NASA Technical Memorandum 110201

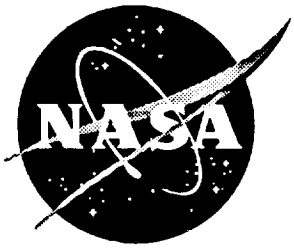

A Study to Determine Methods of Improving the Subsonic Performance of A Proposed Personnel Launch System (PLS) Concept

B. Spencer, Jr., C. H. Fox, Jr., and J. K. Huffman
Langley Research Center, Hampton, Virginia

December 1995

National Aeronautics and
Space Administration
Langley Research Center
Hampton, Virginia 23681-0001

A STUDY TO DETERMINE METHODS OF IMPROVING THE SUBSONIC PERFORMANCE OF A PROPOSED PERSONNEL LAUNCH SYSTEM (PLS) CONCEPT

Bernard Spencer, Jr.; Charles H. Fox, Jr.; and Jarrett K. Huffman

ABSTRACT

An investigation has been conducted in the Langley 7- by 10-Foot High Speed Wind Tunnel to determine the longitudinal and lateral directional aerodynamic characteristics of a series of personnel launch system concepts. This series of configurations evolved during an effort to improve the subsonic characteristics of a proposed lifting entry vehicle (designated the HL-20). The primary purpose of the overall investigation was to provide a vehicle concept which was inherently stable and trimable from entry to landing while examining methods of improving subsonic aerodynamic performance.

Modifications to the original HL-20 were: forebody shaping including the canopy region to minimize drag; changes in body camber to improve positive pitching moment; base area reduction to further reduce drag; and outboard fin dihedral, airfoil section, and fairing to improve lift and lift-drag ratio. Split rudders on the vertical tail were investigated for use as speed breaks in an effort to provide nose up pitching moment. In addition, a canard was added to one configuration for improving both positive pitch and lift. The tests were conducted at a Mach number of 0.30 and Reynolds number per foot of about 1.8×10^6 over an angle of attack range from approximately -4° to 20° at sideslip angles of 0°, -4°, and 4°.

INTRODUCTION

The plans for Space Station Freedom require a small supporting vehicle for ferrying personnel to and from the station. There is also a requirement to have a

vehicle permanently docked at the station to serve as an emergency crew rescue vehicle. This vehicle would be a small personnel-only version; one concept being of the lifting body type vehicle presently designated the HL-20 (see refs. 1-5).

The HL-20 lifting body shape has also been suggested as one candidate for NASA's Assured Crew Return Capability (ACRC) as well as a Personnel Launch System (PLS). Both programs are designed around an entry vehicle with the capability of transporting a crew of 6 to 9 members from the space station. The HL-20 is a small personnel carrier vehicle approximately 28 feet long with aerodynamic characteristics similar to those of the Space Shuttle and earlier lifting body concepts (see ref. 6). The vehicle has a low-aspect-ratio body with a flat under surface and blunt base. Center and outboard fins are mounted on the upper aft body, with the outboard fins set at a dihedral angle of 50°. Control surfaces are mounted on the outboard fins and aft portion of the body. Results of wind tunnel studies to date, indicate; (1) low subsonic lift-to-drag ratios and (2) deficiencies in directional stability at low supersonic speeds with undesirable associated negative trim angle of attack, negative trim lift and lift-to-drag ratios in the Mach range 1.5 to 2.5 (see refs. 7-11).

Therefore, Langley Research Center has initiated an extensive study to investigate methods of improving the overall aerodynamics of a lifting-body vehicle of this type. The refined configurations are referred to herein as the HL-20A and HL-20B series. Modifications to the original HL-20 were forebody shaping including the canopy region to minimize drag; changes in body camber to improve positive pitching moment; base area reduction to further reduce drag, and outboard fin dihedral, airfoil section, and fairing to improve lift and lift-drag ratio. Design philosophy and detailed descriptions of the various modifications are discussed in depth in the models section of this report.

The present investigation was conducted in the Langley 7- by 10-Foot High Speed Wind Tunnel to determine the low speed longitudinal and lateral-directional aerodynamic characteristics of the HL-20A and HL-20B concepts and are compared to

the original HL-20 vehicle. The tests were conducted at a Mach number of 0.30 and Reynolds number per foot of about 1.8×10^6 over an angle of attack range from approximately -4° to 20° at sideslip angles of 0°, -4°, and 4.

SYMBOLS

The data are based on measurements made in the U.S. Customary units. Longitudinal aerodynamic characteristics are referred to the stability axis system and lateral-directional characteristics (including beta derivatives) to body axis system (fig. 1). Longitudinal coefficients are based on projected body planform area and actual length of each body and lateral-directional characteristics on planform area and body span (fins-off). Moment reference point is 54 percent actual body length for each configuration.

b	model reference span, in.
C_A	axial force coefficient, Axial Force/qS
C_l	body axis rolling moment coefficient, Rolling Moment/qSb
$C_{l,\beta}$	beta derivative of body axis rolling moment coefficient computed between $\beta = 4°$, $\beta = 0°$ or $\beta = -4°$
C_D	drag coefficient, Drag/qS
$C_{D,min}$	minimum drag coefficient
C_L	lift coefficient, Lift/qS
ΔC_L	incremental lift between specified configurations
C_m	pitching moment coefficient, Pitching Moment/qSl_b
$C_{m,\alpha}$	longitudinal stability parameter
$C_{m,o}$	pitching moment at alpha = 0°

C_N	normal force coefficient, q normal force/qS
$C_{n,\beta}$	beta derivative of body axis yawing moment coefficient computed between $\beta = -4°$ or $0°$ and $\beta = 4°$ C_n = Yawing Moment/qSb
$C_{Y,\beta}$	β derivative of body axis side force coefficient computed between $\beta = -4°$ or $0°$ and $\beta = 4°$ C_Y = Side Force/qS
l_b	actual body length, in.
L/D	lift-to-drag ratio
$(L/D)_{max}$	maximum lift-to-drag ratio
M_∞	free stream Mach number
q	free stream dynamic pressure, psf
R	Reynolds number per foot
S	model reference area, ft^2
X,	longitudinal station along the body, in.
α	angle of attack, deg
β	angle of sideslip, deg
Γ_h	tip fin dihedral angle, deg (as measured from the horizontal plane)

Abbreviations

Spd Brk	Speed-brake located on centerline vertical tail
Land Gr	Landing gear

DESCRIPTION OF MODELS

Drawings of the HL-20 model are presented in figure 2 and drawings of the HL-20A/B configurations are presented in figure 3. Photographs of the HL-20, with landing gear deployed, and HL-20B-1 configurations mounted in the High Speed 7- by 10-Foot Tunnel are presented in figure 4(a) and 4(b), respectively. Additional photographs showing the various configuration changes made during the investigation are presented as follows:

Fig. 4(c) - Composite of the HL-20A/B series.

Fig. 4(d) - HL-20; HL-20A/B Planform, upper surface base, tip-fin and center fin comparison.

Fig. 4(e) - HL-20A-1; A-2; A-4 showing under surface camber changes.

Fig. 4(f) - HL-20A-1; HL-20A-3 showing increase base boattailing and tip fin fairing changes.

Fig. 4(g) - Formation of HL-20B-1 and B-2 from HL-20A-4 and A-3, respectively by removal of upper surface downslope.

Fig. 4(h) - Comparison of AFN and slab configurations.

Fig. 4(i) - Comparison of 25° AFO and AFN tip fin configurations.

Fig. 4(j) - Comparison of AFN faired and unfaired.

Fig. 4(k) - Partial-span speedbrake deflected 45° per side.

Fig. 4(l) - Canard planform on HL-20B-2.

HL-20

The baseline configuration is the HL-20 and a detailed discussion of its geometry is presented in reference 7 and 8. Basically, this configuration is a flat bottom low aspect ratio body with a large, blunt nose section, a blunt canopy, and a downsloping -6.5° upper surface (see fig. 2). The body, aft upper surface region is fixed as an upward deflected elevon at approximately -20° for obtaining trimmed pitching moments

over the range of entry-to-landing Mach numbers. The outboard fins are set at 50° dihedral and a small vertical tail is located at the centerline of the body. Both fins and vertical tail have a slab cross section with a full radius leading edge.

HL-20A-1

The HL-20A-1 configuration (figure 3, part 1) retained the basic features of the HL-20 except that the forebody was modified to a lower drag, ogive shape and the canopy was modified and highly swept. These modifications resulted in an increase in both plan-form area and length. The double-sloped forebody and therefore the "cheeks" located aft of the canopy were eliminated, as well as the large upper surface, negatively deflected elevons (see figure 4(d)). These modifications were incorporated to reduce profile drag, base drag and eliminate entry "hot spots," which have been noted in unpublished aeroheating results. It is anticipated that these vehicles (HL-20A/B) would reenter the Earth's atmosphere at higher angles of attack than the baseline HL-20, around 56° to 60° near $C_{L,max}$ compared to 40°. This higher angle of attack entry should move the stagnation heating line aft of the nose region to the underside of the body. The resulting lower heating rates should allow the smaller equivalent nose radii used on the HL--20A/B configurations. Normal rotation of the vehicle from near 56° to 60°, to lower trim angles of attack will occur inherently due to the natural center of pressure movement with decreasing Mach number.

HL-20A-2

The lower surface of the HL-20A-2 configuration (figure 3 - part 2) was cambered by adding a NACA 65A006 airfoil camber distribution to the centerline section to the HL-20 flat-bottom, while retaining HL-20A-1 forebody and planform (figure 4(e)). This was incorporated to improve positive $C_{m,o}$ for subsonic trim and possibly eliminate the trim at negative angles of attack noted at low supersonic speeds (ref. 8).

HL-20A-3

The base area of the HL-20A-3 (figure 3, part 3) configuration was somewhat reduced by increasing the HL-20A-2 base boattailing towards the outboard fins. This modification was incorporated primarily to provided a smoother fairing between the fins and body leading edges. See figure 3, part 3(b) and also figure 4(f).

HL-20A-4

The lower surface camber was further increased on the HL-20A-4 configuration (figure 3, part 4) by replacing the NACA 65A06 section of the HL-20A-3 configuration with a NACA 65A012 (see figure 4(e) comparison). This was incorporated to provide even more positive $C_{m,o}$ for trim than the HL-20A-2. Cross-sectional shapes were elliptic, thereby again giving a smoother fairing to the body leading edges as well as the outboard fins.

HL-20B-1 and HL-20B-2

The HL-20B-1 and B-2 series (figure 3, parts 5, 6, and 7; respectively) are the HL-20A-4 and HL-20A-3 bodies with the 6.5° upper surface downslope removed (i.e., upper surface made parallel to free stream). These modifications were formed by adding a 6.5° pie shaped wedge aft of the canopy. This increased the camber effect and was incorporated in an effort to push the subsonic $(L/D)_{max}$ to angles of attack nearer those anticipated for landing (i.e., $\alpha \approx 16°$), and to further increase positive $C_{m,o}$. See figure 4(g). Representative cross-sections accompany each configuration as digitized for a smaller model, appropriately noted (figure 3).

Outboard Fin Configurations

The original HL-20 outboard slab fins were modified by changing the airfoil section from a slab section with a blunt base to a NACA 0012 at the tip and NACA 0008 at the root (figure 3, part 8(b) and figure 4(h) and 4(i)). This eliminated the large blunt base areas on each of the fins, thereby reducing $C_{D,\,min}$.

The fins were modified such that the cross section was an airfoil shape on one side and a flat plate on the other. The airfoil-in (AFN) configuration has the flat surface facing outboard and airfoil section inboard to increase positive C_L. Airfoil sections are NACA 0012 at the tip and NACA 0008 at the root.

The airfoil-out (AFO) configuration has the flat surface facing inward and airfoil section outboard to increase positive $C_{m,o}$ for trim; however, at a loss in C_L. Both of these also eliminated the base area of the slab fin. Airfoil sections are NACA 0012 at the tip and NACA 0008 at the root.

The fins on the HL-20 are located above the flat bottom lower surface, therefore, leaving a "ridge" between fin-body junction and body lower surface. During entry this could cause flow separation and impingement, thereby creating hot spots on the fin. The designation "faired" (i.e., AFN-faired, SLAB-faired) indicates the fins were moved outboard and lowered down the side to form a smooth fairing into the vehicle lower surface (see figure 4(j)). Some increase in fin exposed planform area resulted, which also gave a slight increase in wing span.

Vertical Tail and Speed Brake

The small blunt vertical fin of the HL-20 was replaced by a large, symmetrical vertical tail to enhance subsonic directional stability (figure 4, part a and b). The root is an NACA 0008 and the tip a NACA 0012 airfoil section. Split rudders (speedbrakes)

were also tested with the large vertical tail (see figure 4(k)). Full span speedbrakes were deflected 30° per side and partial span (upper 1/3 of rudder) were deflected 45° in an effort to produce positive $C_{m,o}$ without reducing C_L.

Canard

A canard was also tested on the HL-20B-2 configuration(see figure 3, part 8(a) and figure 4(l)). This is considered a fold-down device which could be stowed along the body contour aft of the canopy during entry and then deployed subsonically to produce positive increments in both C_m and C_L. The canard had a flat bottom and highly cambered NACA 0012 upper surface, and was trapezoidal in planform.

APPARATUS, TESTS, AND CORRECTIONS

The investigation was conducted in the Langley 7- by 10-Foot High Speed Wind Tunnel (see ref. 11). Forces and moments were measured on a six component strain gage balance mounted internally in the model. The test was run at a Mach number of 0.30, with the average test Reynolds number approximately 1.8×10^6 per foot. The models were tested over an angle of attack range from approximately -4° to 20° at sideslip angles of 0°, -4°, and 4°. The corrected angles of attack and sideslip include the effects of sting bending under load. Beta derivatives were obtained between $\beta = 0°$; -4°, and +4° incrementally, and therefore do not account for any nonlinearities which may exist in this β range.

Jet boundary and blockage corrections have been applied to the data based on the equations found in references 12 and 13; respectively. The balance chamber pressure and the base pressures were monitored for selected configurations. However, no corrections were made to the data for the effects of base and chamber pressure. Transition strips 0.0625 inches in width of No. 100 Carborundum grain were located 0.3 inch aft of the leading edges of the fins and vertical tail as well as 1.0 inch aft of the

nose of the model. For the canards, number 80 Carborundum grains were placed 0.55 inches aft of the leading edges. All transition strips were applied according to the methods prescribed in reference 14.

RESULTS AND DISCUSSIONS

Presentation of Results

The parametric nature of the test permits one to generate numerous comparison plots showing the effects of various configurational variables in combination. The data are presented such that systematic analysis of the various modifications can be made, with results presented in the following figures:

	Figures
Effect of body contouring on the longitudinal aerodynamic characteristics for the HL-20A series bodies alone.	5
Effect of body contouring on the longitudinal aerodynamic characteristics for the HL-20A series bodies with slab tip fin at $\Gamma_h = 50°$, and compared to the baseline HL-20 configuration.	6
Effect of the addition of tip fins with different airfoil sections on the aerodynamic characteristics for the HL-20A-4 configuration.	7
Effect of speed brakes on the aerodynamic characteristics for the HL-20A-4 configuration.	8
Effect of removal of upper surface downslope on the longitudinal aerodynamic characteristics for configurations with tip fins off. HL-20A-4 and A-3 to HL-20B-1 and B-2; respectively.	9

DISCUSSION

Effects of body contouring.- As previously noted the primary purposes of changes in body contour from the HL-20 shape (HL-20A1-A4) was to reduce profile drag, reduce base area and thereby base drag and provide positive increment in pitching moment in order to minimize large negative control surface deflections required for trim. The effects of body contouring for bodies A1-A4 alone and bodies A1-A4 with 50° slab-fins are presented in figures 5 and 6; respectively, the latter includes the original HL-20 configuration. Since no body alone data are available on the HL-20 configuration below $M_\infty = 0.60$, and blunt bodies are well into compressibility effects at $M_\infty = <0.30$ no comparisons with the body alone data have been presented.

An examination of the aerodynamic characteristics of the HL-20 versus the HL-20A-1 indicates a reduction in $C_{D,min}$ from 0.065 to 0.044 along with a positive increment in C_L of about 0.1. This combination resulted in an increase in $(L/D)_{max}$ from about 3.5 to 4.2. This resulted, however, in a large negative shift in $C_{m,o}$ of about 0.03. The use of body camber on the HL-20A-2 and HL-20A-4 configurations greatly alleviated this adverse effect through a positive shift in $C_{m,o}$ without adversely affecting either $(L/D)_{max}$ or $C_{D,min}$. However, C_L was reduced back to the level of the original HL-20. All of these favorable effects of body shaping and boattailing are emphasized in figure 5 (body-alone), indicating the HL-20A-3 (additional boattailing) and HL-20A-4 to have the lowest drag and slightly higher $(L/D)_{max}$.

Effects of tip-fin section (HL-20A-4).- Changing the tip-fin configuration from 50° slab to 50° AFN results in increases in $(L/D)_{max}$ from 4.2 to 6.6 (figure 7). The resultant $C_{m,o}$ values, however, shift from positive (0.019) to negative -0.004 and herein lies the

problem with vehicles of this type. How does one generate higher lift and lift-drag ratio and still retain positive stable trim without large negative control surfaces? It becomes an iterative process: efficient lifting surface and reductions in base area to increase L/D, and body camber for $C_{m,o}$ to provide trim.

Speedbrake for trim.- An alternate method of producing the large $C_{m,o}$ needed for stable trim is to deploy split rudders (speedbrakes) and use the resulting drag force located well above the configuration center of gravity. The idea is to produce a pitching moment without having a significant affect on the total lift. Speedbrakes have been shown to be very effective pitch control devices, compared to the elevons, on the Space Shuttle Orbiter at supersonic speeds and are used by the shuttle during the approach and landing maneuver. Both full span and partial span speedbrakes were tested and, as shown in figure 8(a), both produced significant positive increments in $C_{m,o}$ such that trim was obtained around 8° - 9° angle of attack. The configuration without the speedbrake was significantly out of trim with large negative C_m in this angle of attack range. For this case, however, the speedbrakes did have an affect on C_L causing a loss of about 0.1. This and the normal increase in drag resulted in large reductions in L/D such that $(L/D)_{max}$ was only about 3.3. While the speedbrakes did provide good trim characteristics, the performance penalty would appear to be too large. The inefficiency of full-span speedbrake results from induced flow separation on the body aft end causing lift loss (as evidenced by the additional large $+C_{m,o}$ obtained). Use of a partial-span speedbrake deflected 45° per side (upper 1/3 of vertical tail) in combination with the 50° slab-faired fins, resulted in $C_{m,o}$ increases with resultant increased C_D from 0.041 to 0.068 and $(L/D)_{max}$ loss from 4.5 to 3.2; a more efficient control, but still too large a penalty. Speedbrakes are therefore, not efficient devices for low (L/D) vehicles at subsonic speeds.

Removing body upper-surface negative slope.- (HL-20B series) As previously noted, removing the negative 6.5° body upper surface downslope was accomplished by

adding a 6.5° wedge aft of the canopy thereby making the vehicle upper surface parallel to free stream using the HL-20A-4 and HL-20A-3 configurations to form the HL-20B-1 and HL-20B-2 configurations; respectively. (See figure 4(e)). The desired effect was to increase positive C_m due to increased body camber and to shift $(L/D)_{max}$ to higher angles of attack (i.e., nearer those for landing) while accepting some losses in lift.

Removing the 6.5° upper surface downslope (HL-20B-series) had the desired effect of shifting α for $(L/D)_{max}$ to angles of attack near 16° or near landing conditions (see figure 9). The HL-20B-1 with the 50° slab fin on (figure 10) shows stable trim near α = 16° at $(L/D)_{max}$ with an $(L/D)_{max}$ of about 4.1 or the same value as the HL-20A series near 8° to 10° angle of attack.

Effect of fin airfoil section and fairing.- (HL-20B-1) The effect of changing the fin airfoil section on the HL-20B-1 configuration from slab to AFN results in increases in $(L/D)_{max}$ from about 4.1 to 6 with an accompanying reduction in trim angle of attack from 15° to 6° (figure 12). This again emphasizes the continual trade-off between efficient lifting surfaces for improving performance while still maintaining the desired trim characteristics.

Fairing the fin into the bottom of the body had no effect on any aerodynamic characteristics for the HL-20B-1 AFN configuration but did have a significant effect on the slab configuration (as shown in figure 12(a)) where $(L/D)_{max}$ and lift curve slope were improved. Significant increases in longitudinal stability, $C_{m,\alpha}$ were noted. However, fairing the fin on the HL-20B-2 produced improvements in aerodynamic characteristics for both the AFN and slab configurations (figure 14). For example, $(L/D)_{max}$ was increased for both configurations.

Fin-dihedral/airfoil contours.- (AFN/AFO) HL-20B-1. Decreasing outboard fin dihedral for the AFN configuration from 50° to 25° resulted in an increase in α, trim from 6° to 9°. Reversing airfoil section from AFN to AFO produced the large positive pitch

desired, however, not without accompanying lift losses and losses in $(L/D)_{max}$ to about 4.8 (see figure 13). Similar results are noted for the HL-20B-2 configuration (figure 15).

Effect of addition of canards.- The addition of canards to the HL-20B-2 body resulted in large increases in positive pitching moment, with some increases in lift coefficient (figure 16). Not all of the positive lift generated by the canards is realized, however, due to the down-wash from the canard reducing somewhat the lift on the body-fin combination (compare ΔCL between body-canard and ΔCL between body-fin canard). This phenomena (canard efficiency factor) is explained in depth in reference 15. Use of a canard is an efficient method of producing the desired pitch for trim on lifting bodies of this type, while still taking advantage of the favorable C_L produced by the AFN fins.

Lateral-directional characteristics.- The primary purpose of the present study was to investigate methods of improving aerodynamic subsonic performance, therefore only a limited amount of lateral-directional stability as affected by the various configurational changes were obtained. These were done primarily to see if large adverse effects occurred as a result of configurational modifications.

As may be noted from the "b" parts of selected configurations, no large adverse affects on the directional stability parameter $C_{n\beta}$ nor on the positive effective dihedral parameter $C_{\iota\beta}$ occurred due to the various configurational modifications employed, with the new large center vertical tail on.

Landing Gear Deployment.- Because of the low values of subsonic $(L/D)_{max}$ noted for the original HL-20 configuration, the question arose as to how much further reduction in performance would result from landing gear deployment?

Figure 18 presents the effects of landing gear deployment on the aerodynamic characteristic of the original HL-20 with 50° slab fins. The major effect is on C_D and $(L/D)_{max}$ where an increase in $C_{D,min}$ from about 0.065 to 0.09 is noted with resultant loss in $(L/D)_{max}$ from about 3.4 to 2.9. A slight reduction in C_L versus a and

accompanying downward shift in C_m also results for the gear on configuration. Some increases in $C_{n\beta}$ at the low to moderate angles of attack also occur with no effect on $C_{\iota\beta}$.

SUMMARY OF RESULTS

An investigation has been made to determine methods of improving the subsonic performance of lifting body vehicles, by use of body contouring, and tip-fin airfoil section and fin dihedral. In addition, the use of split rudders on the vertical tail (speedbrake) and the addition of a canard to provide positive moment were also examined. Results of this study are summarized as follows:

Body contouring and cambering and reducing blunt base areas (in non-essential areas) combined with properly tailoring the outboard fins can significantly enhance subsonic performance of lifting-body type entry vehicles. Use of a canard can improve lift and provide large positive increments in pitching moment with losses in maximum lift-to-drag ratio occurring. Further investigation into optimizing canard-body-fin arrangements appears warranted, in order to minimize losses in landing performance, since such large reductions in landing speeds results from deployment of these devices. Using a split rudder (speed-brake) as a pitch control can provide the desired positive pitch increments, however, the penalties in performance are significant, thereby, making this type of pitch control device undesirable at subsonic speeds. No large adverse affects on lateral-directional stability parameter occurred due to the various configurational modifications employed.

REFERENCES

1. DeMeis, Richard: Fleeing Freedom. Aerospace America, pp. 38-41, May 1989.

2. Covault, Craig: NASA to Seek Design Concepts for Station Crew Escape Vehicle. Aviation Week and Space Technology, pp. 30, August 17, 1987.

3. Hook, W. R.; and Freeman, D. C.: Lifting Body Option for a Space Station Rescue Vehicle. IAF Congress, Malaga, Spain, October 1989.

4. Naftel, J. Chris; Powell, Richard W.; and Talay, Theodore A.: Ascent, Abort, and Entry Capability Assessment of a Space Station Rescue and Personnel/Logistics Vehicle. AIAA Paper 89-0635, January 1989.

5. Ware, G. M.; Spencer, B., Jr.; and Micol, J. R.: Aerodynamic Characteristics of Proposed Assured Crew Return Capability (ACRC) Configurations. AIAA 89-2172, July 1989.

6. Spencer, Bernard, Jr.: An Investigation of Methods of Improving Subsonic Performance of a Manned Lifting Entry Vehicle. NASA TM X-1157, 1965.

7. Ware, George M.: Transonic Aerodynamic Characteristics of A Proposed Assured Crew Return Capability (ACRC) Lifting-Body Configuration. NASA TM 4117, June 1989.

8. Ware, George M.: Supersonic Aerodynamic Characteristics of A Proposed Assured Crew Return Capability (ACRC) Lifting-Body Configuration. NASA TM 4136, November 1989.

9. Micol, J. R.: Experimental and Predicted Aerodynamic Characteristics of A Proposed Assured Crew Return Vehicle (ACRV) Lifting Body Configuration at Mach 6 and 10. AIAA 90-1403, June 1990.

10. Horvath, T. J.; Rhode, M. N.; and Buck, G. M.: Aerothermodynamic Measurements on A Proposed Assured Crew Return Vehicle (ACRV) Lifting Body Configuration at Mach 6 and 10 in Air. AIAA 90-1744, June 1990.

11. Fox, Charles H., Jr.; and Huffman, Jarrett K.: Calibration and Test Capabilities of the Langley 7- by 10-Foot High Speed Tunnel. NASA TM X-74027, 1977.

12. Gillis, Clarence L.; Polhamus, Edward C.; and Gray, Joseph L., Jr.: Charts for Determining Jet-Boundary Corrections for Complete Models in 7- by 10-Foot Closed Rectangular Wind Tunnels. NACA WR L-123, 1945. (Formerly NACA ARR L5G31)

13. Herriot, John G.: Blockage Corrections for Three-Dimensional-Flow Closed-Throat Wind Tunnels, With Consideration of the Effect of Compressibility. NACA Report 995, 1950. (Supersedes NACA RM A7B28)

14. Braslow, Albert L.; Hicks, Raymond M.; and Harris, Roy V., Jr.: Use of Grit-Type Boundary-Layer-Transition Trips on Wind-Tunnel Models. NASA TN D-3579, 1966.

15. Spencer, Bernard, Jr.; and Sleeman, William C., Jr.: Low-Speed Longitudinal Characteristics of an Airplane Configuration Including Effects of Canard and Wing Trailing-Edge Flap Controls in Combination. NASA Memo 4-22-59L, April 1959.

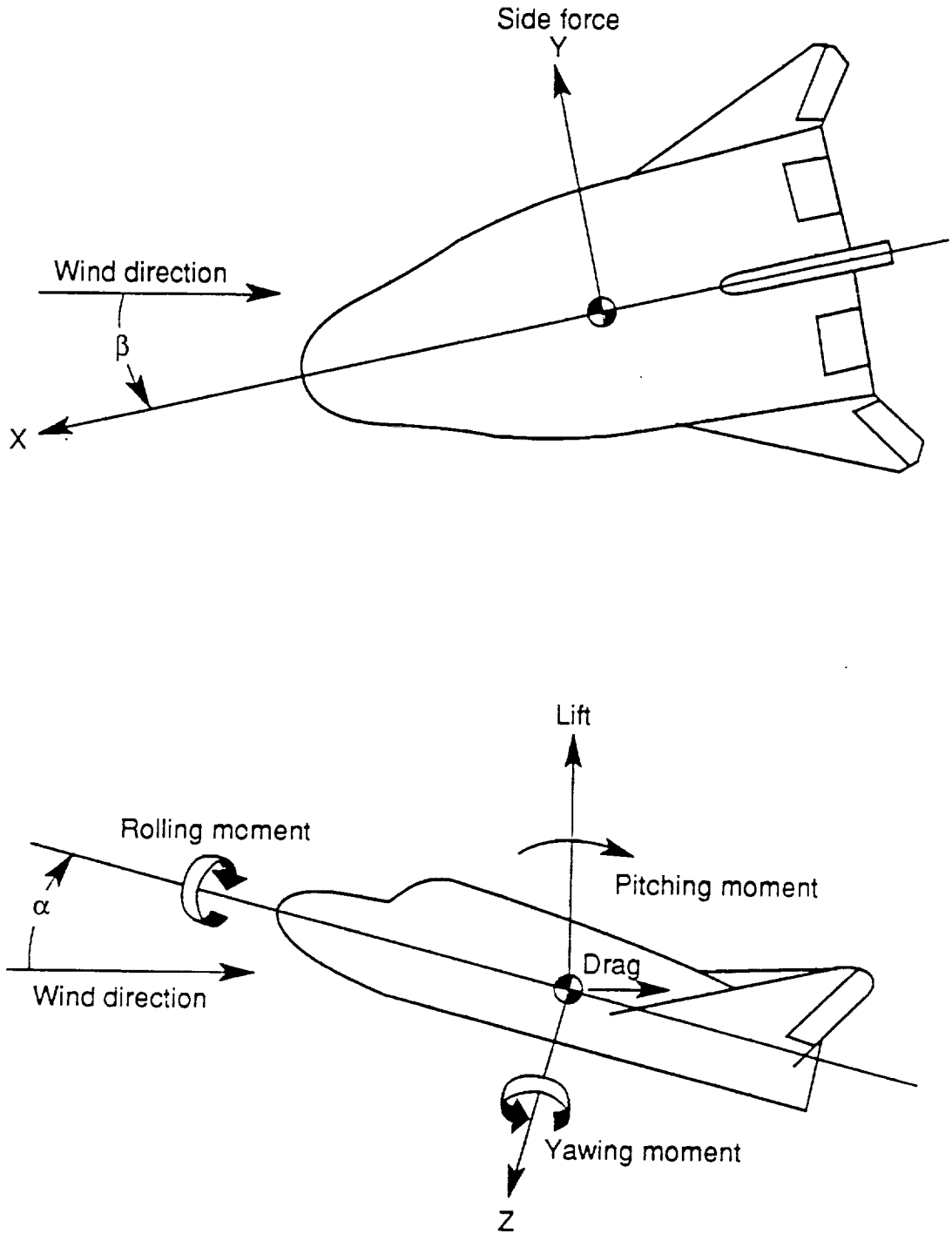

Figure 1. Sketch of system of axes used in investigation showing positive direction of forces, moments, velocities, and angles.

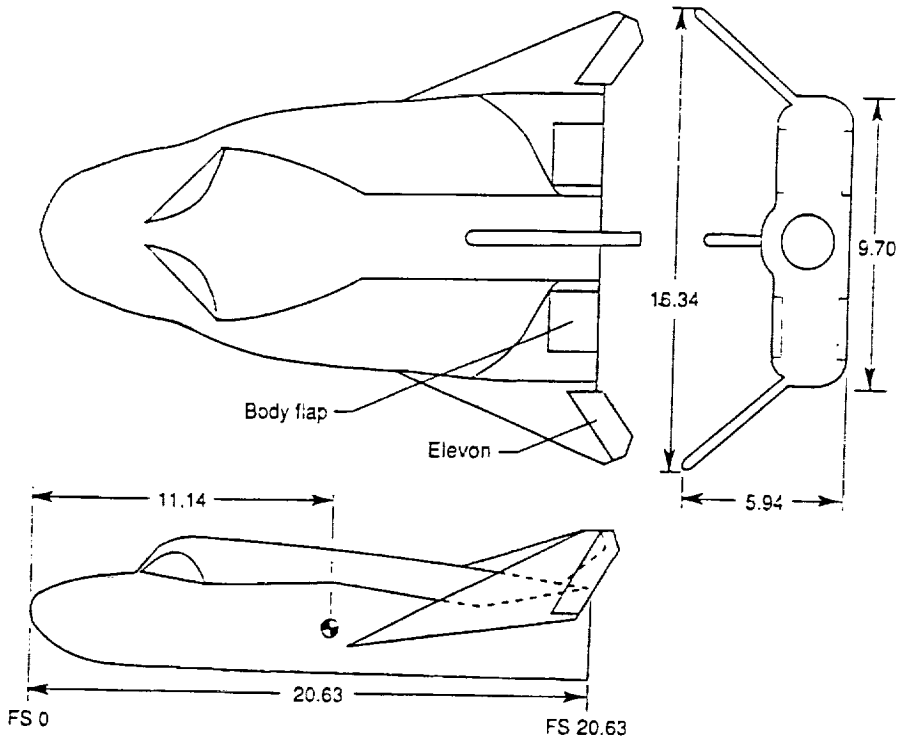

(a) General arrangement.

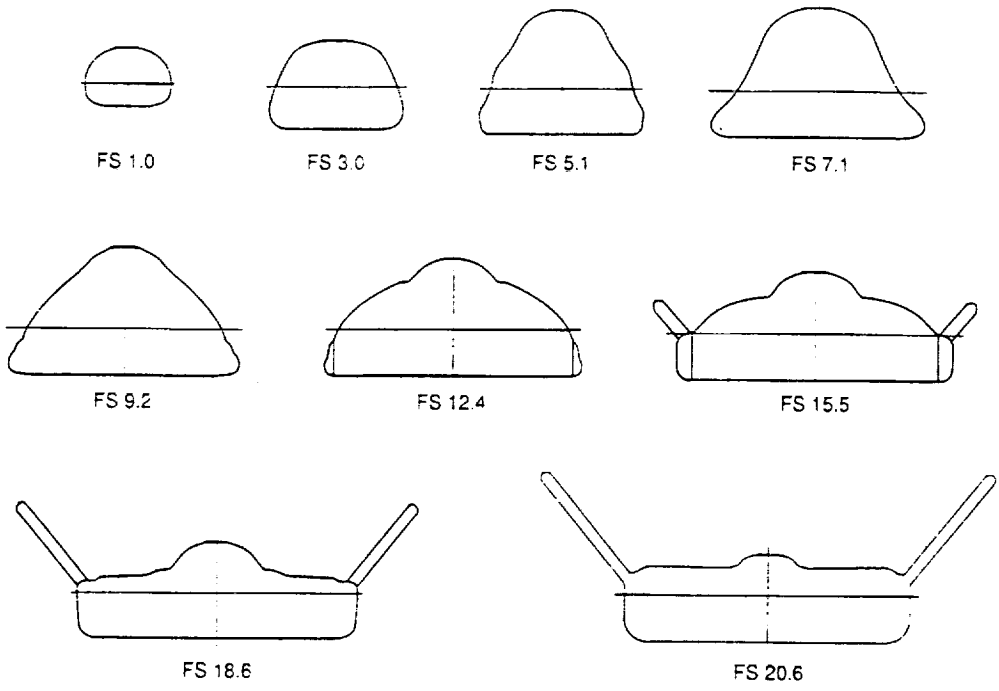

(b) Body cross sections.

Figure 2. Sketches of model used in investigation. All dimensions are in inches.

HL-20A-1:

Reference area, sq. in.	172.92816
Reference span, b, in.	9.694
Reference chord, l_b, in.	21.574
Moment center	0.54 l_b

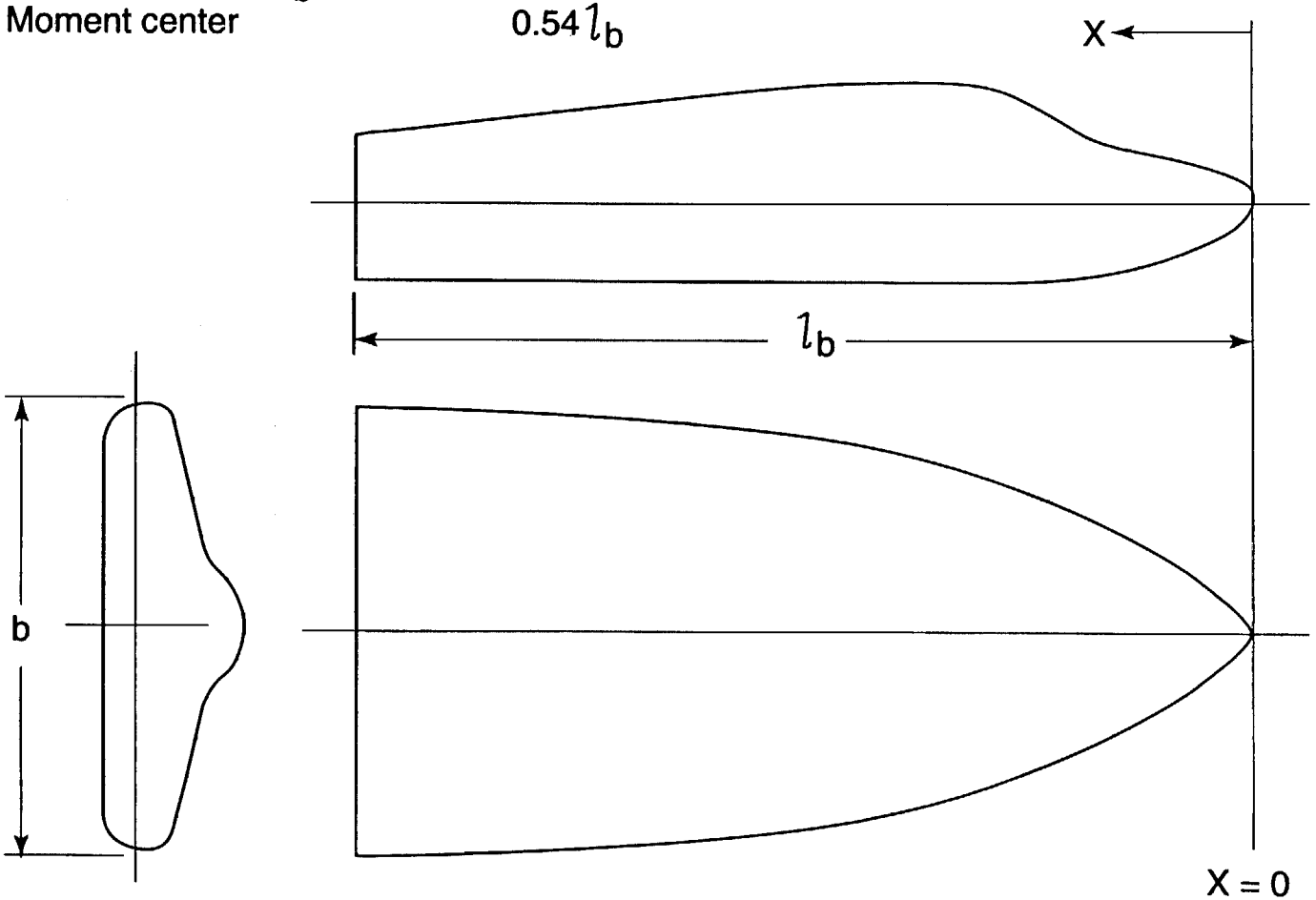

(a) Planform, profile and base.
Part 1 - HL-20A contiguration.

Figure 3. Sketches of body lised in the investigation, including cross-sections.

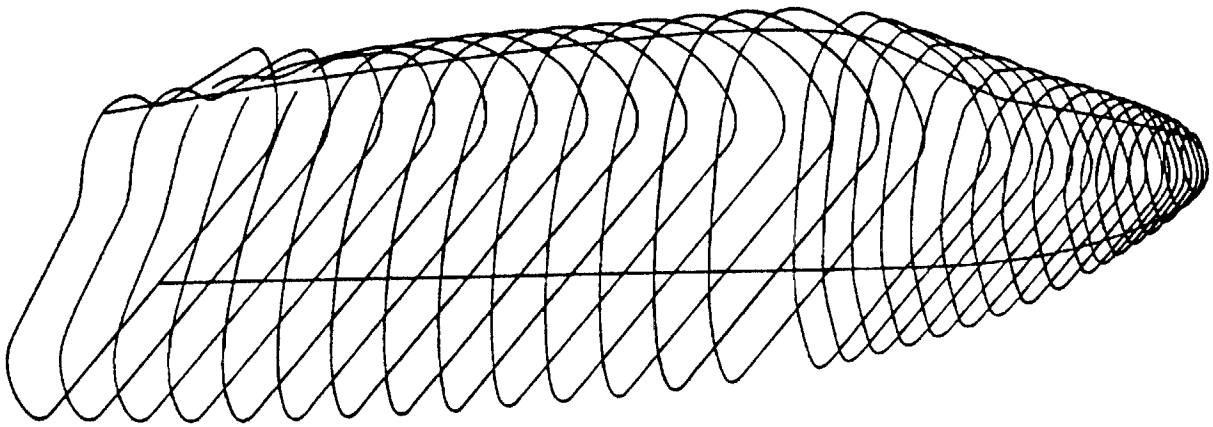

(b) Schematic of body A-1
Part 1 - Continued

Figure 3 - Continued.

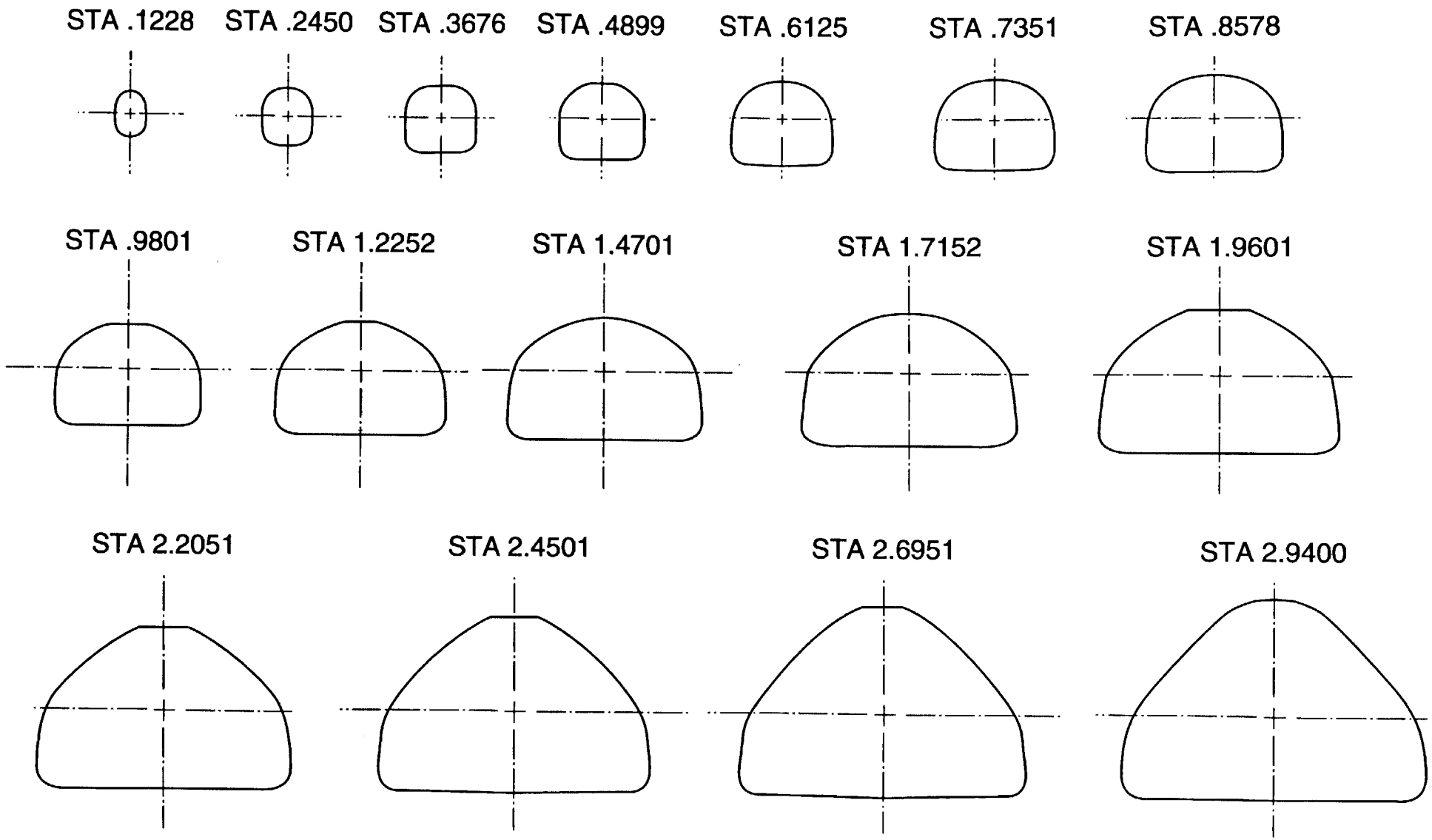

(c) Cross-sections based on X_{max} = 10.2908
Part 1 Continued A-1

Figure 3. Continued.

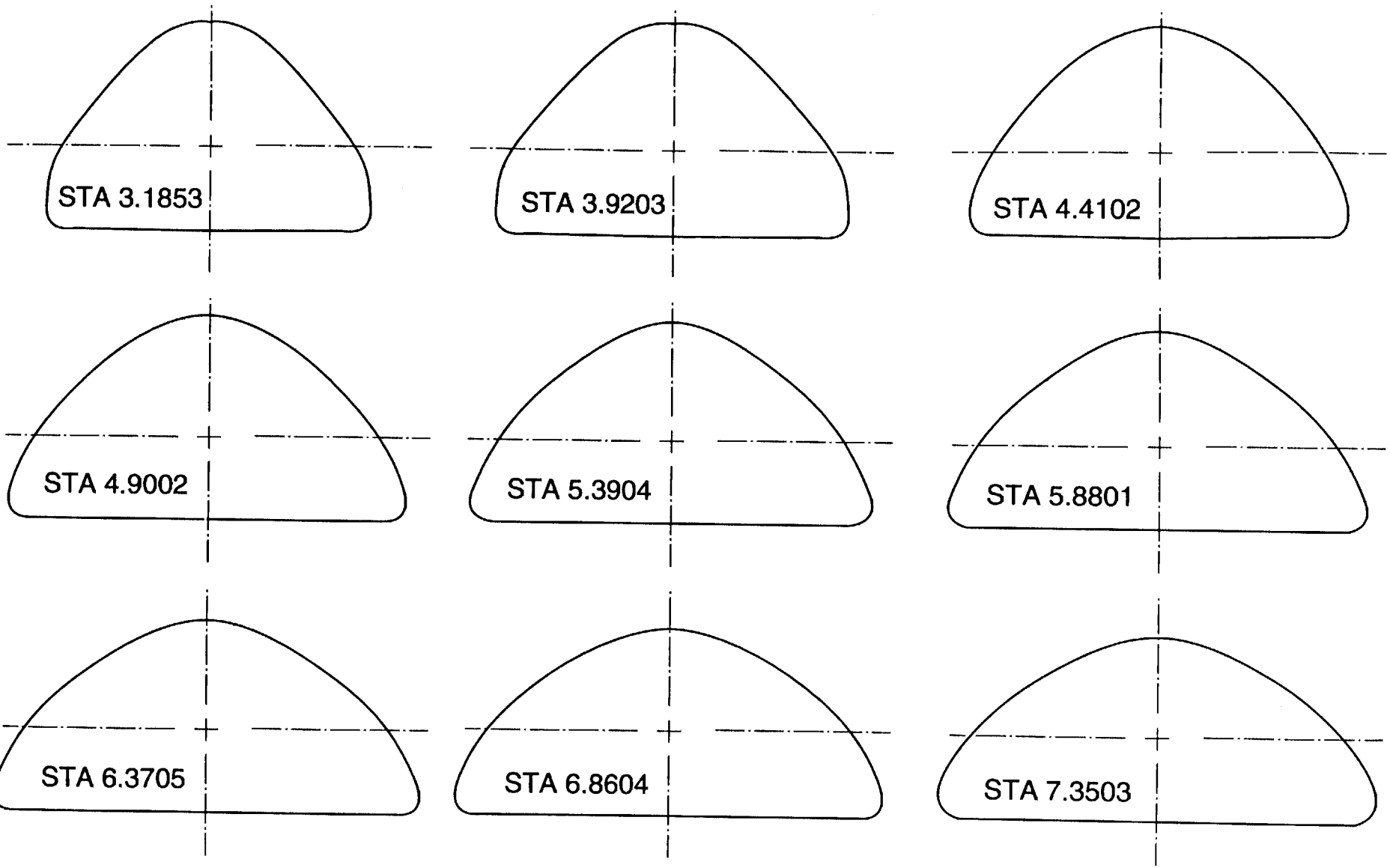

(c) Continued
Part 1 Continued

Figure 3. Continued.

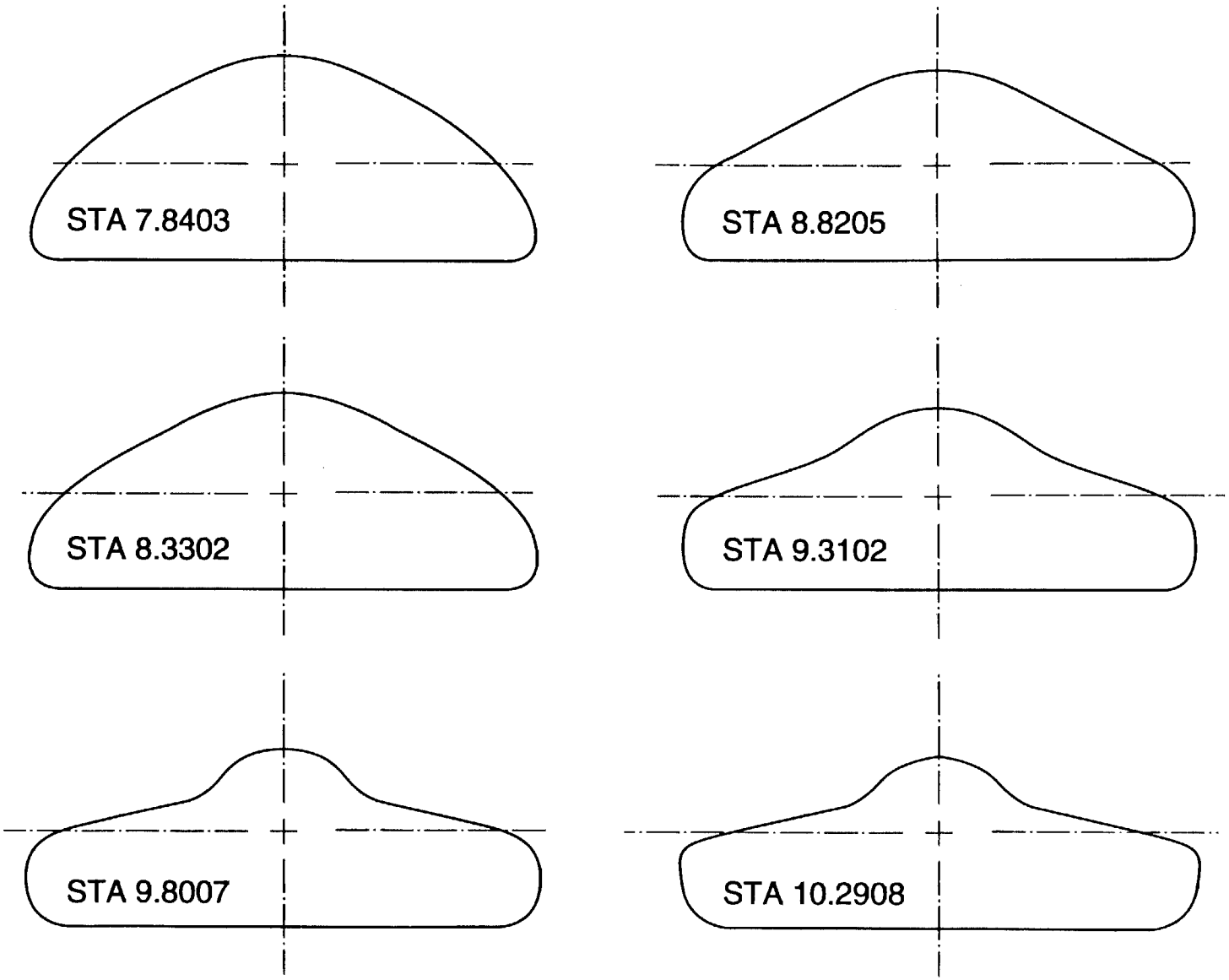

(c) Concluded
Part 1 Concluded

Figure 3. Concluded.

HL-20A-2:

Reference area, sq. in.	172.92816
Reference span, b, in.	9.694
Reference chord, l_b, in.	21.565
Moment center	0.54 l_b

Schematic of body A-2

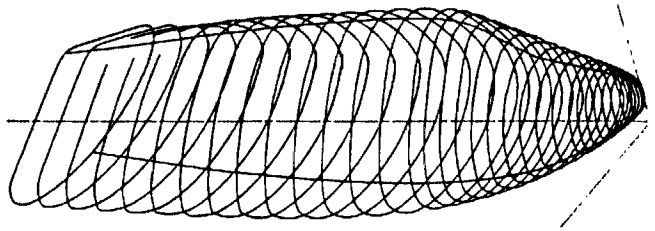

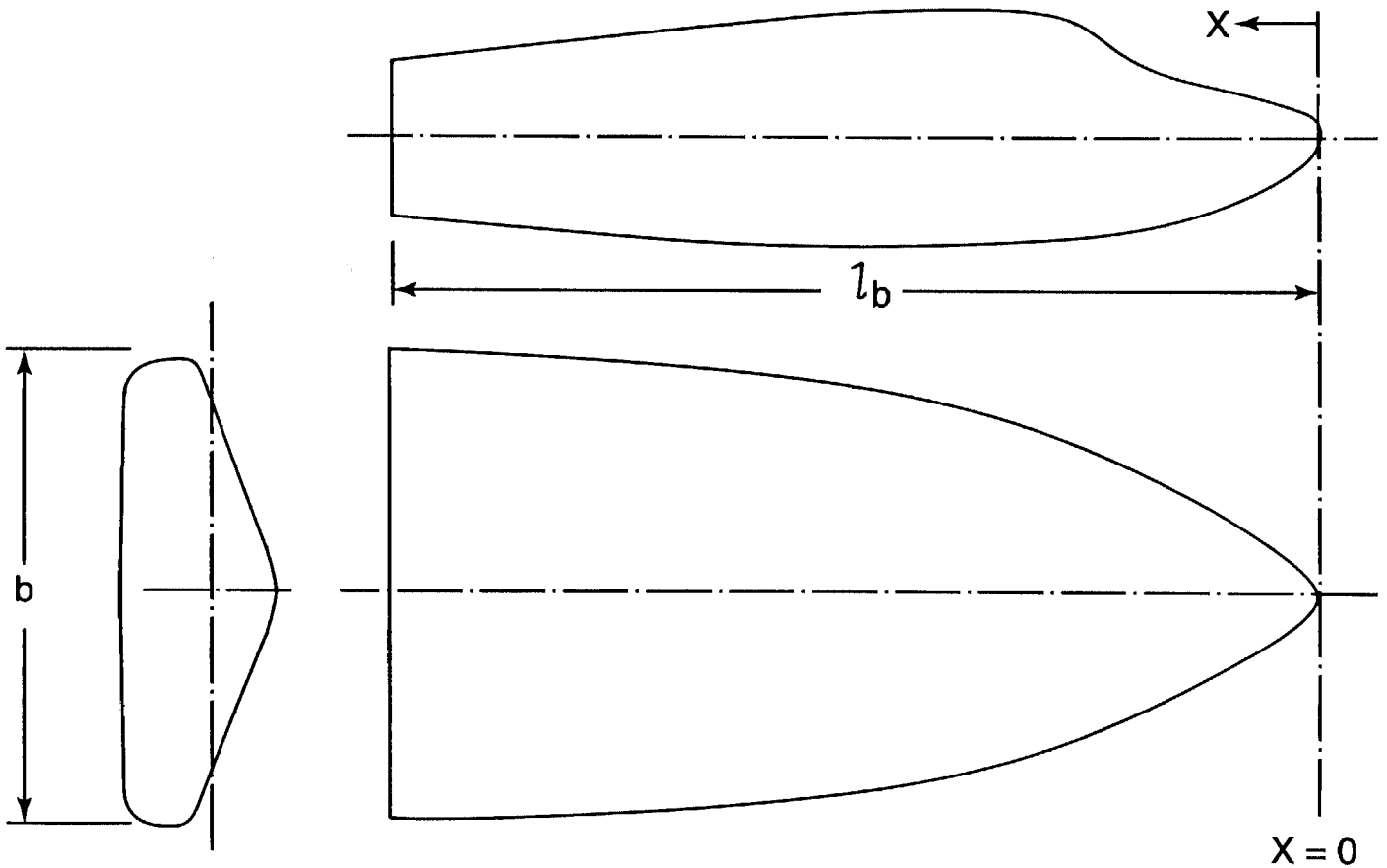

(a) Planform, profile and base views.

Part 2 - HL-20A-2 configurations

Figure 3 Continued.

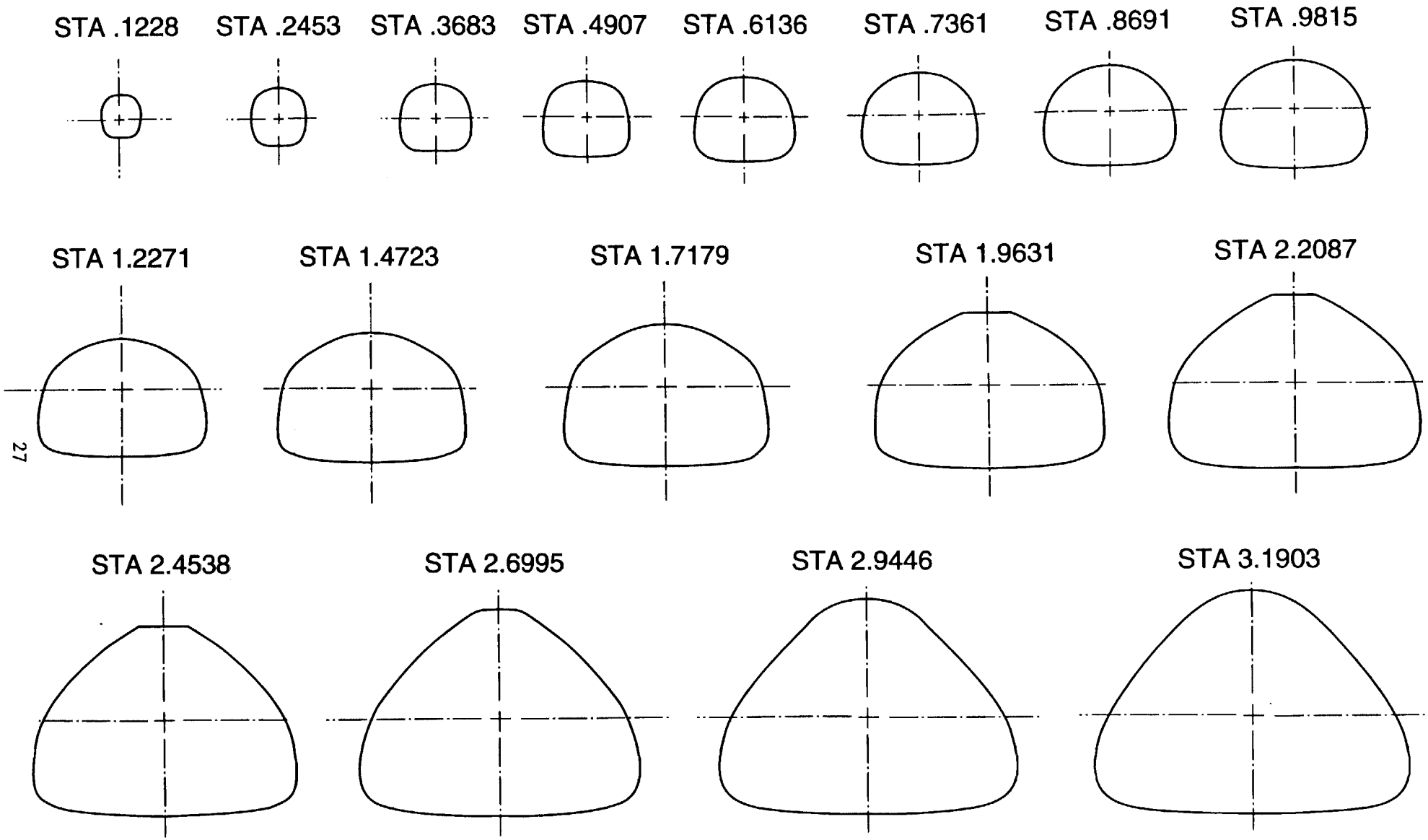

(c) Cross-sections for $_b$ body = 10.3067 inches.

Part 2 - Continued.

Figure 3. Continued.

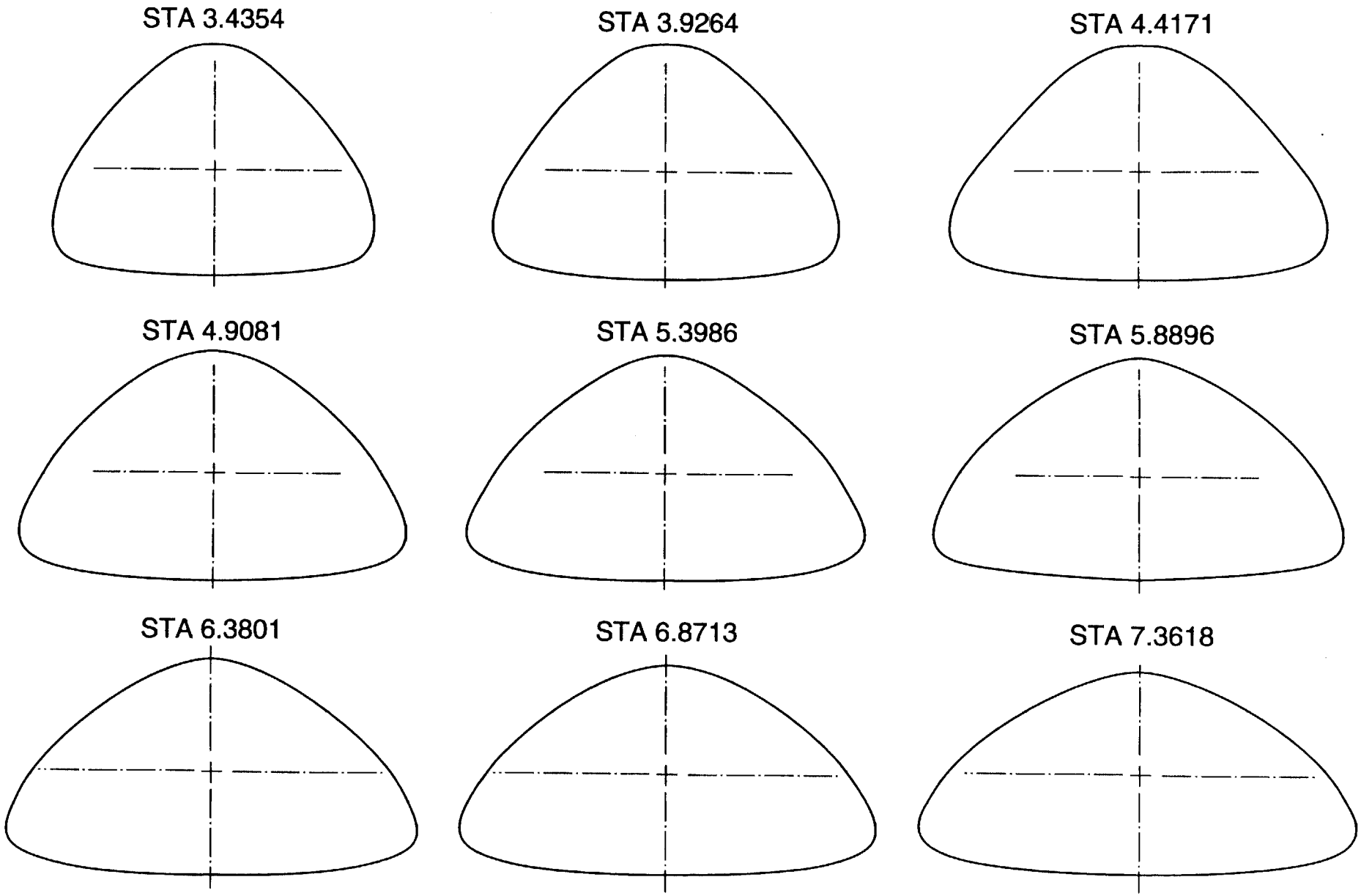

(c) Continued.

Part 2 - Continued.

Figure 3. Continued.

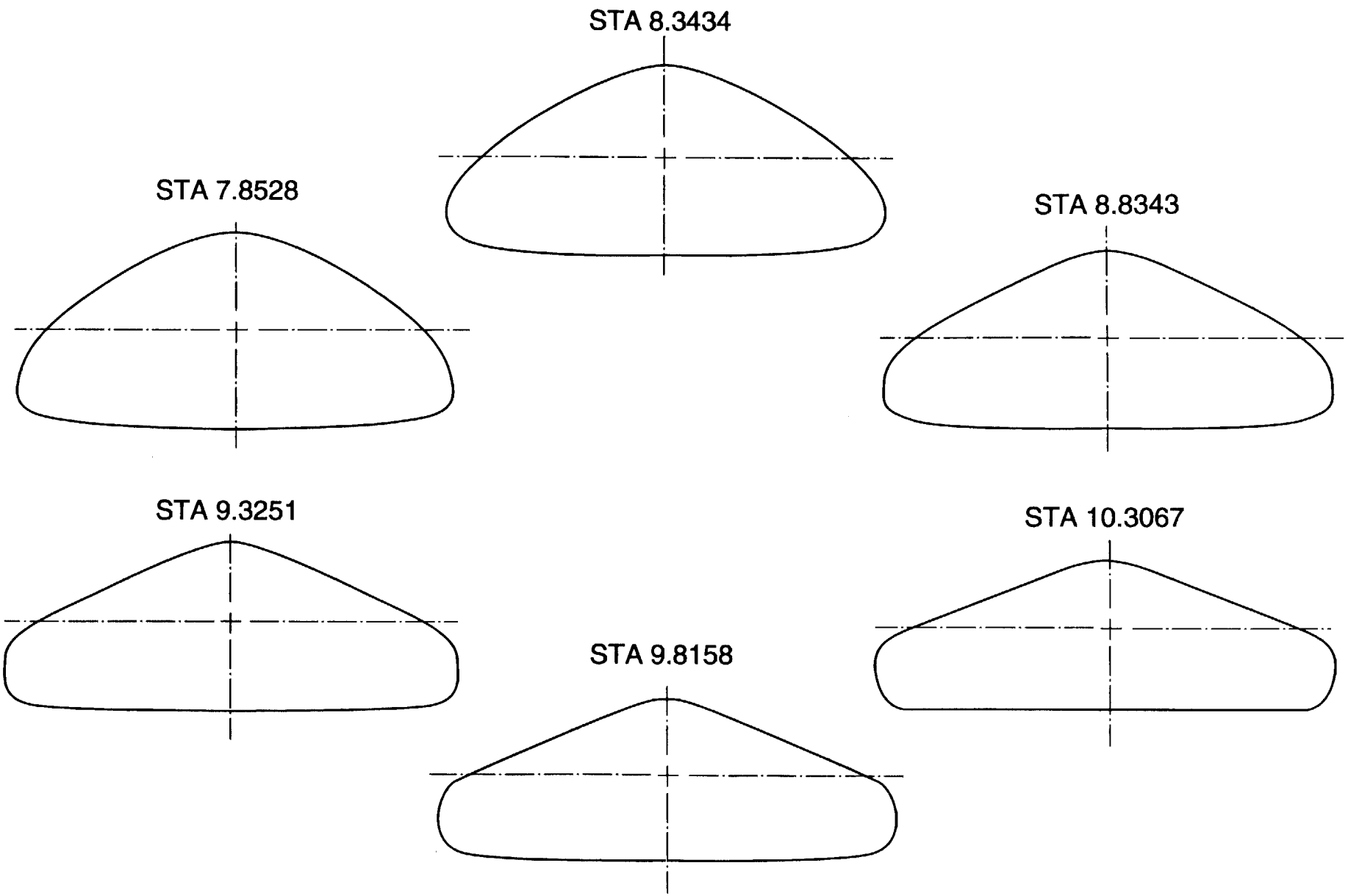

(c) Concluded.

Part 2 - Continued.

Figure 3. Continued.

HL-20A-3:

Reference area, sq. in.	172.92816
Reference span, b, in.	9.694
Reference chord, l_b, in.	21.420
Moment center	0.54 $\bar{c}$

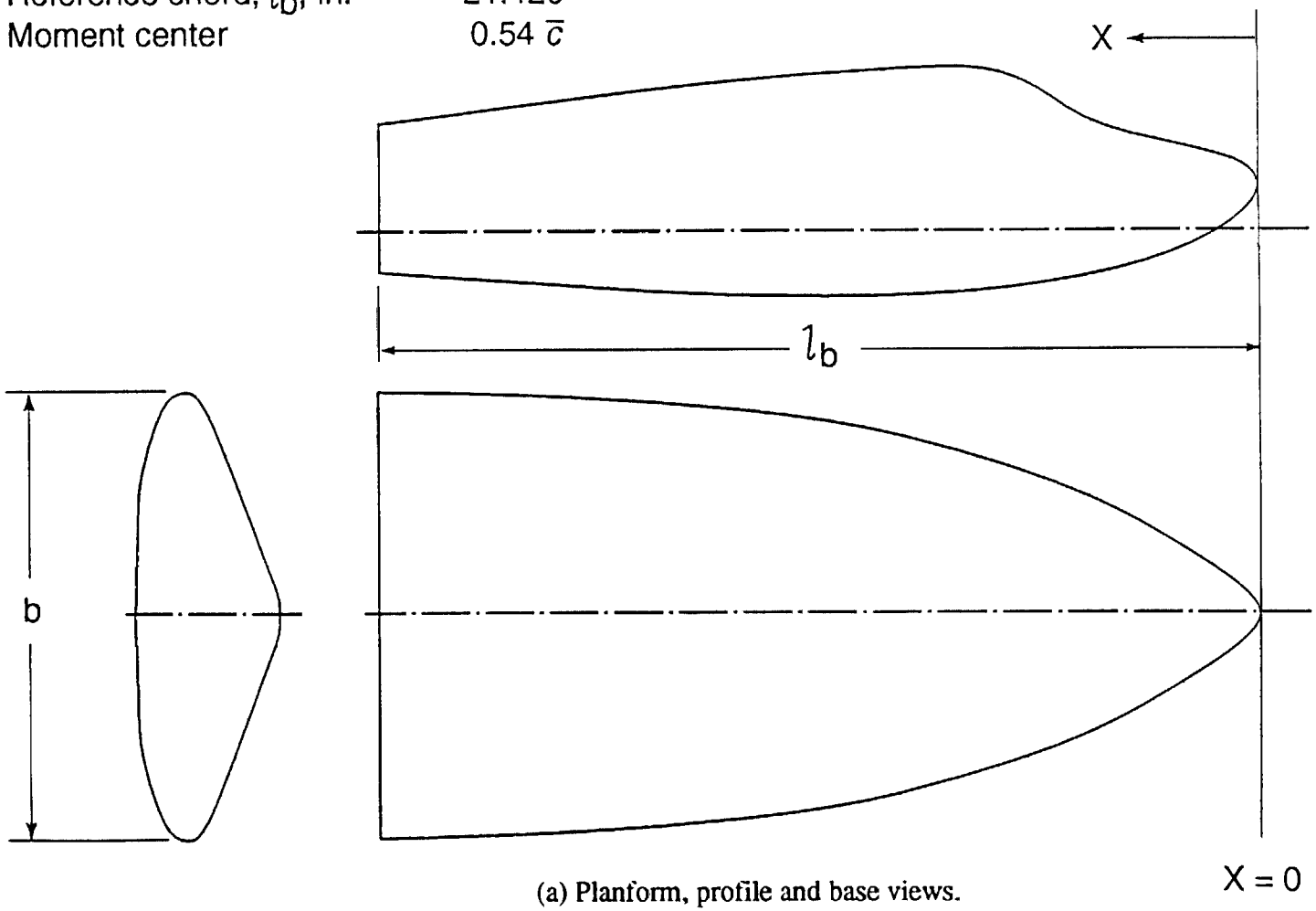

(a) Planform, profile and base views.

Part 3 - HL-20A-3 configuration.

Figure 3 Continued.

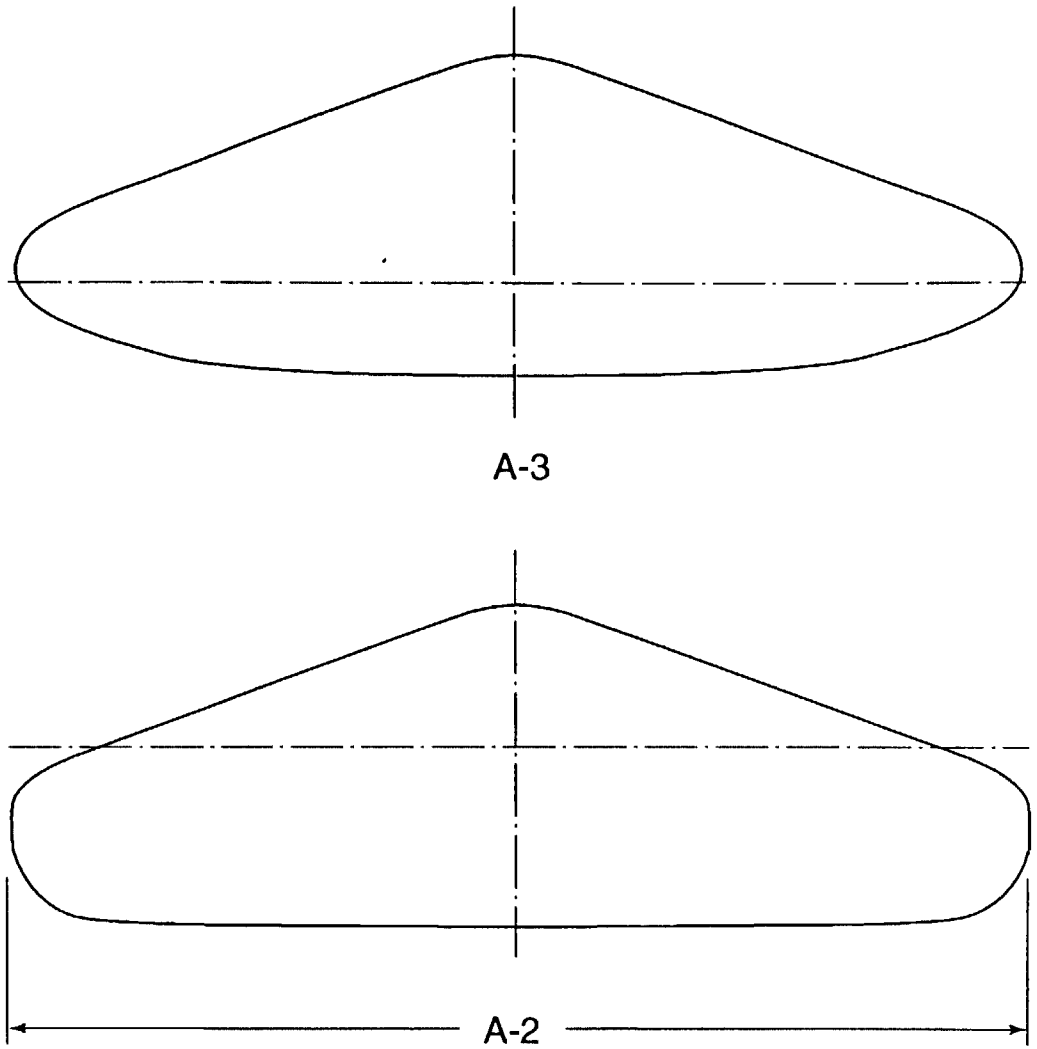

(b) Comparison of A-2 & A-3 base configurations.

Part 3 Continued.

Figure 3 Continued.

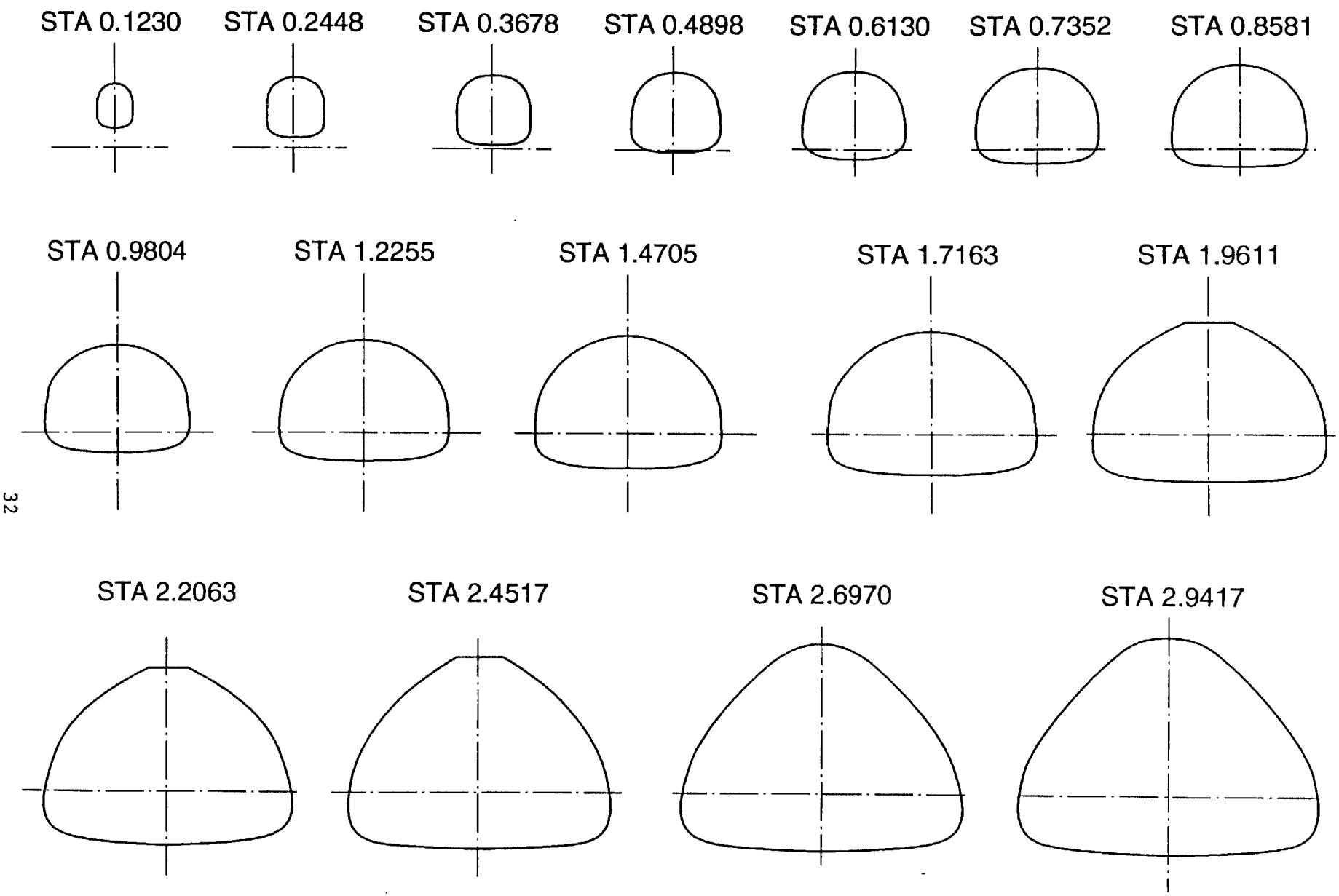

(c) Cross-section based on Xmax = 10.2986 in. (A-3)

Part 3 Continued.

Figure 3 Continued.

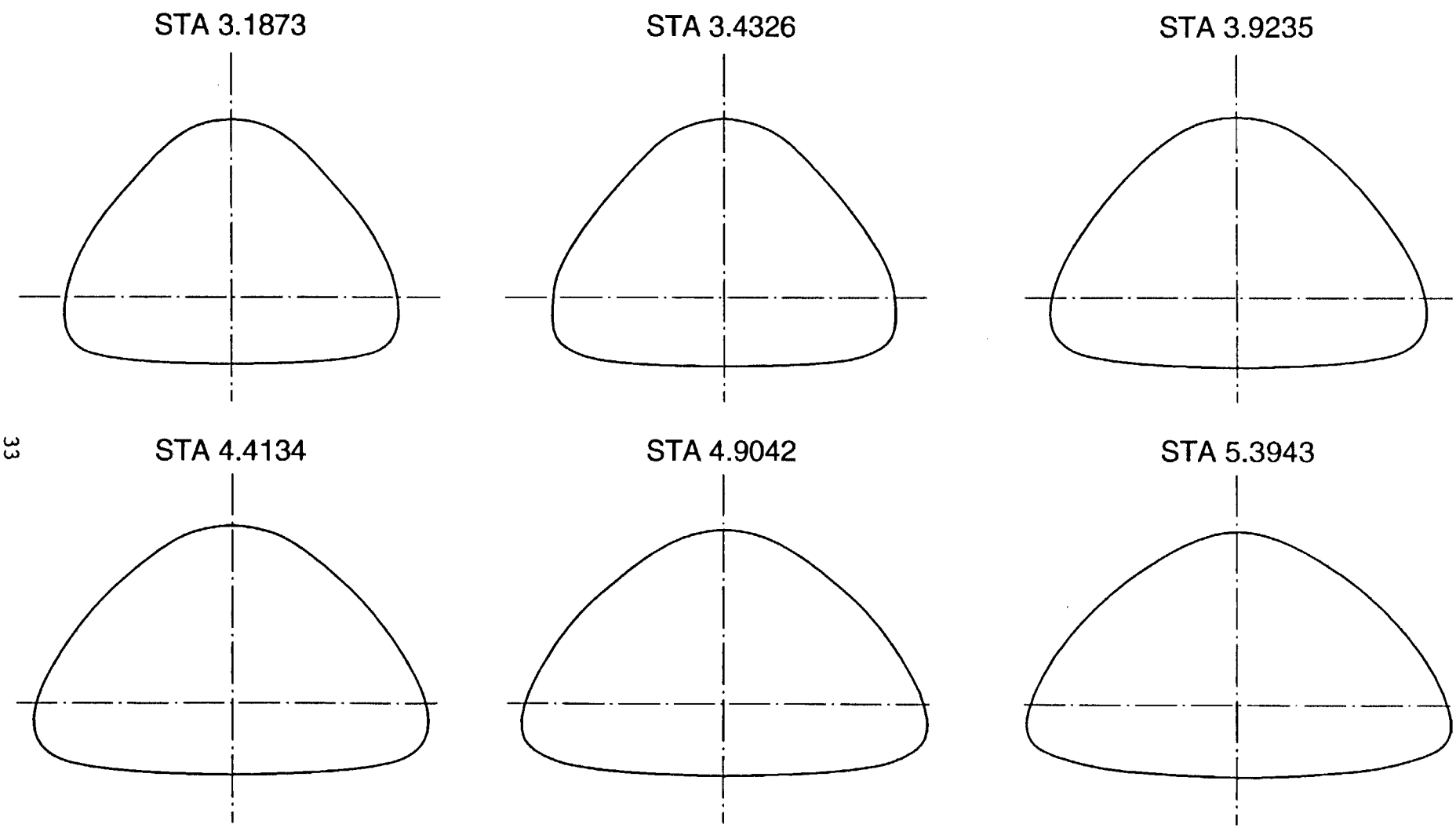

(c) Continued.

Part 3 Continued.

Figure 3 Continued.

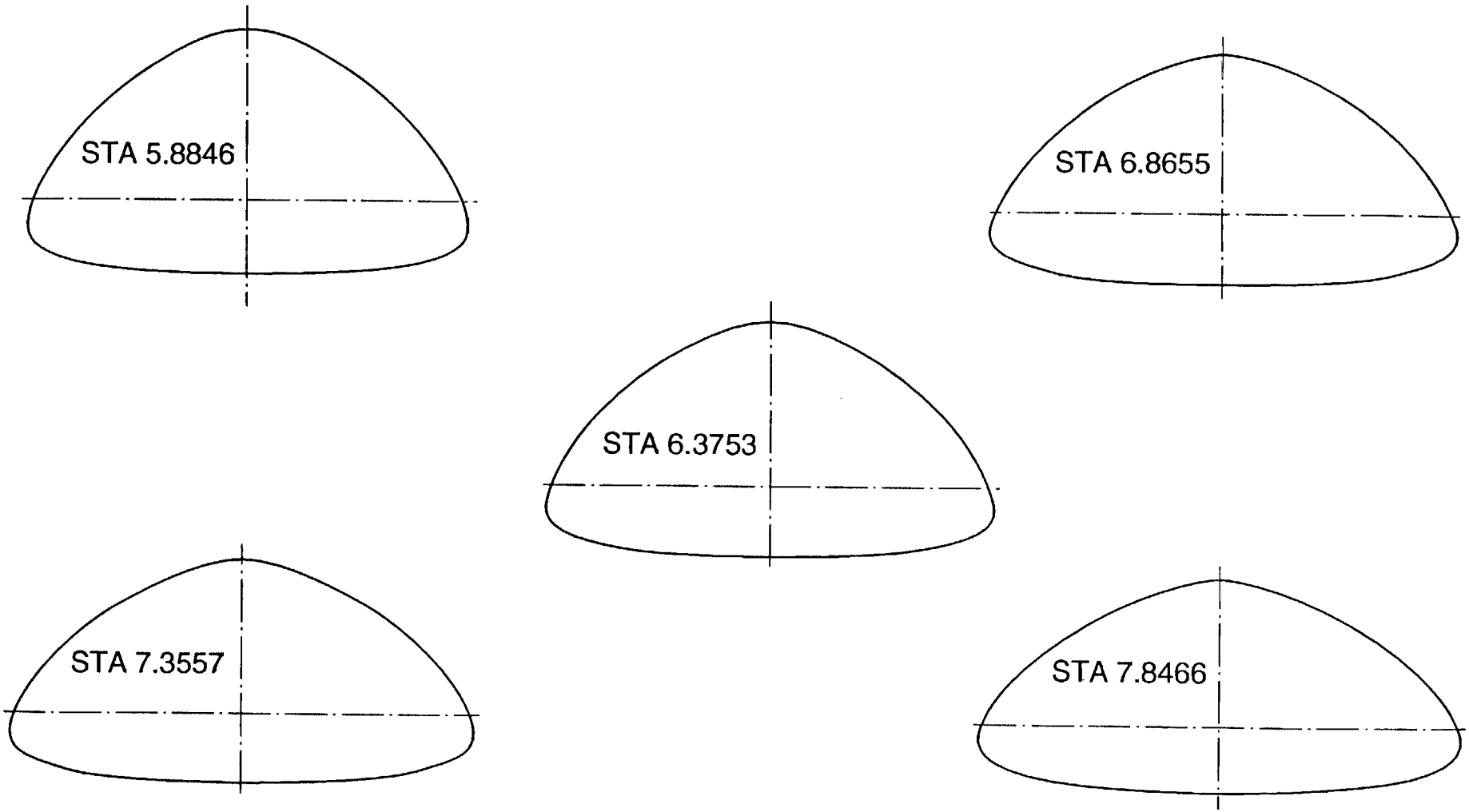

(c) Continued.

Part 3 Continued.

Figure 3 Continued.

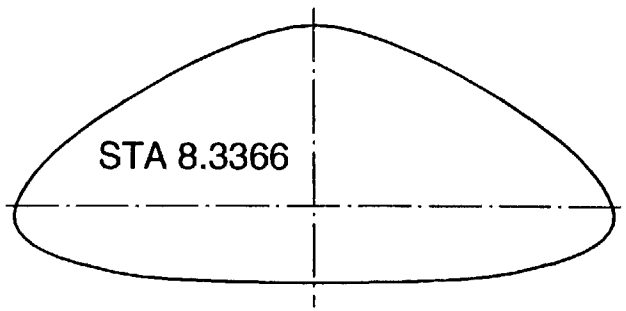

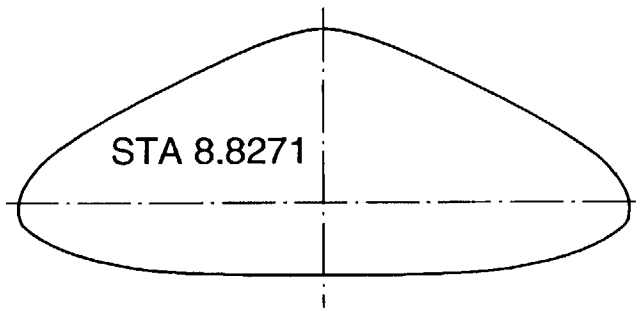

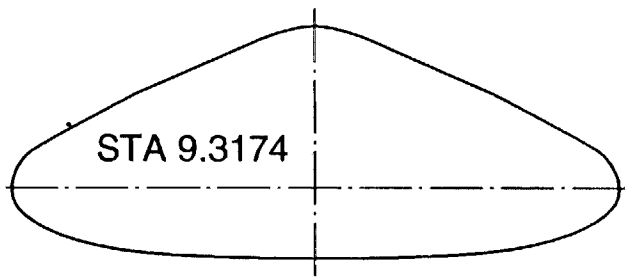

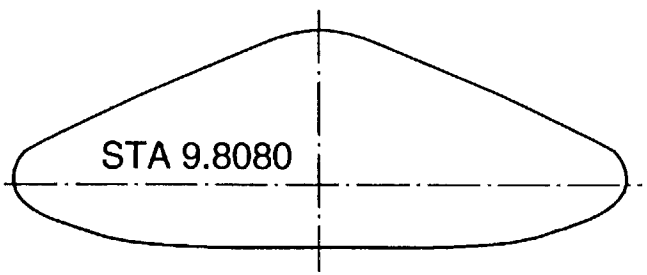

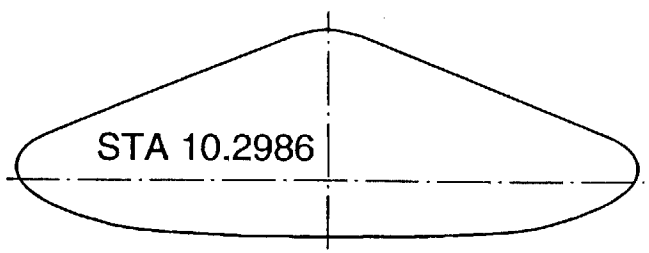

(c) Continued.

Part 3 Continued.

Figure 3 Continued.

HL-20A-4:

Reference area, sq. in.	172.92816
Reference span, b, in.	9.694
Reference chord, l_b, in.	21.527
Moment center	0.54 l_b

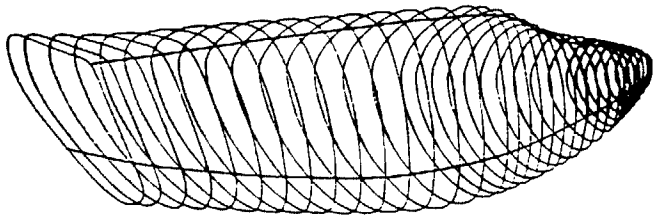

Schematic A-4

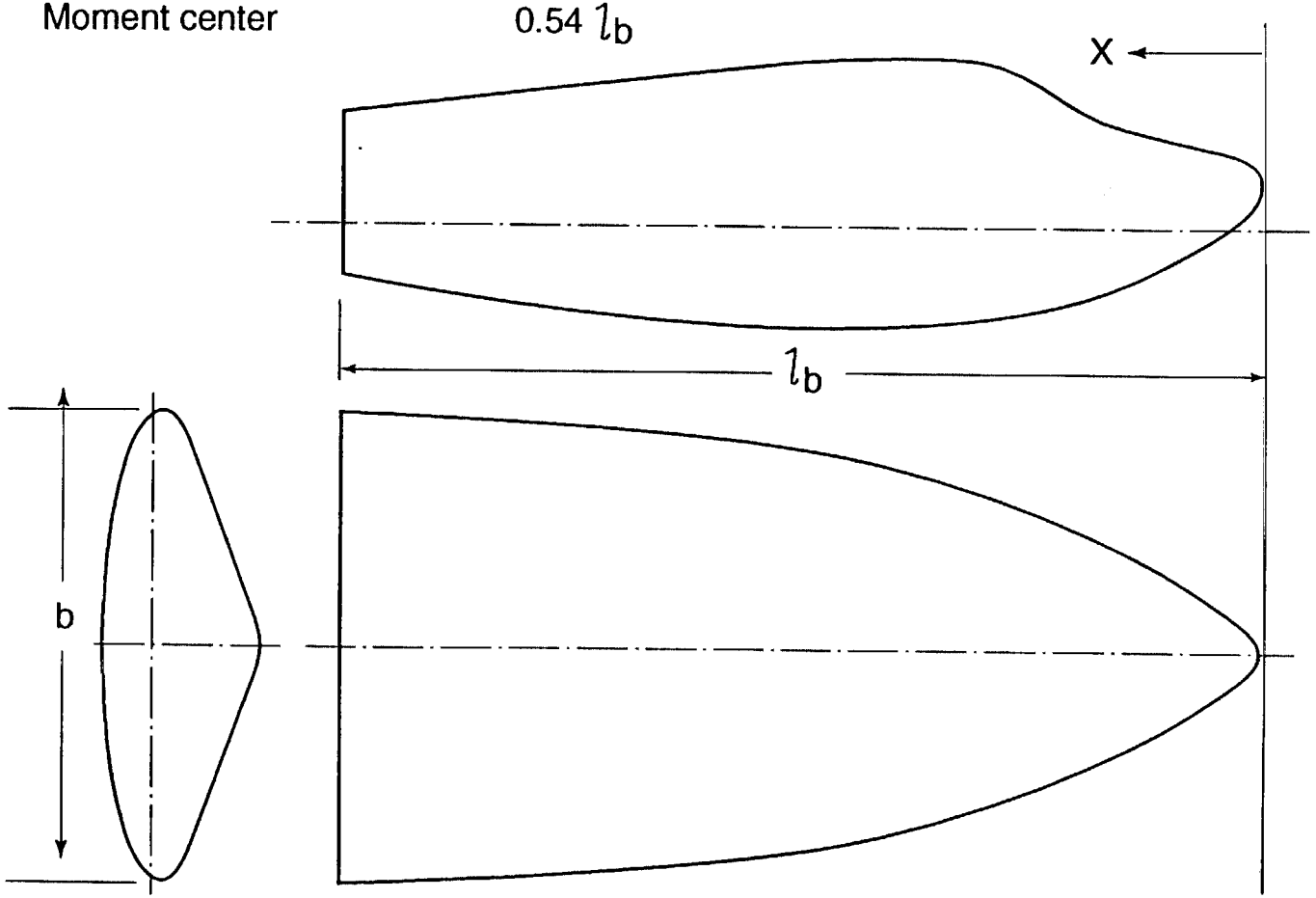

(a) Planform, profile and base views.

Part 4 - HL-20A-4 configuration.

Figure 3 Continued.

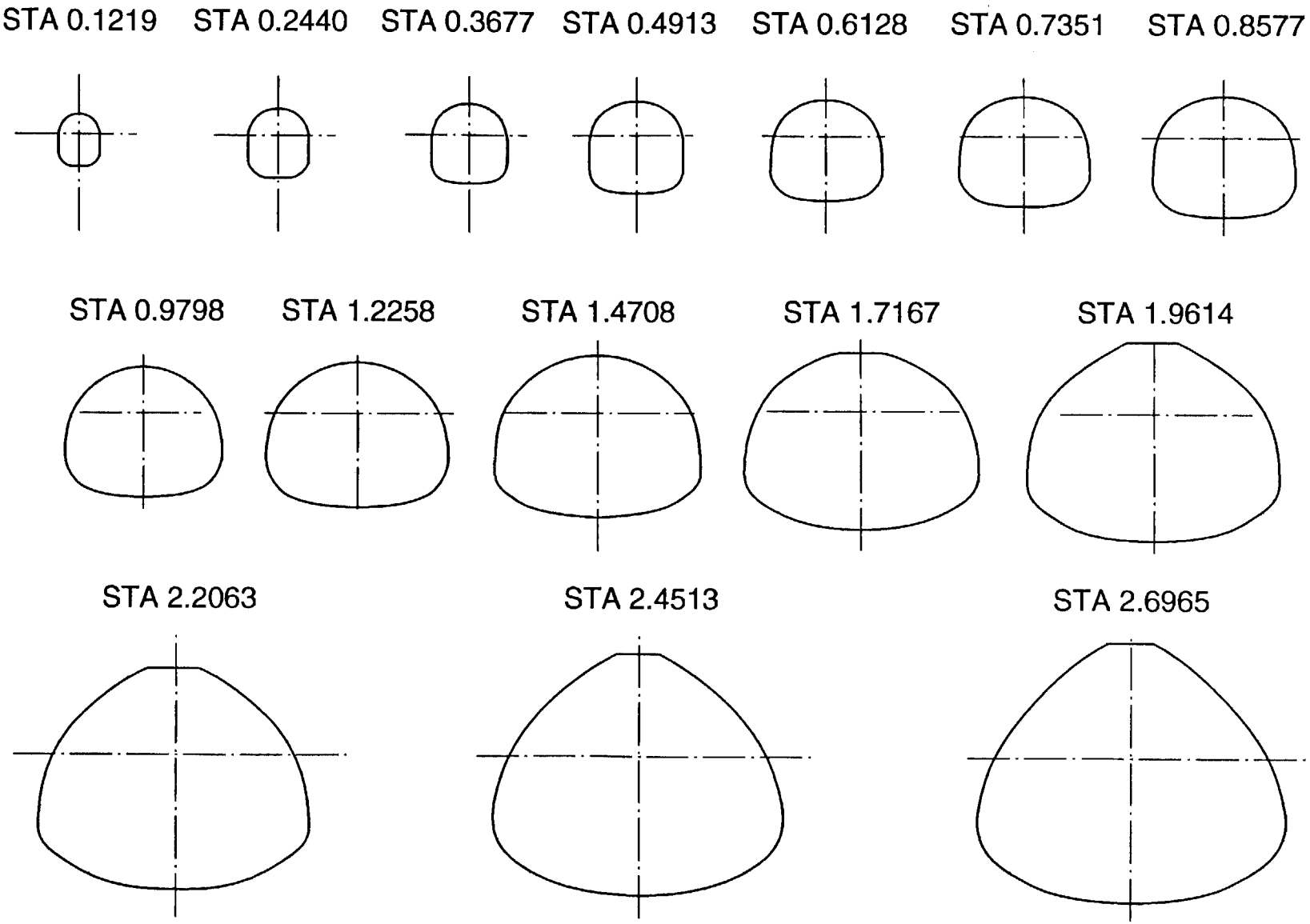

(b) Body cross-section based on X = 10.2973 in.

Part 4 - Continued.

Figure 3 Continued.

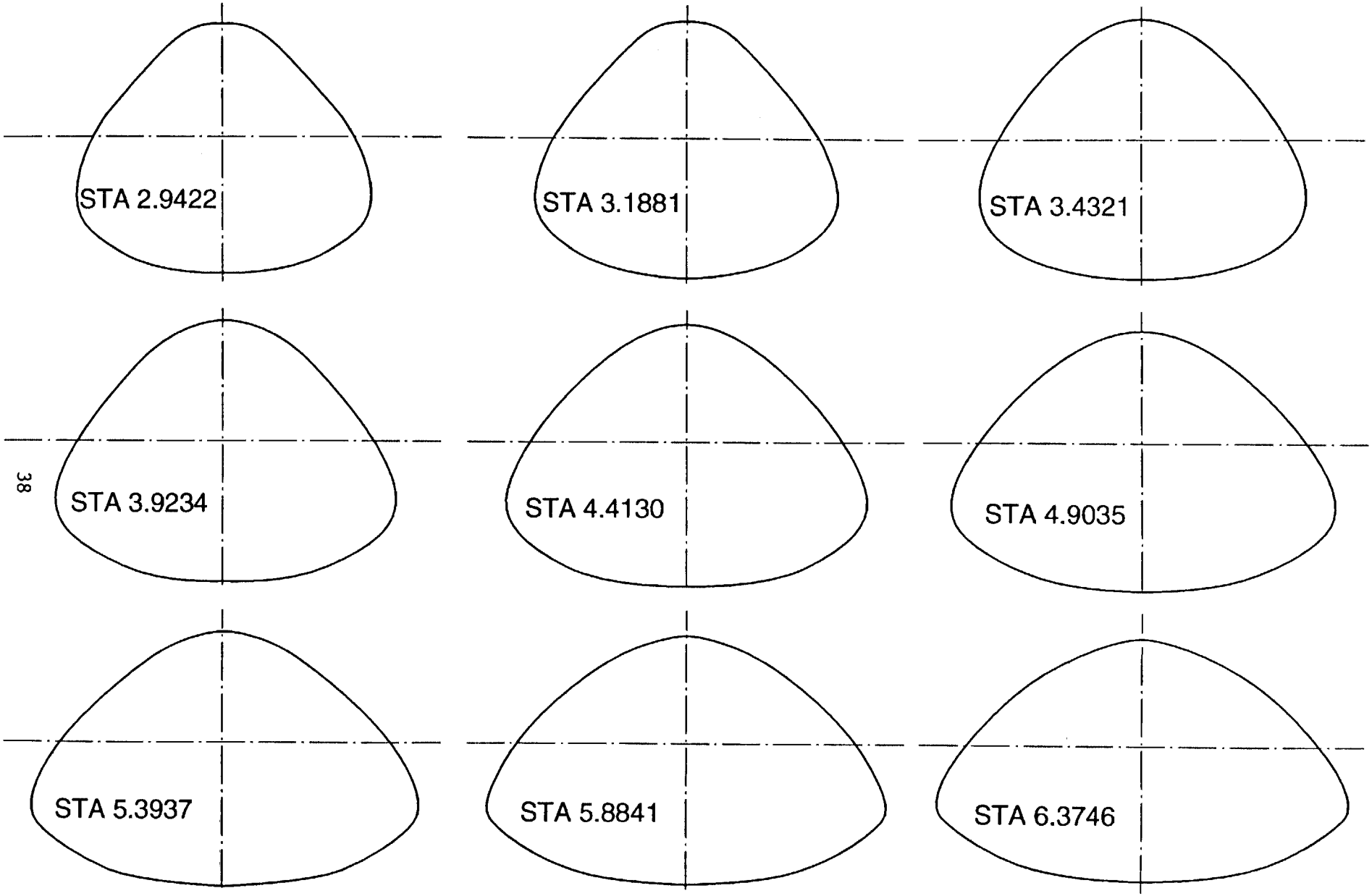

(b) Continued.

Part 4 - Continued.

Figure 3 Continued.

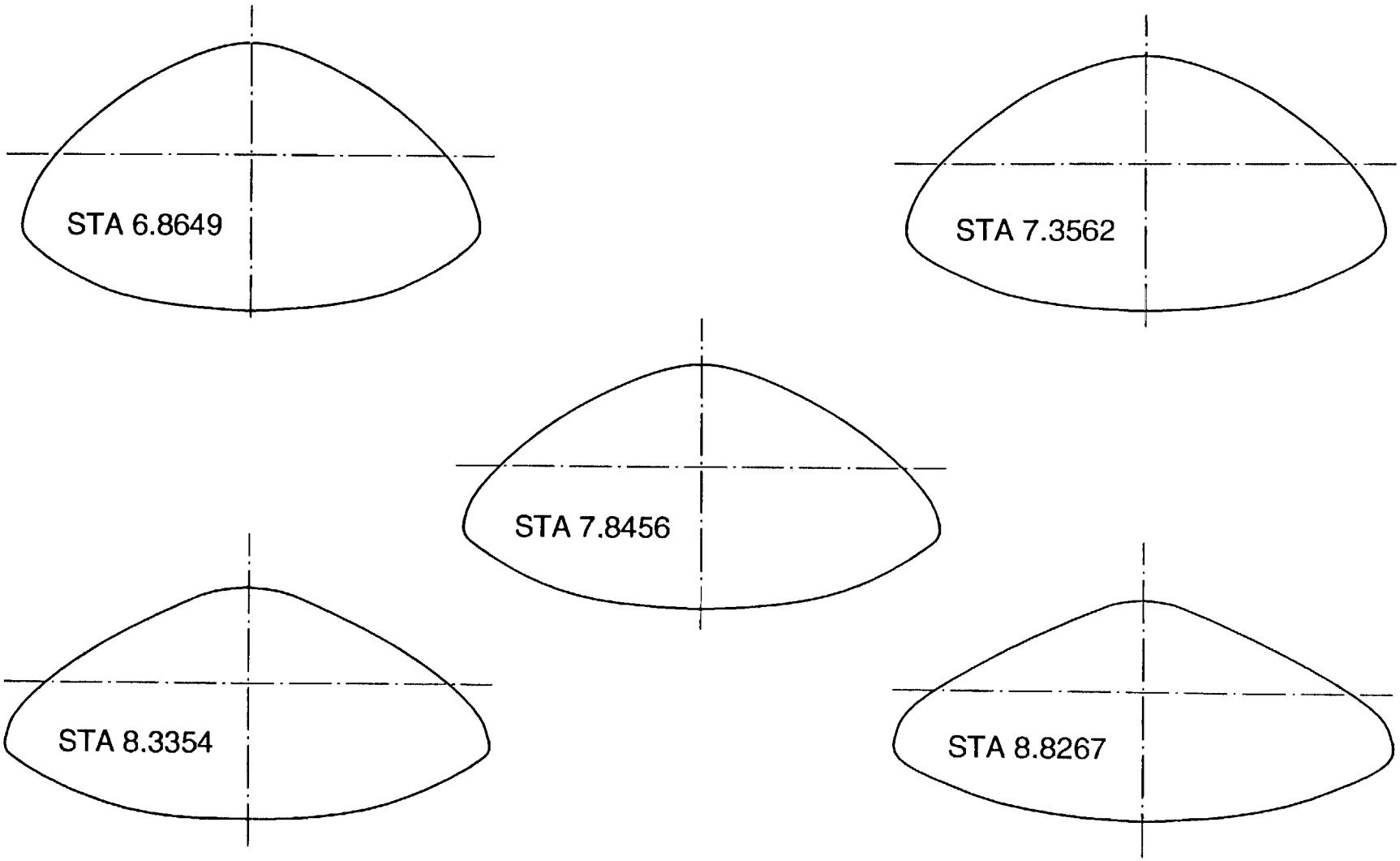

(b) Continued.

Part 4 - Continued.

Figure 3 Continued.

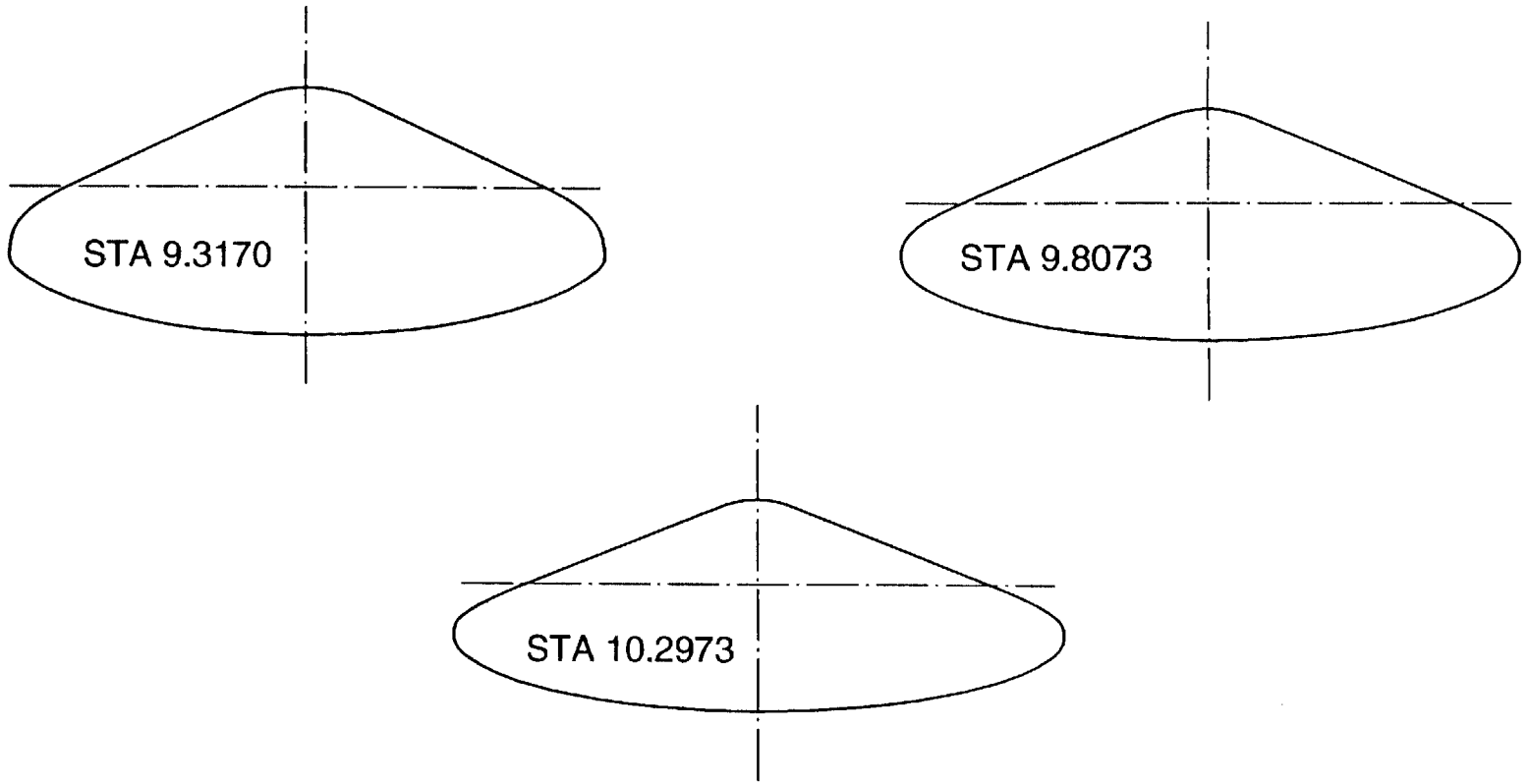

(b) Concluded.

Part 4 - Concluded.

Figure 3 Continued.

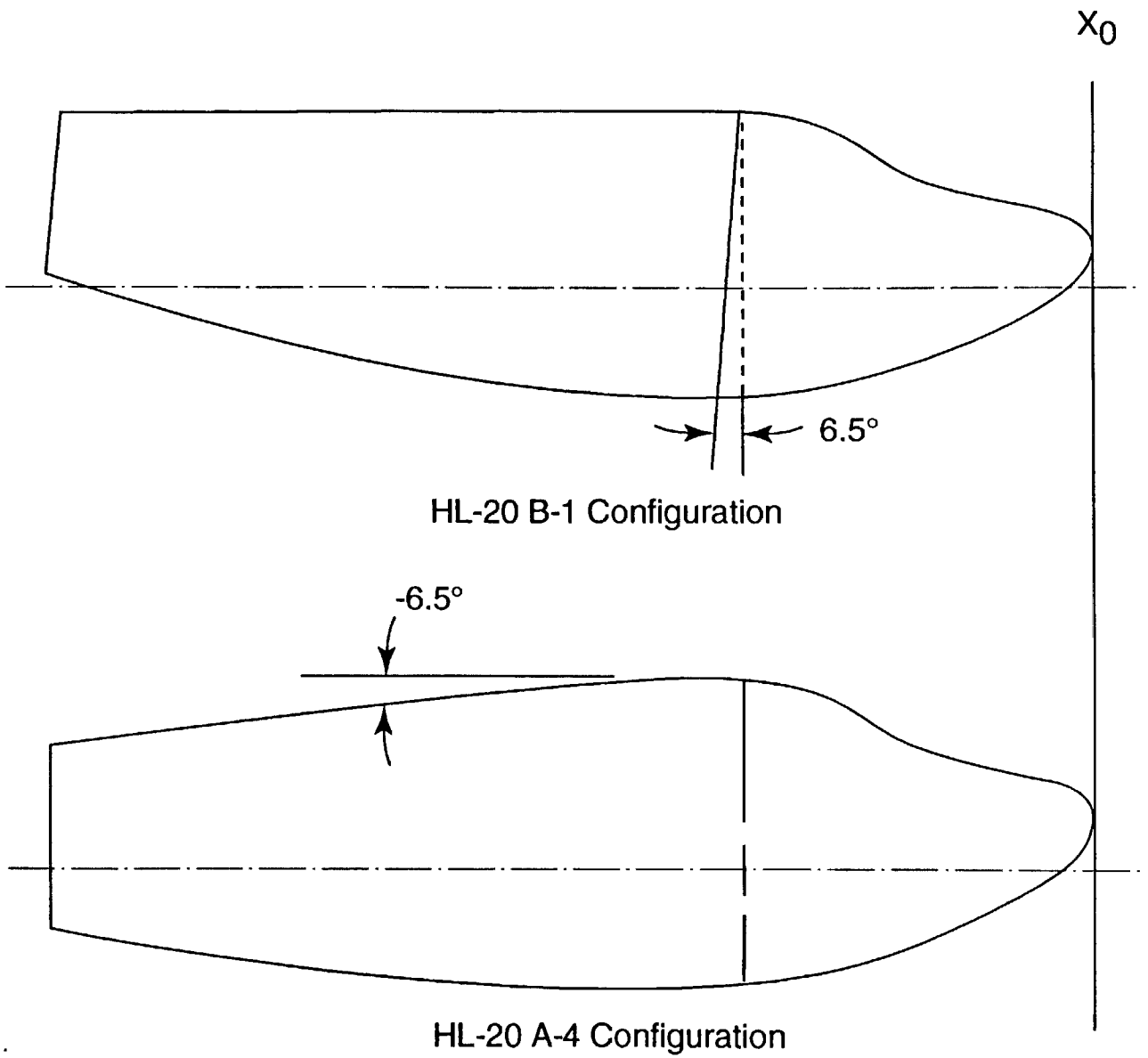

Part 5 - Formation of "B" series from A configurations. Addition of 6.5° wedge aft of canopy.

Fig 3 Continued.

HL-20B-1:

Reference area, sq. in.	172.92816
Reference span, b, in.	9.694
Reference chord, l_b, in.	21.754
Moment center	0.54 l_b

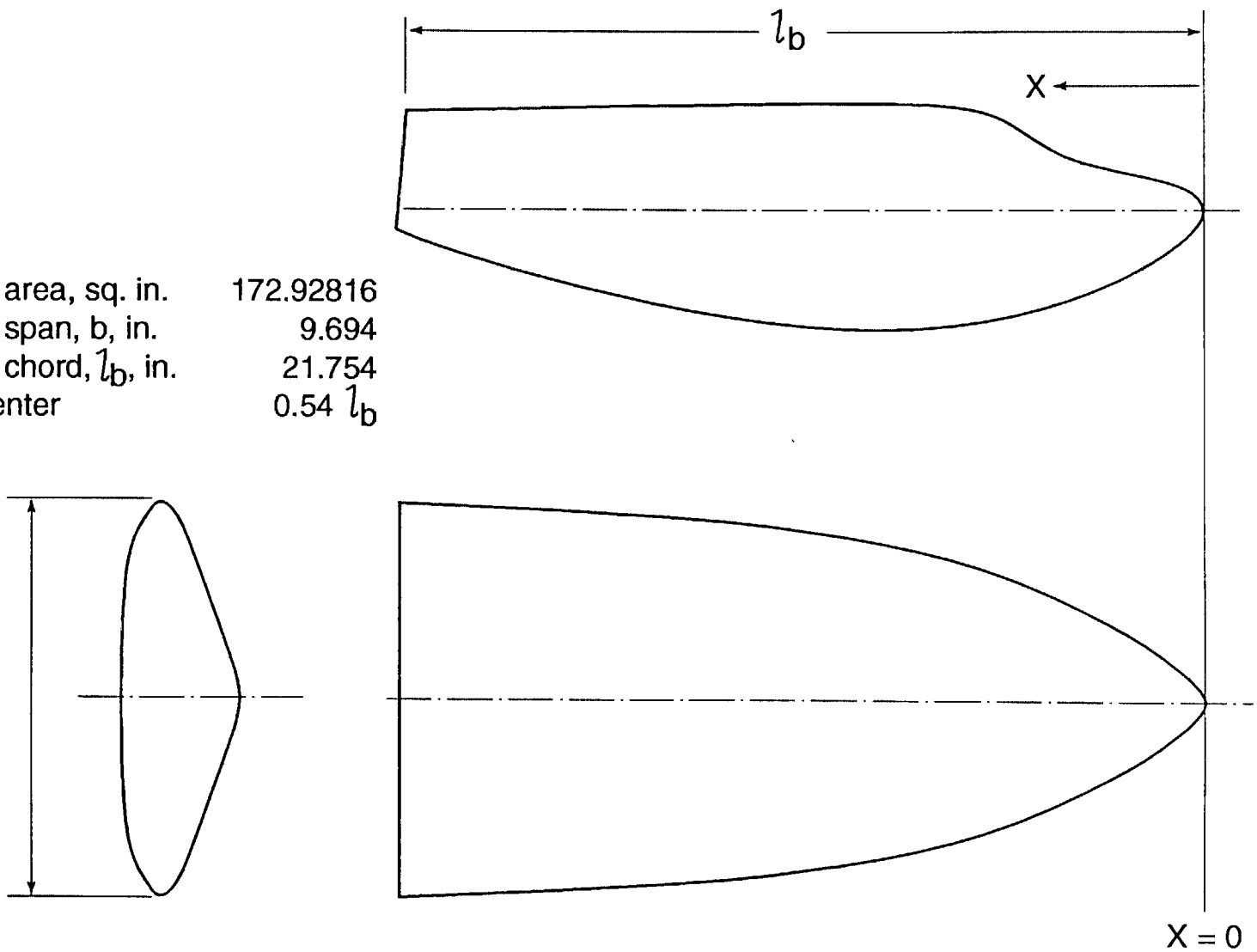

(a) Planform, profile and base views.

Part 6 - HL-20B-1

Figure 3 Continued.

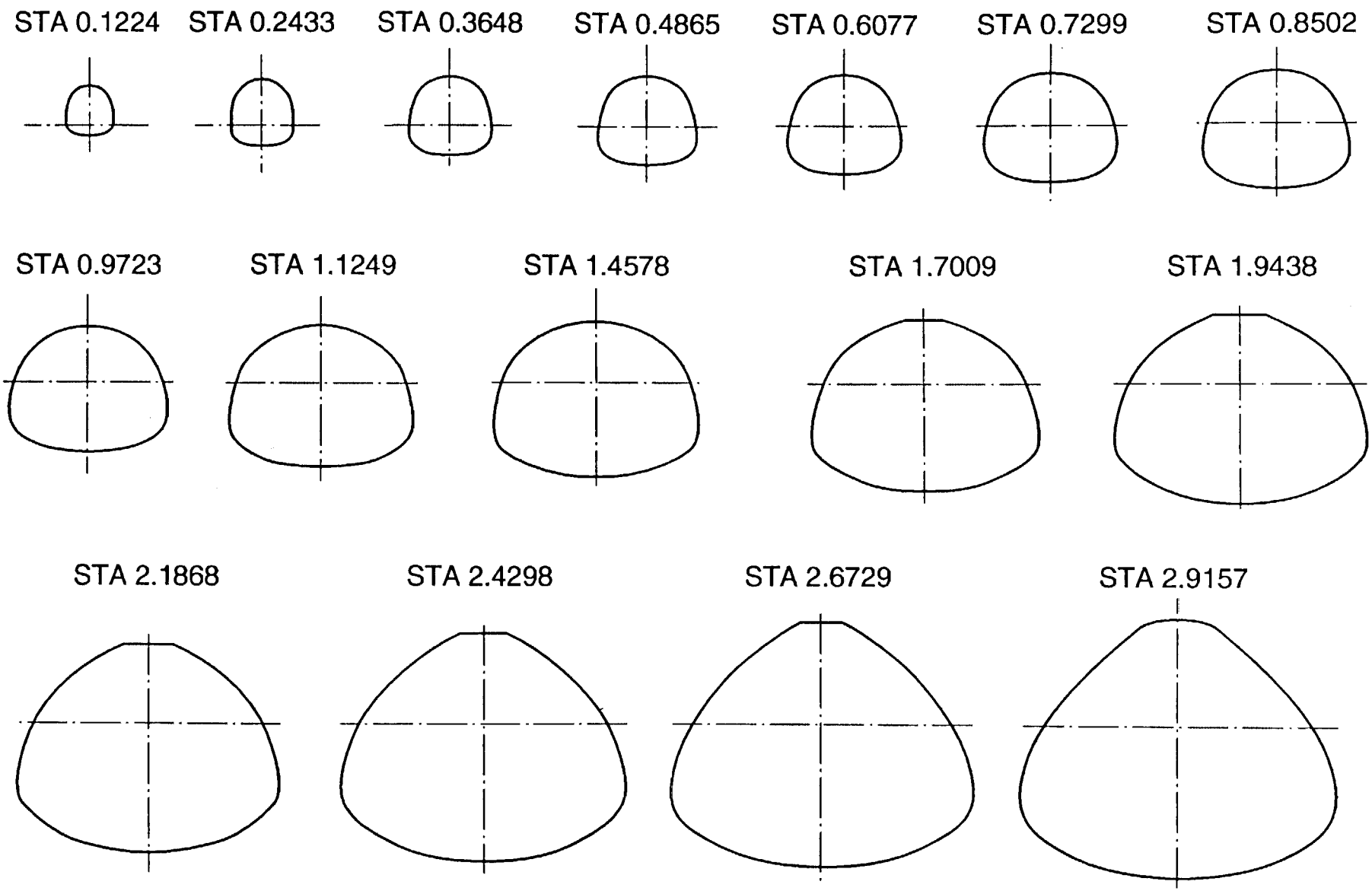

(b) Body cross-section based on X = 10.5253 in.

Part 6 - Continued.

Figure 3 Continued.

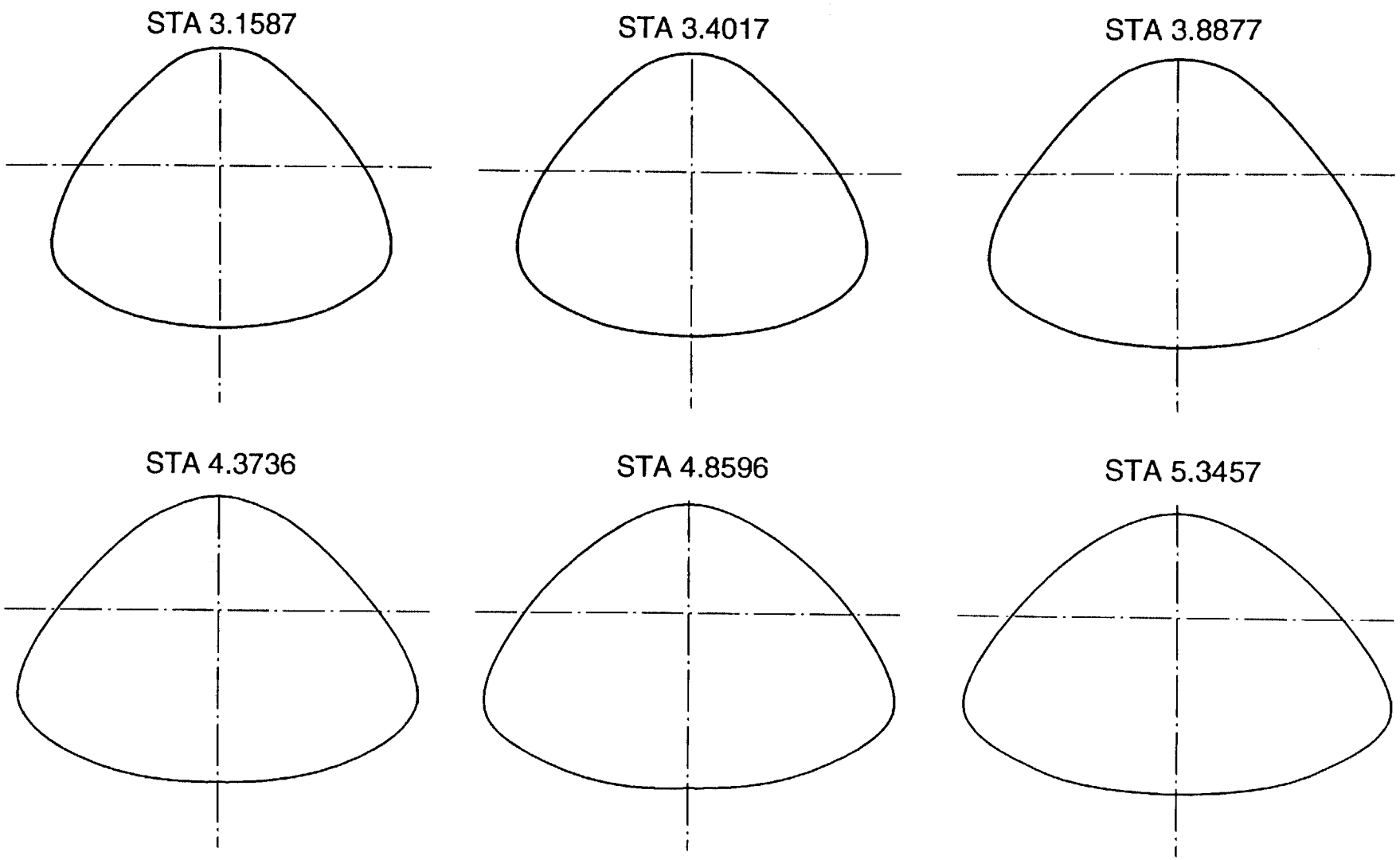

(b) Continued.

Part 6 - Continued.

Figure 3 Continued.

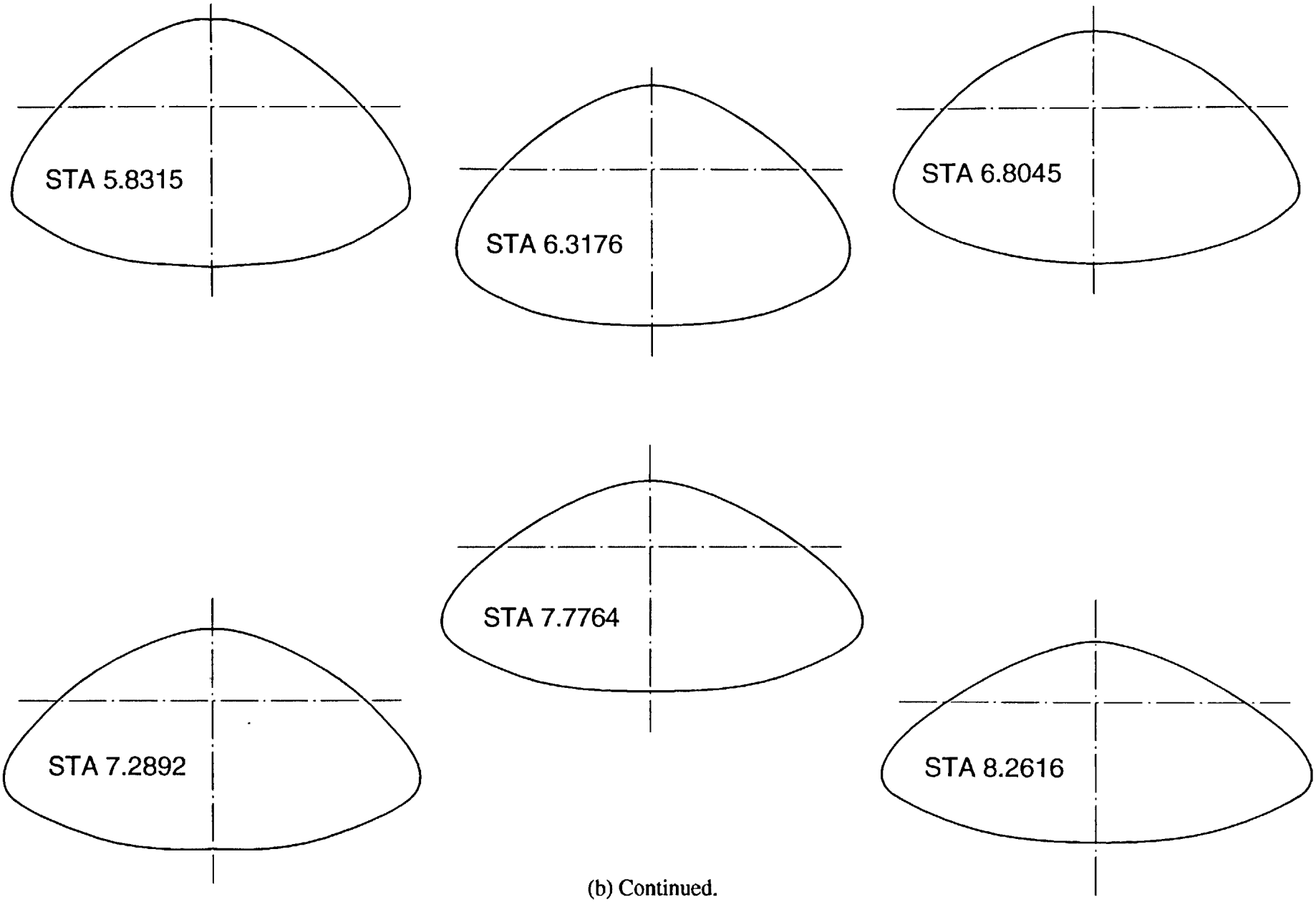

(b) Continued.

Part 6 - Continued.

Figure 3 Continued.

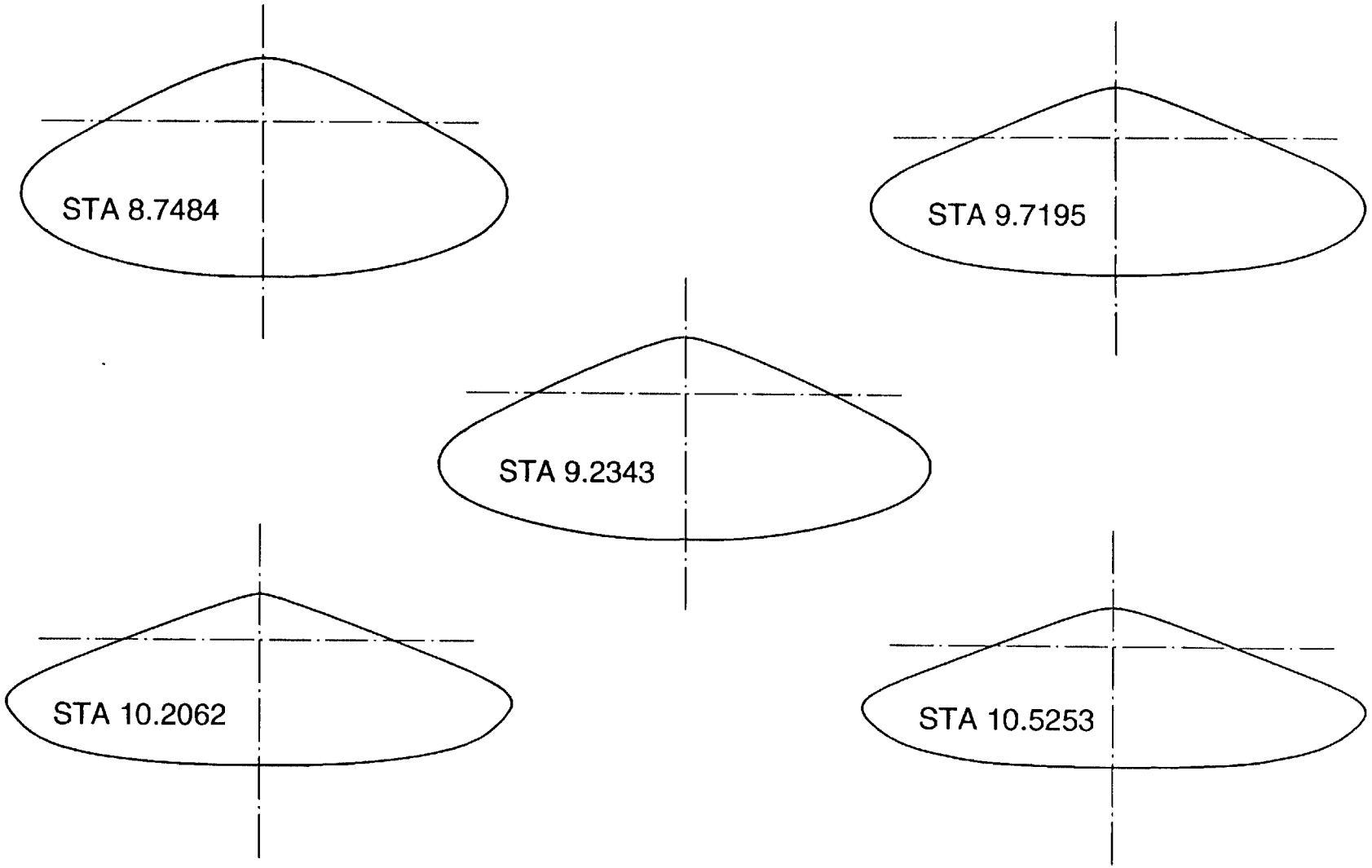

(b) Concluded.

Part 6 - Concluded.

Figure 3 Concluded.

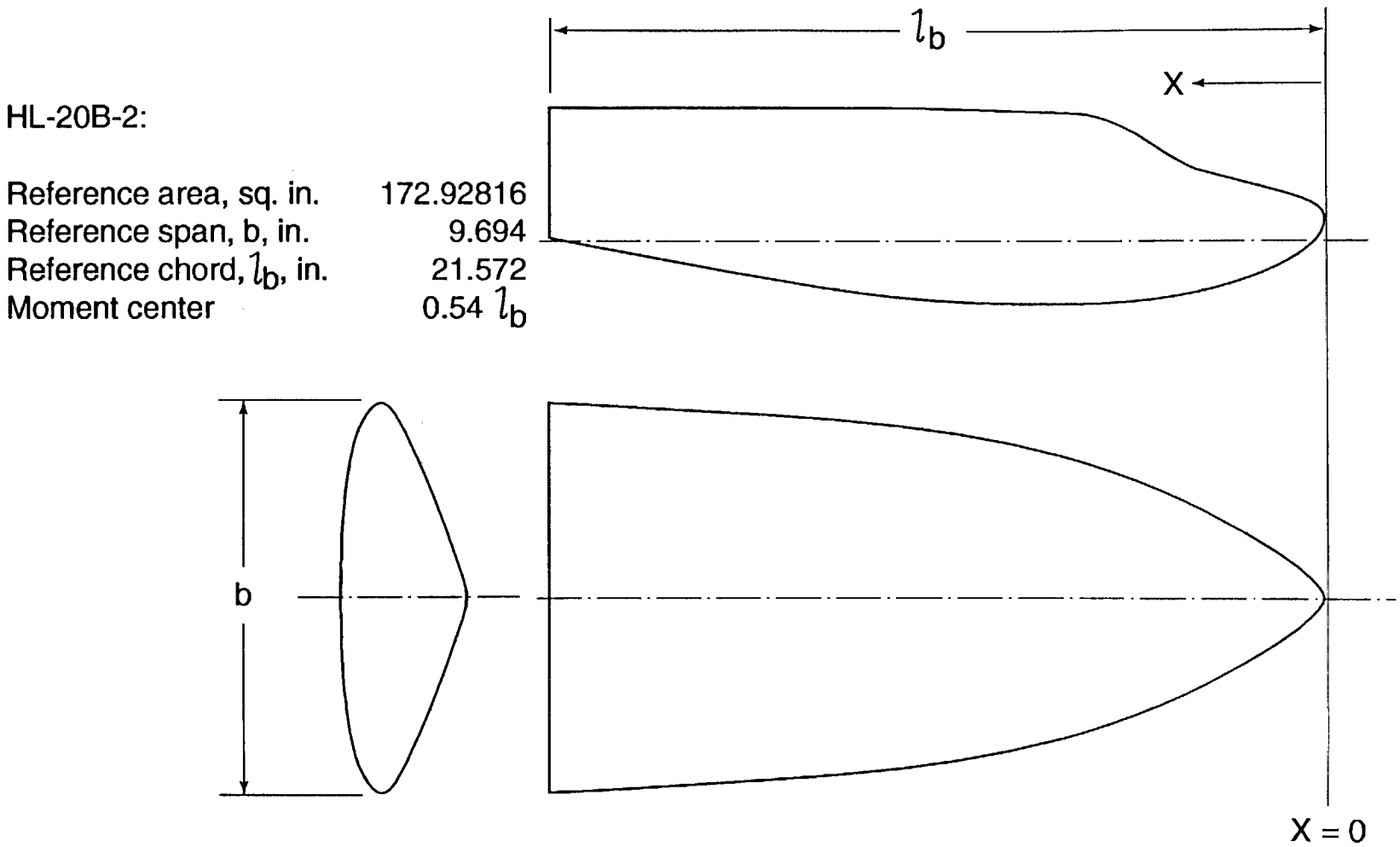

(a) Planform, profile and base views.

Part 7 - HL-20B-2

Figure 3 Continued.

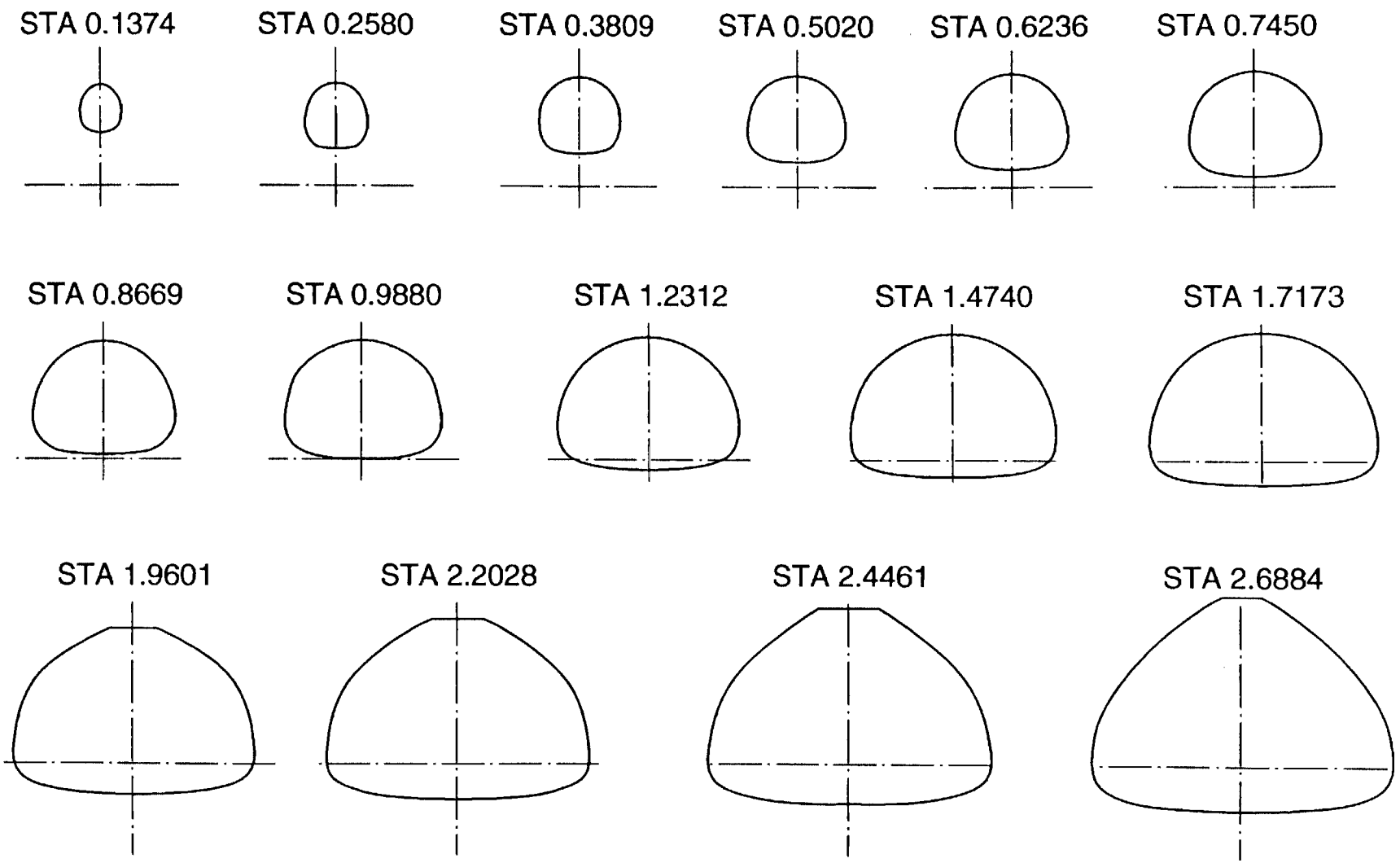

(b) Body cross-section based on X = 10.2212 in.

Part 7 - Continued.

Figure 3 Continued.

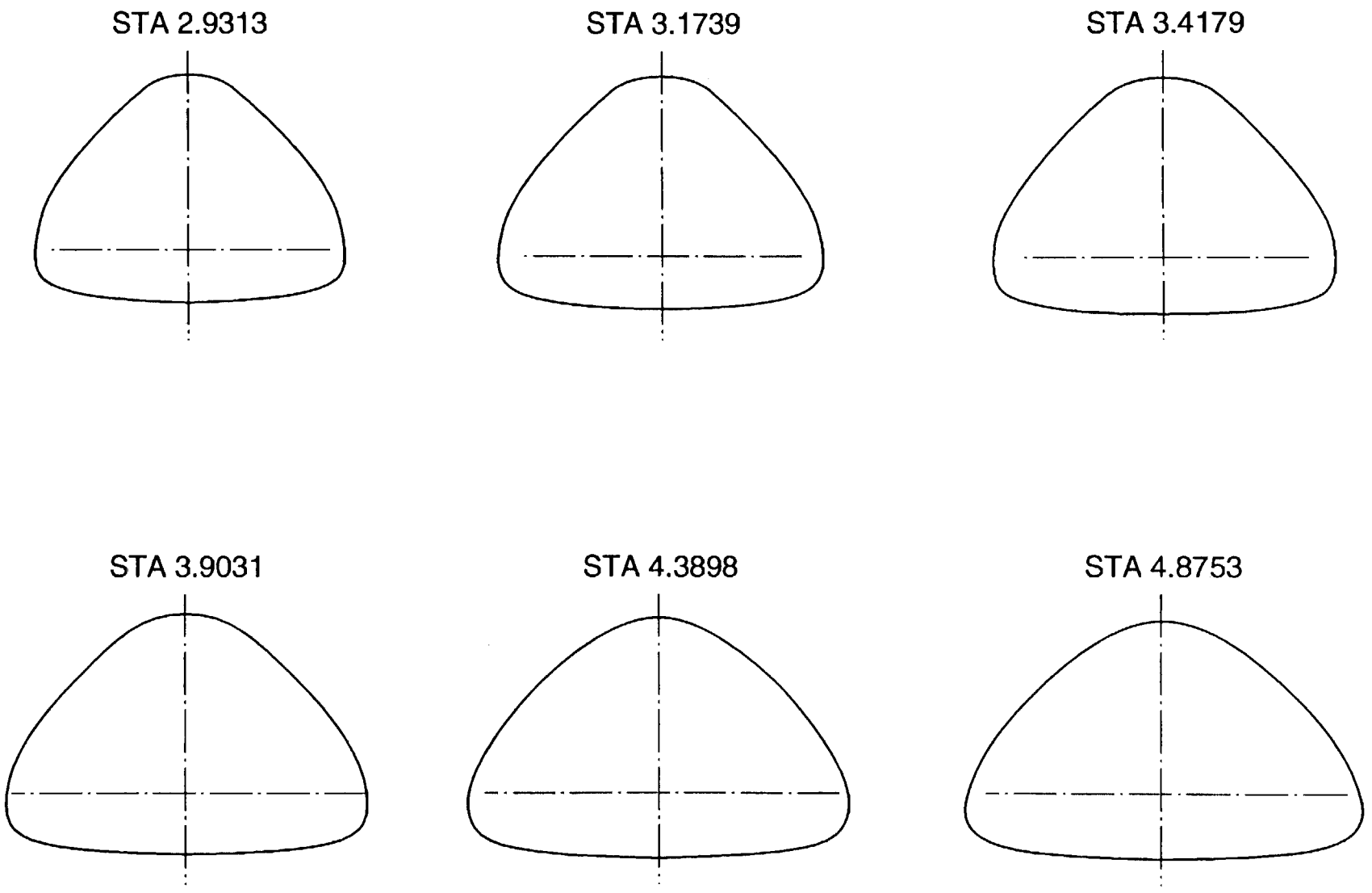

(b) Continued.

Part 7 - Continued.

Figure 3 Continued.

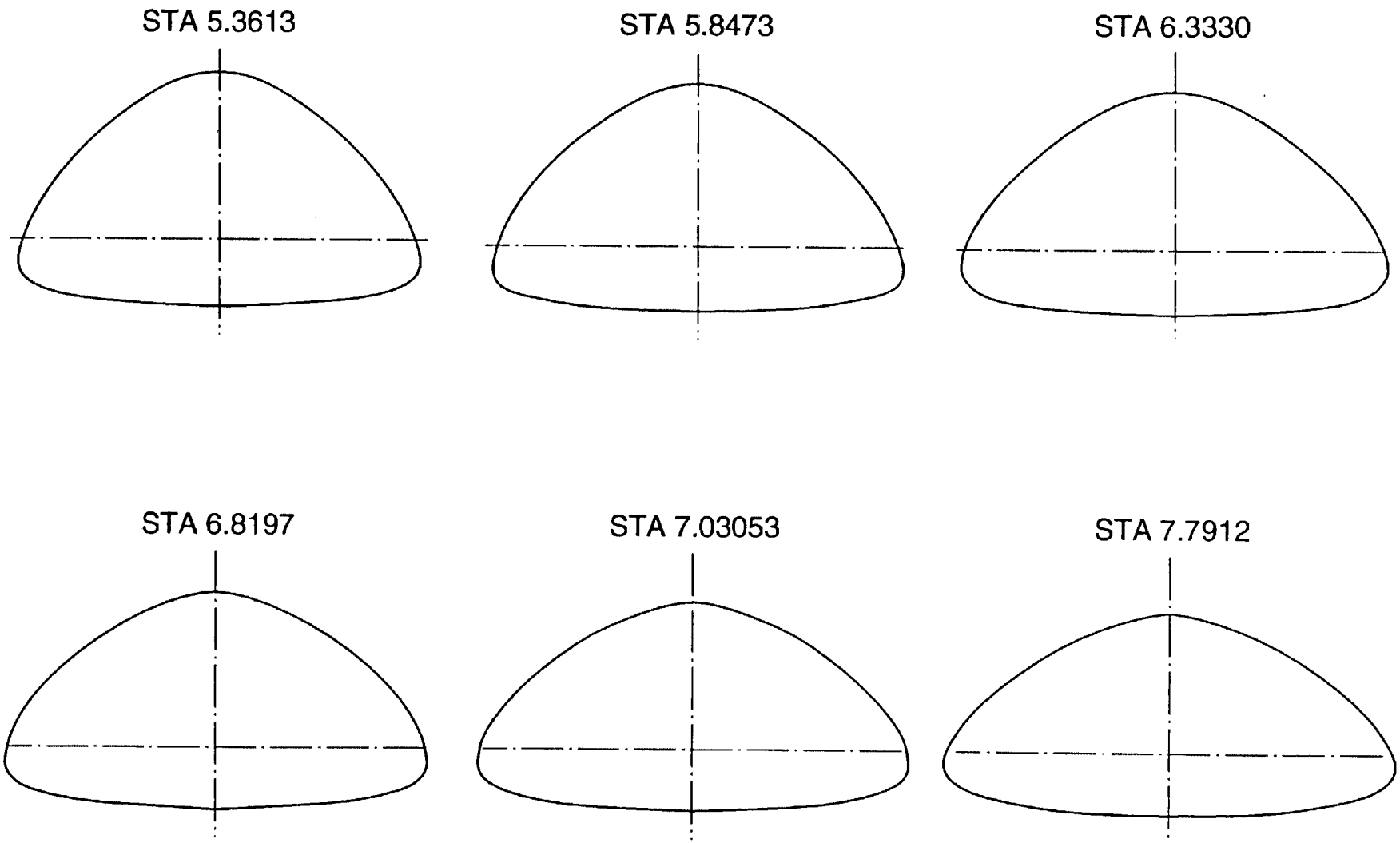

(b) Continued.

Part 7 - Continued.

Figure 3 Continued.

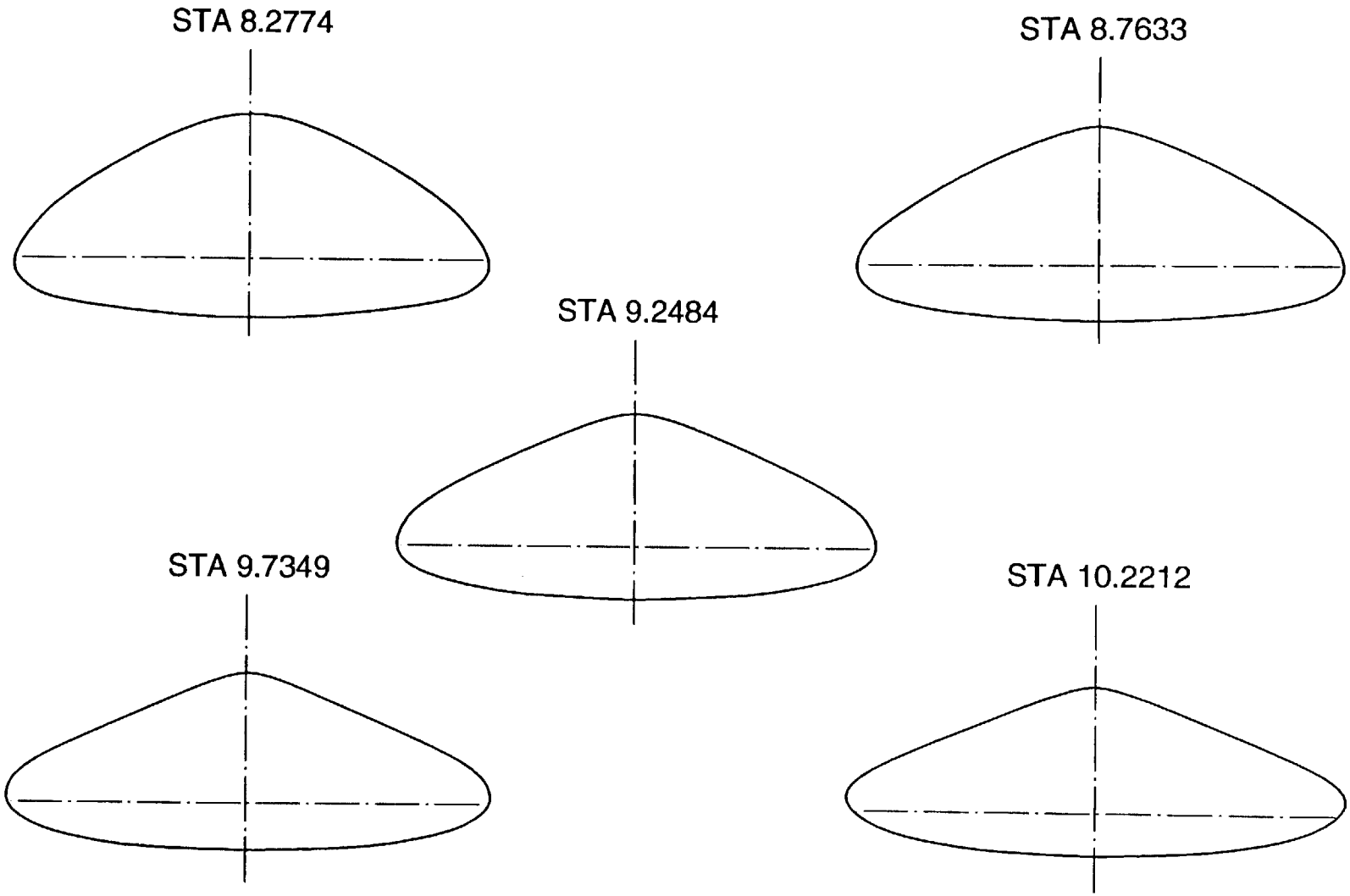

(b) Concluded.

Part 7 - Concluded.

Figure 3 Continued.

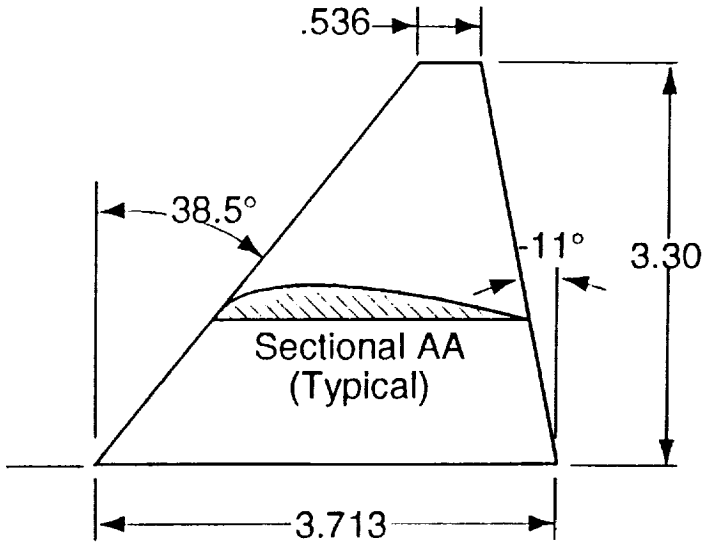

Canard Planform

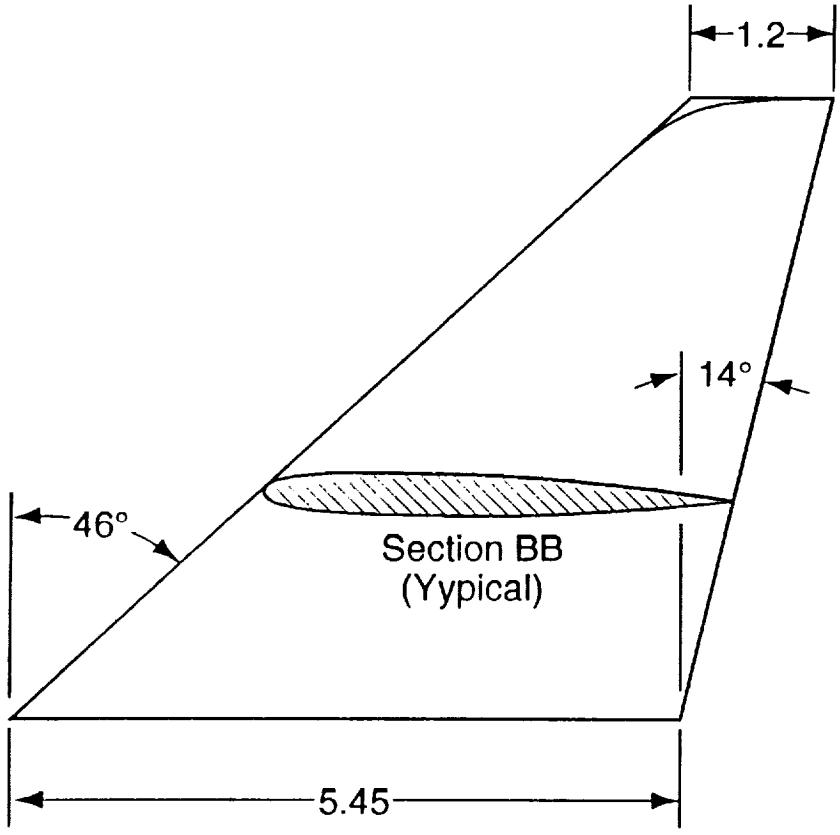

Vertical Tail
Planform

(a) Canard and vertical tail

Part 8 - Canard and stabilizer details.

Figure 3 Continued.

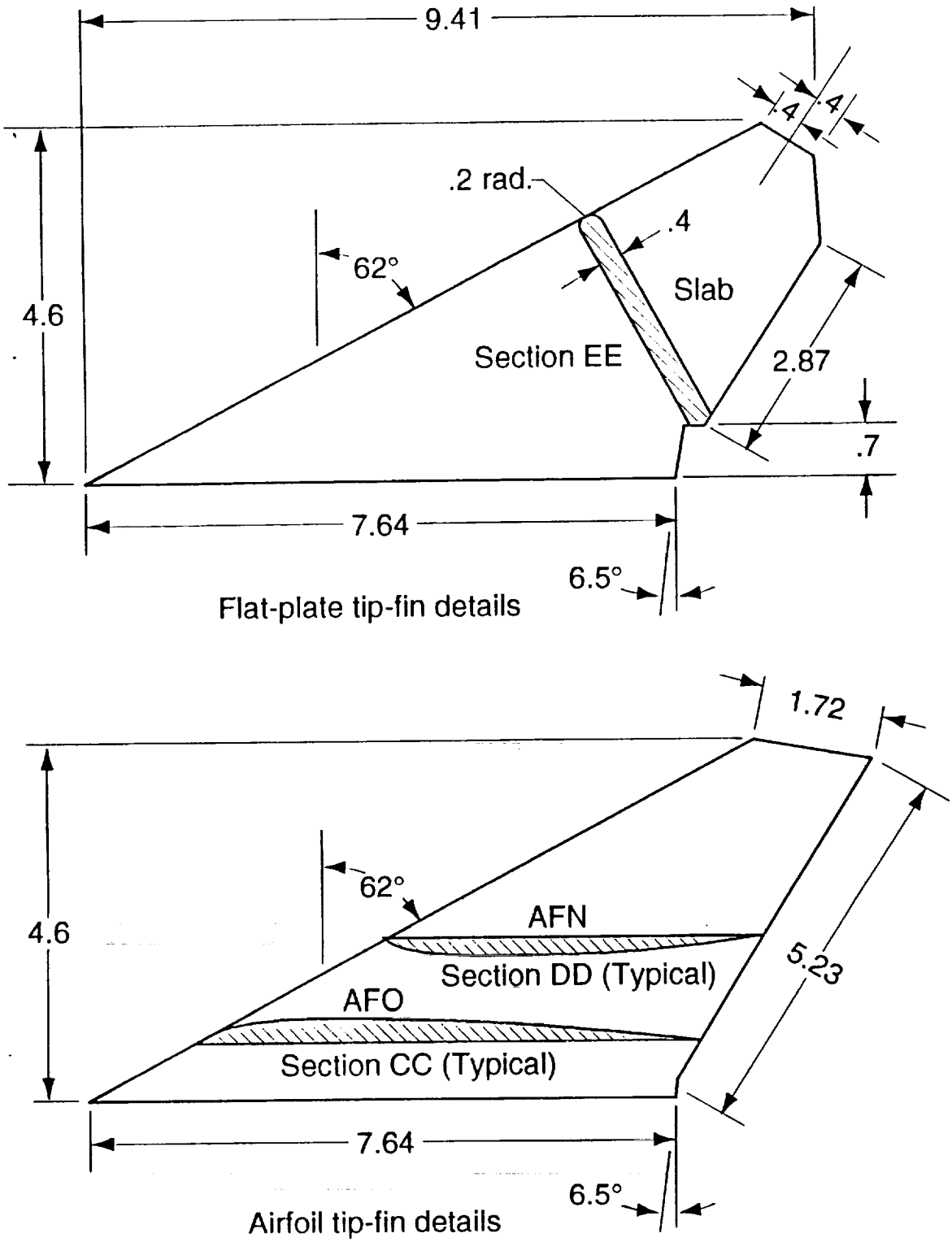

(b) AFO, AFN and Slab-fins

Part 8 - Concluded.

Figure 3 Concluded.

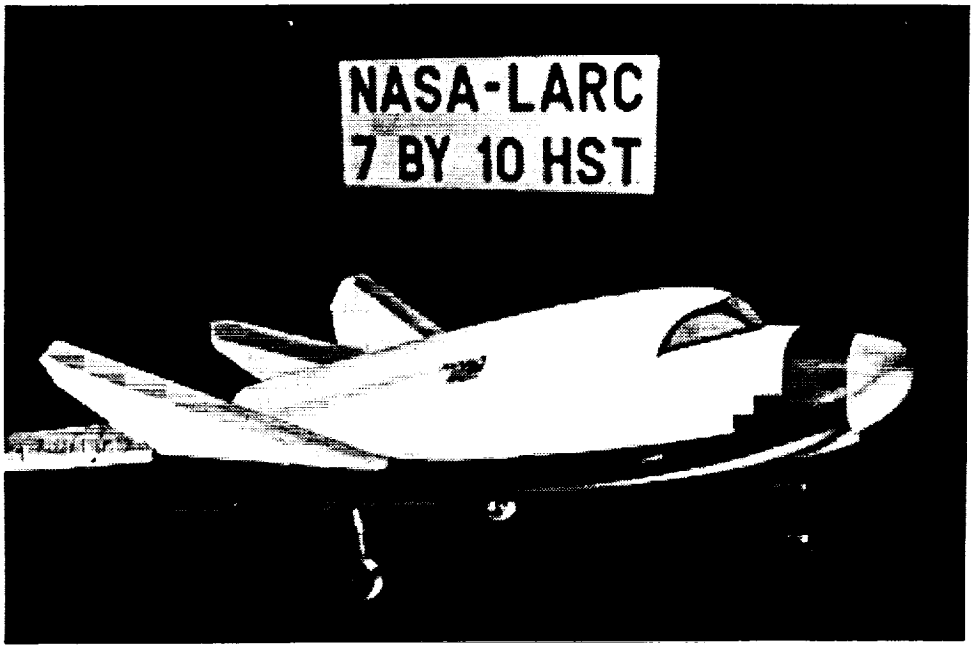

(a) HL-20 with landing gear, in the 7x10 foot wind tunnel.

Figure 4 - Photographs of the HL-20 Model and HL-20A/B series of models depicting the various modifications made during the investigation.

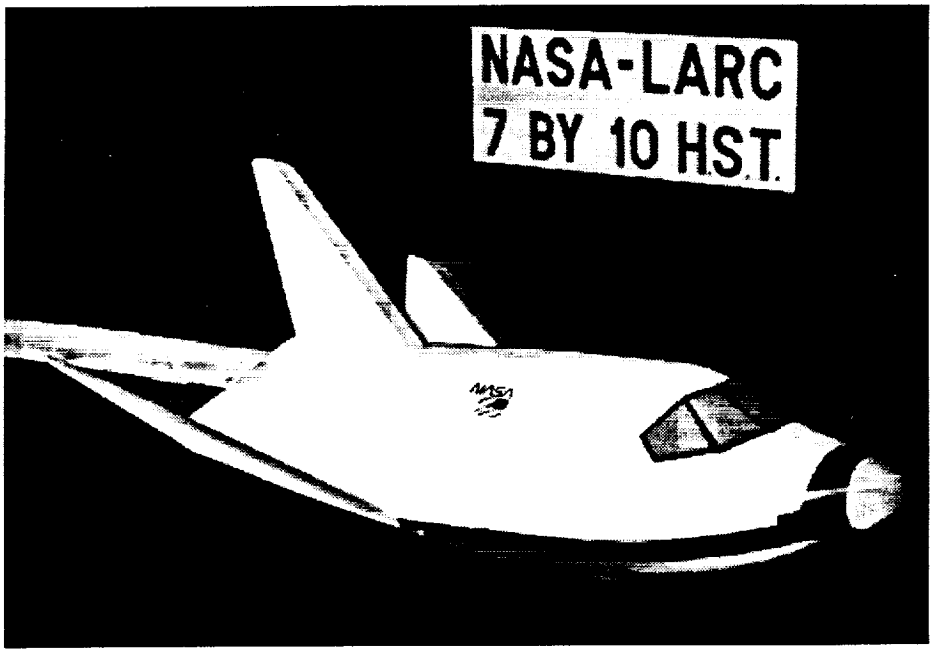

(b) HL-20B-1 with 50° AFN-faired, in the 7x10 foot wind tunnel.

Figure 4 - Continued.

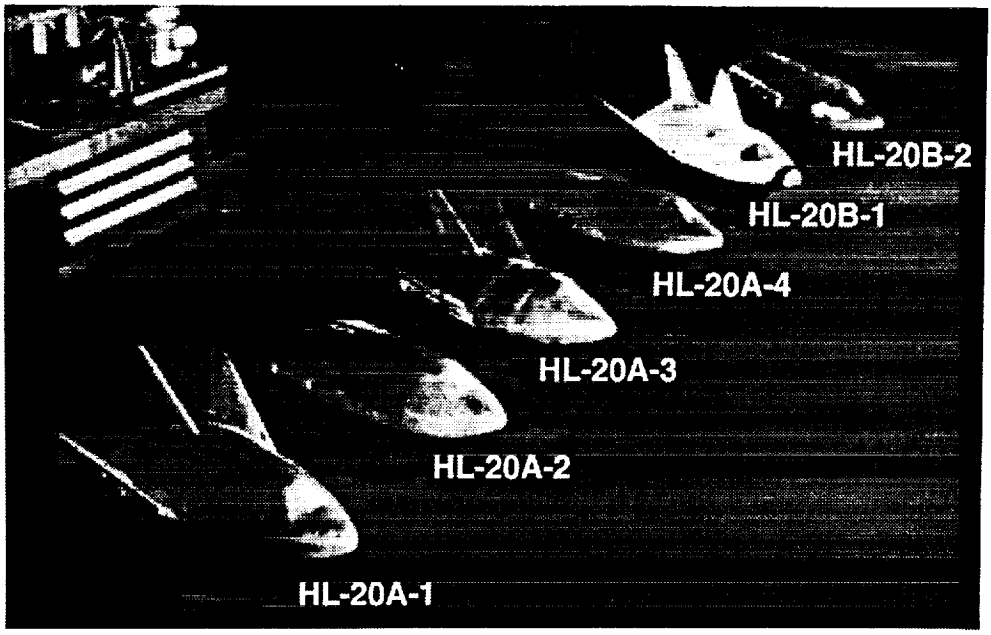

(c) Composite of the HL-20A/B series of bodies tested.

Figure 4 - Continued.

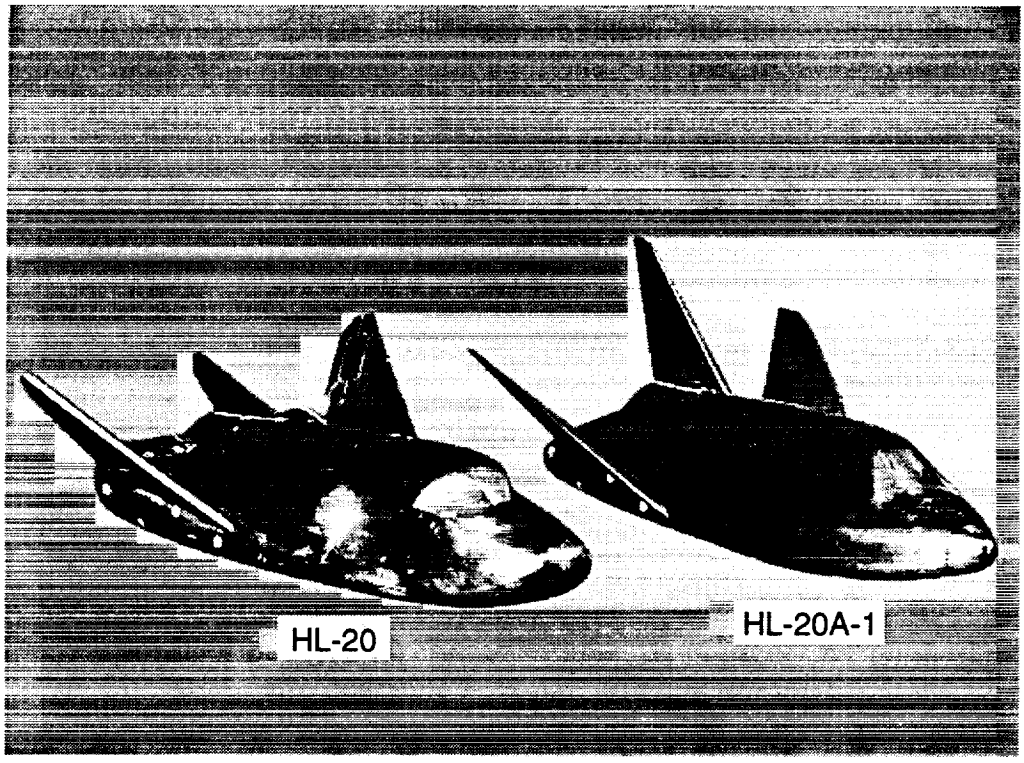

(d) HL-20 and HL-20A-1: Comparison showing forebody, planform, upper surface base, tip fin and center vertical tail modifications.

Figure 4 - Continued.

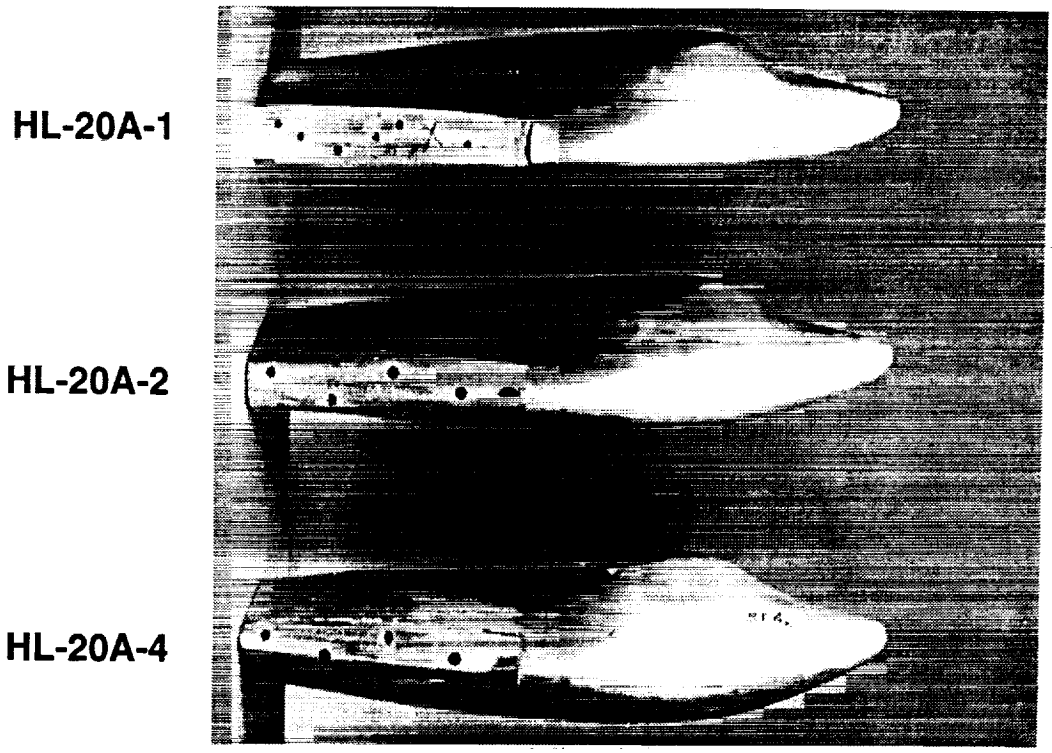

(e) Comparison of HL-20A-1; A-2 and A-4 showing under-surface camber changes.

Figure 4 - Continued.

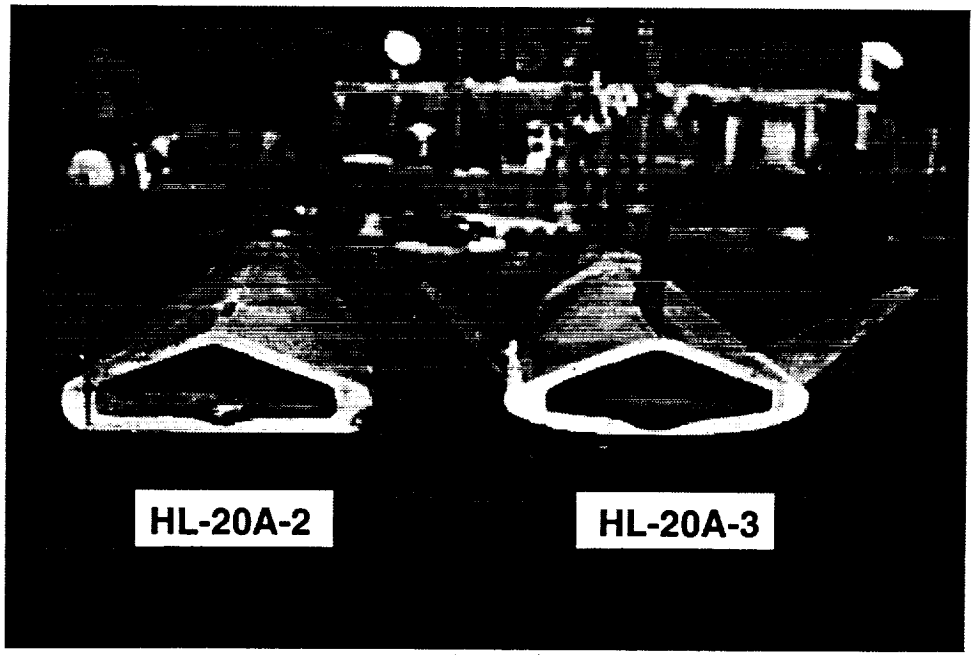

(f) Base view of HL-20A-2; A-3 showing lateral-elliptic faring to body leading edge and reduced base area.

Figure 4 - Continued.

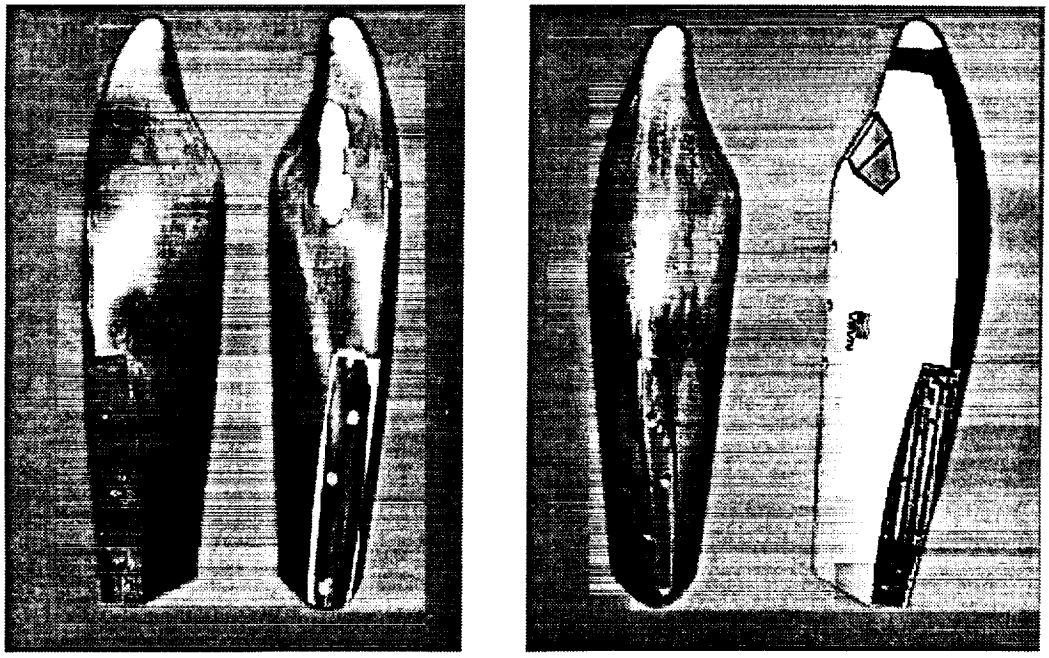

HL-20A-3 to HL-20B-2 HL-20A-4 to HL-20B-1

(g) Comparison of HL-20B-1; B-2 from HL-20A-4 and A-3, respectively, by removal of 6.5° body upper surface down slope.

Figure 4 - Continued.

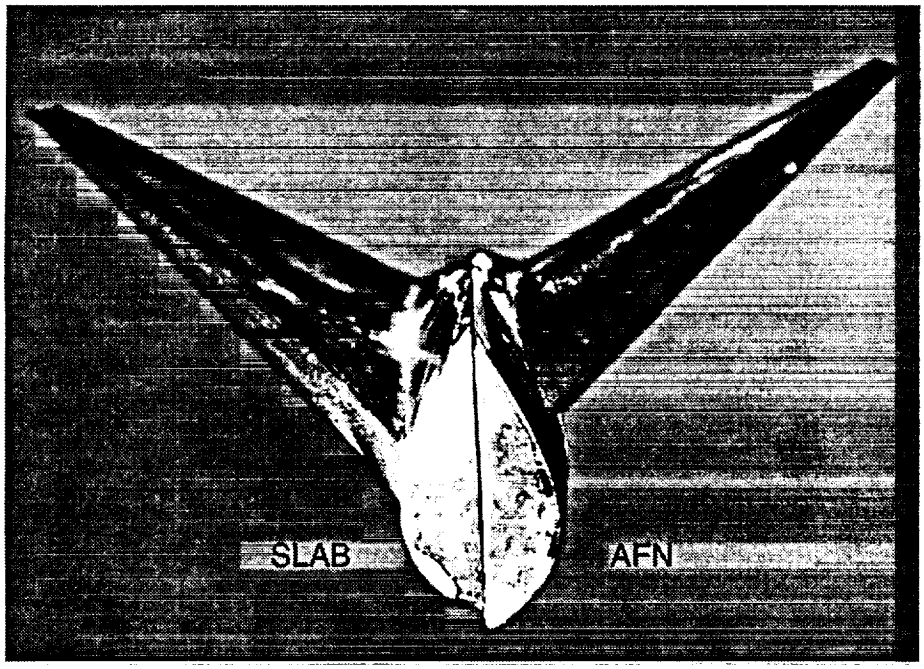

(h) Comparison of SLAB and AFN tip-fin configurations.

Figure 4 - Continued.

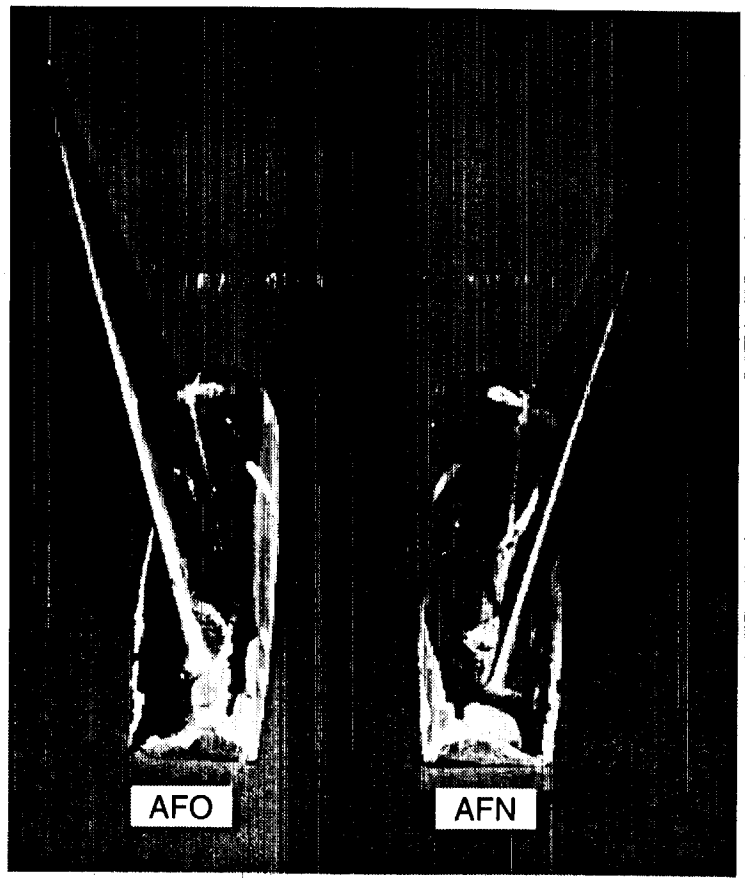

(i) Comparison of 25° AFO and AFN tip-fin configurations.

Figure 4 - Continued.

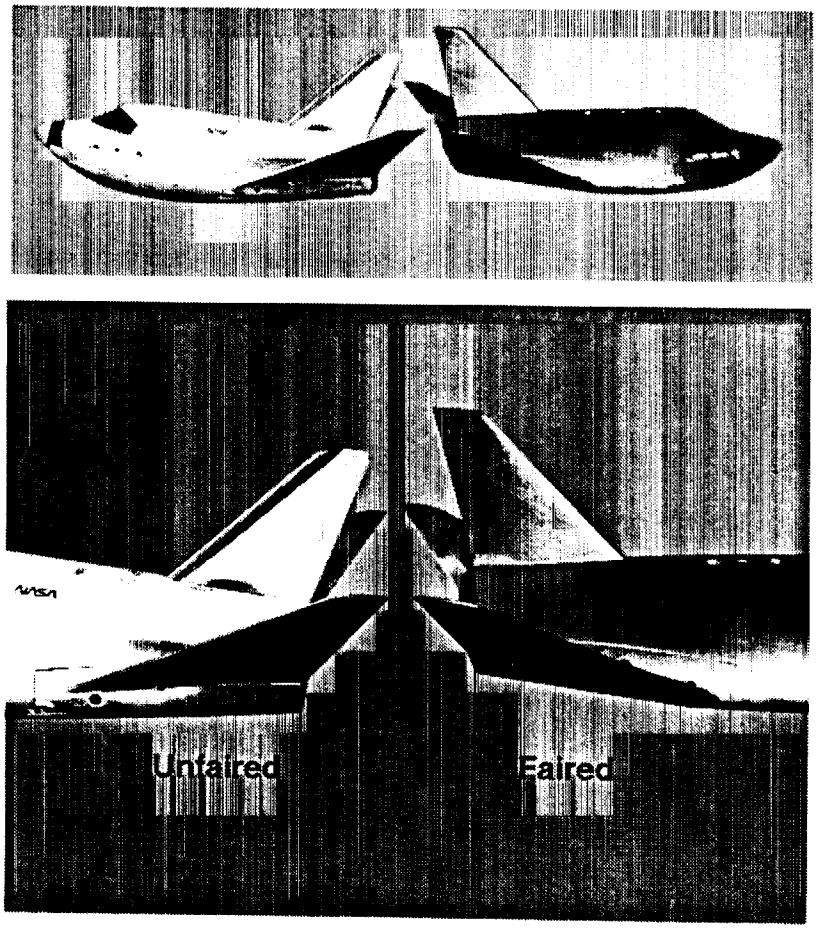

(j) Comparison of AFN faired and unfaired.

Figure 4 - Continued.

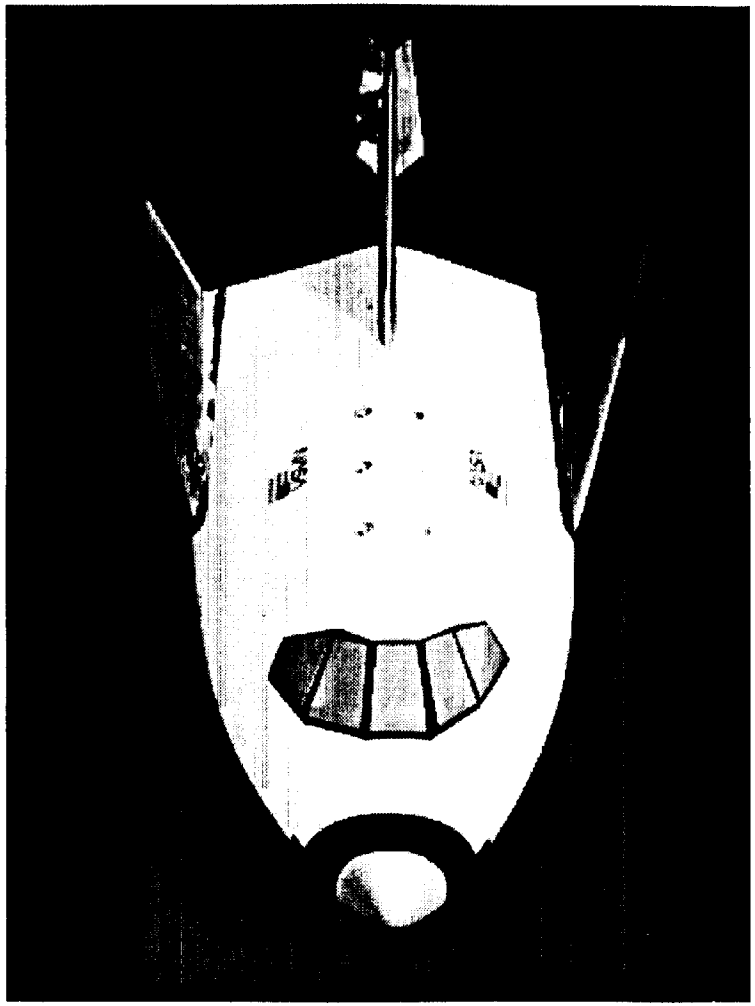

(k) Partial-span speed-brake deployed 45° per-side.

Figure 4 - Continued.

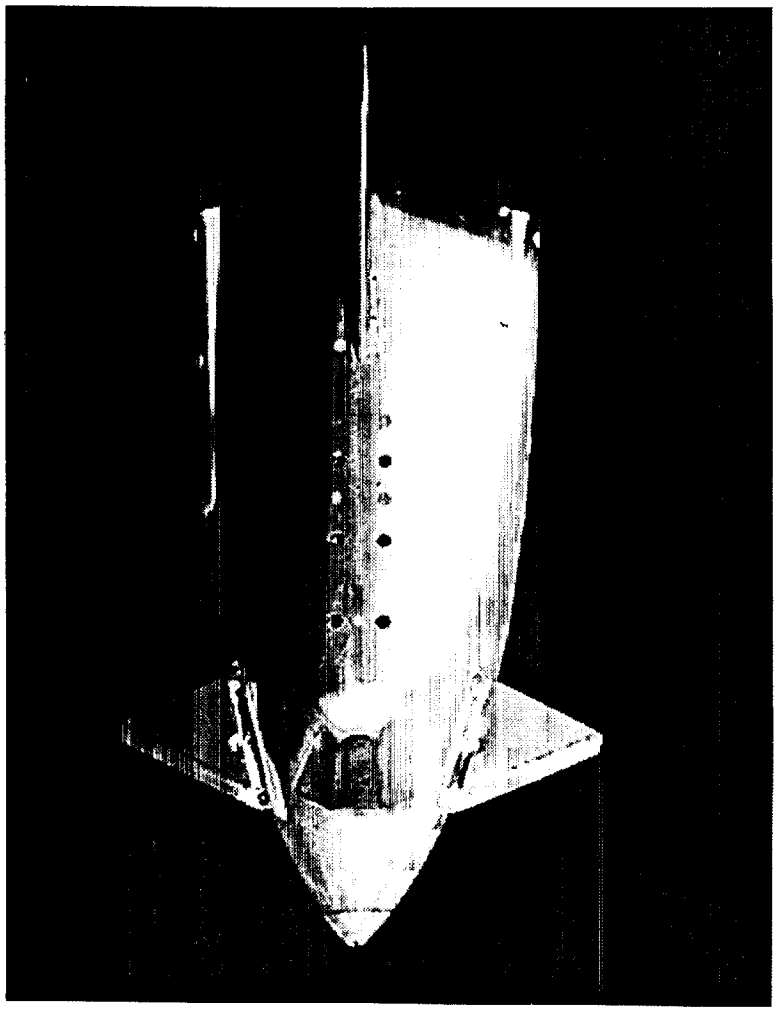

(l) Canard planform.

Figure 4 - Concluded.

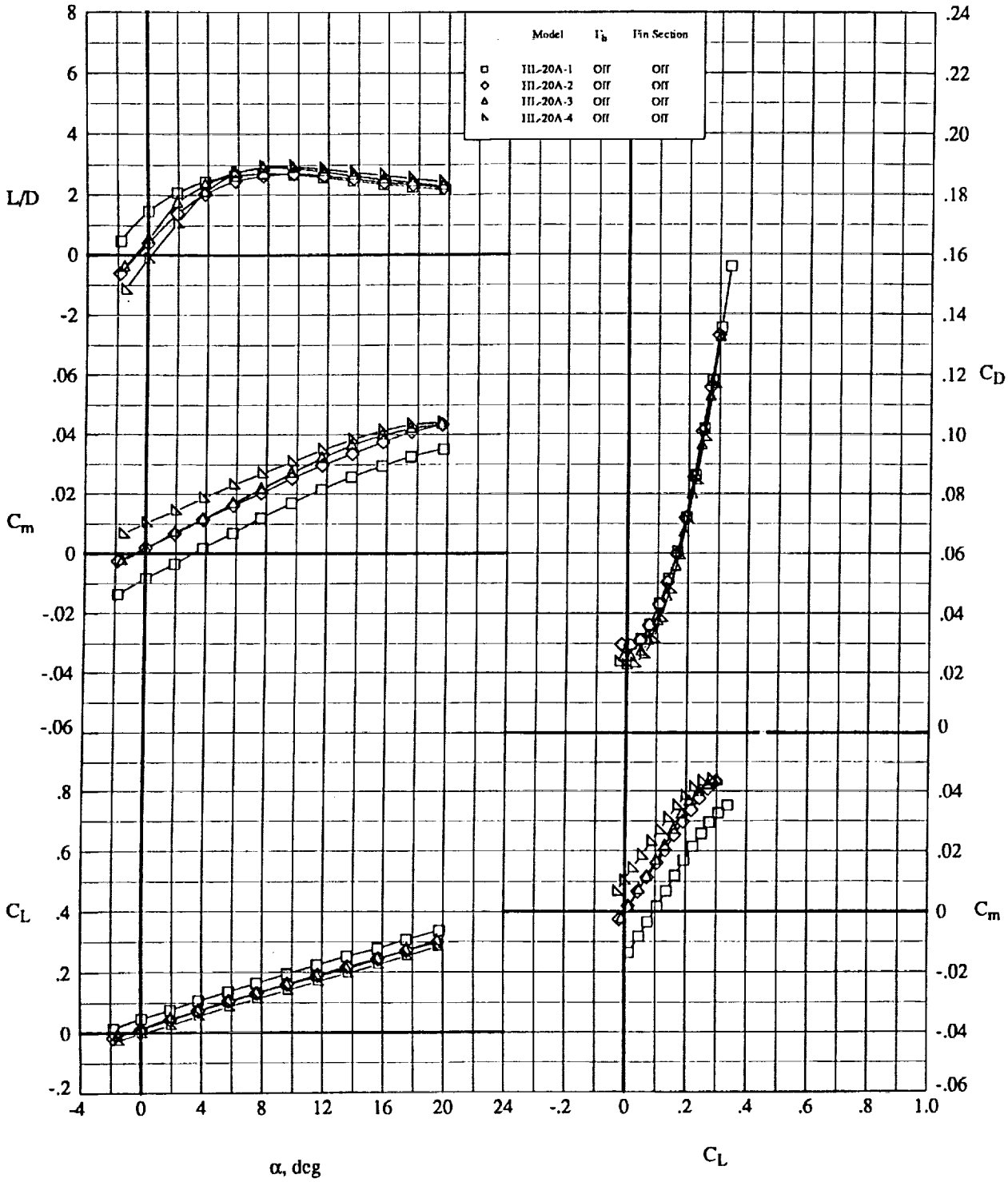

Figure 5. Effect of Body Contouring and Camber on the Longitudinal Aerodynamic Characteristics at $M_\infty = 0.3$ for the HL-20A Series bodies alone.

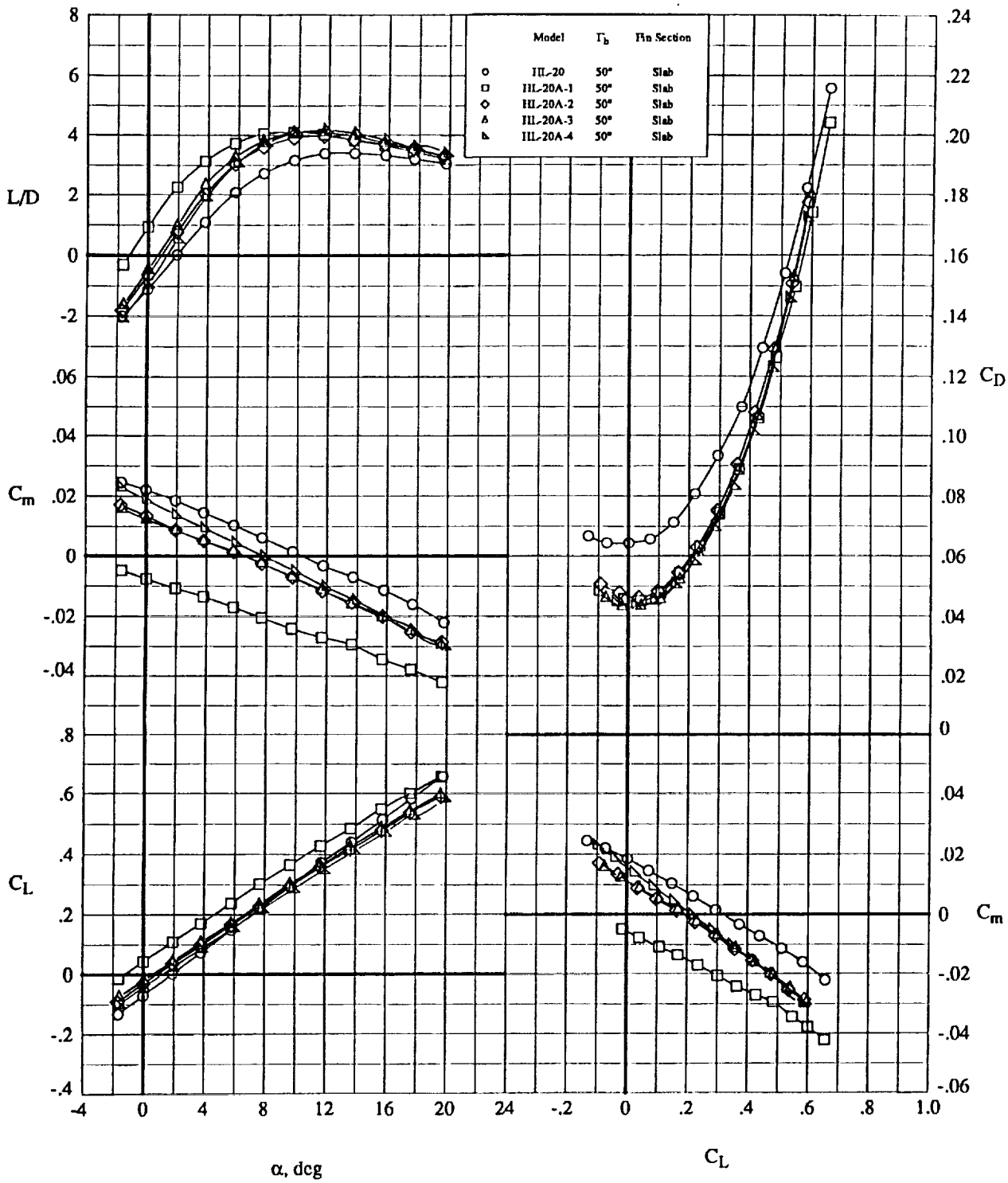

Figure 6. Effect of Body Contouring and Camber on the Longitudinal Aerodynamic Characteristics at $M_\infty = 0.3$ for the HL-20A Series bodies with the slab tip fin at $\Gamma_h = 50°$, compared to the original HL-20 configuration.

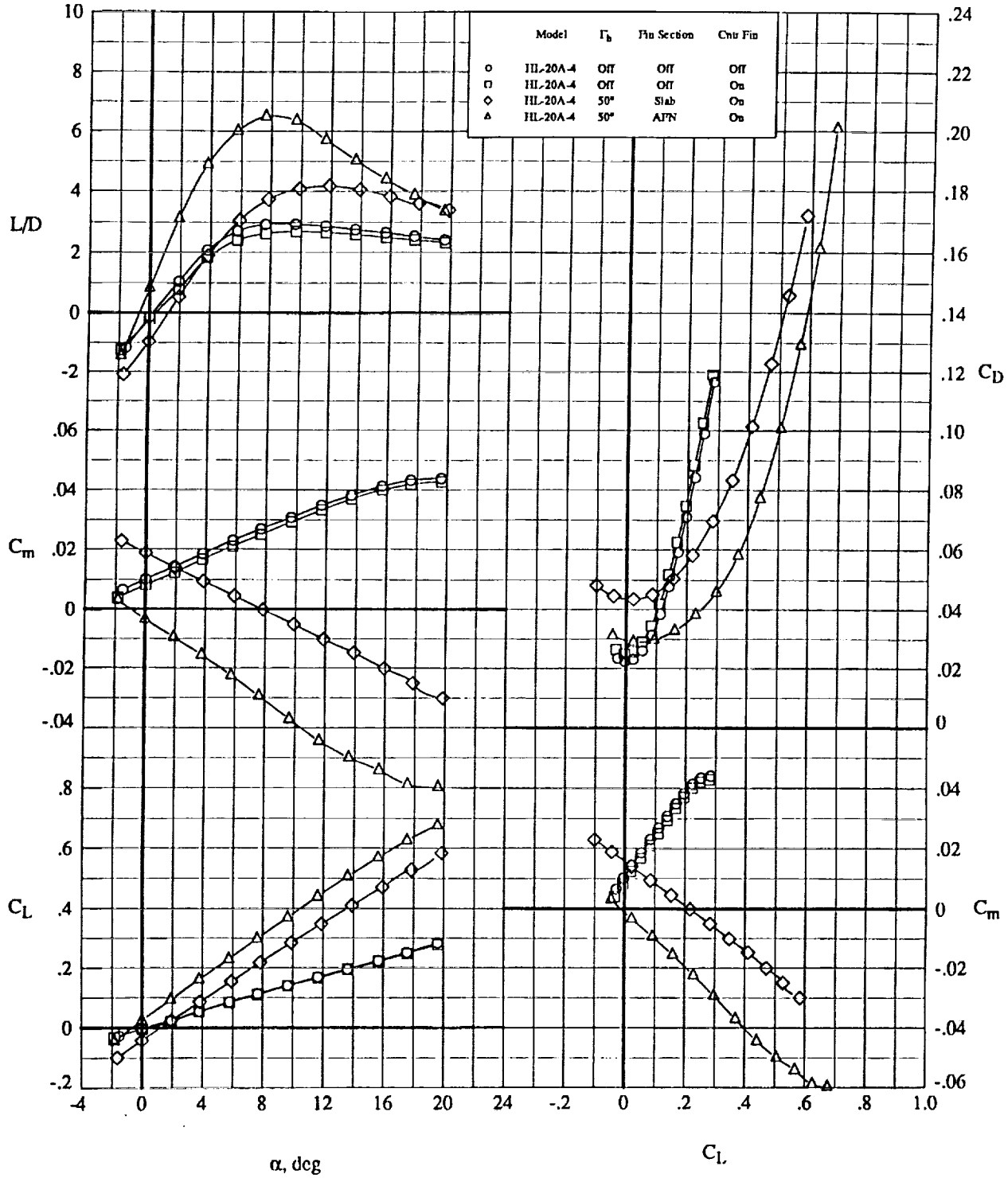

(a) Longitudinal Characteristics

Figure 7. Effect of Addition of Fin and of Fin Section on the Aerodynamic Characteristics at $M_\infty = 0.3$ for the HL-20A-4 configuration.

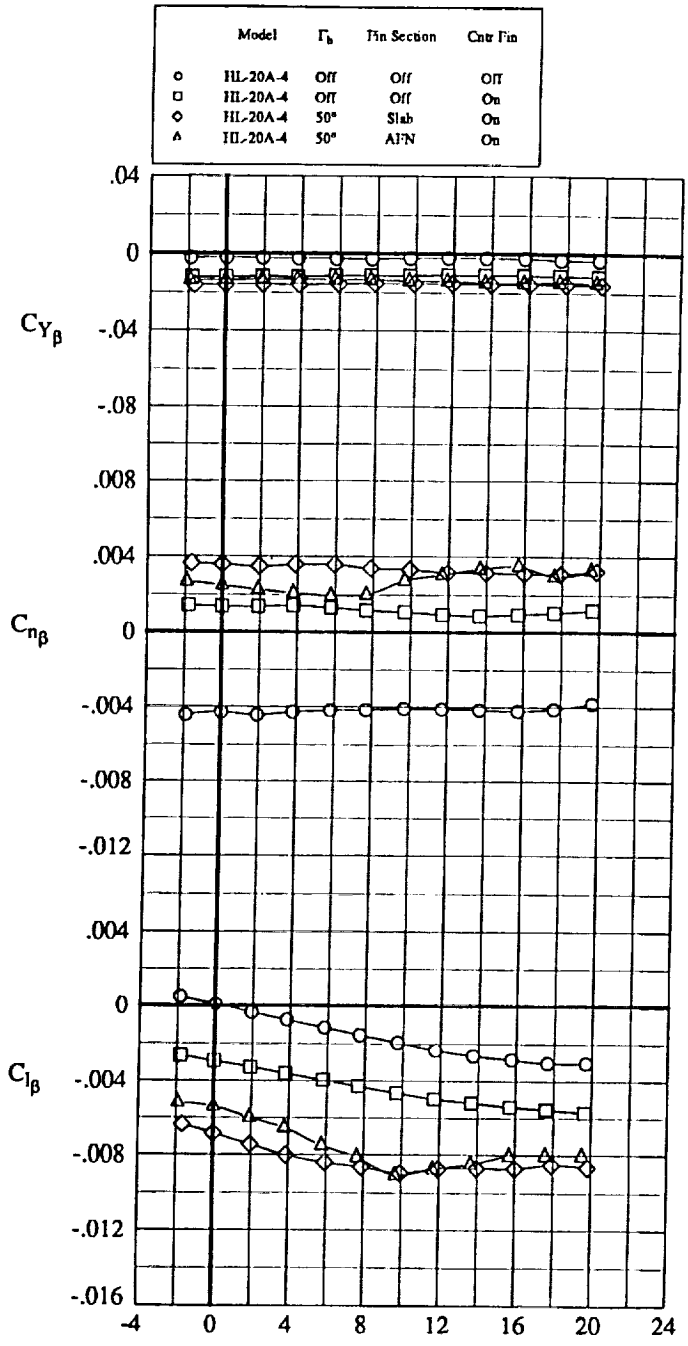

(b) Lateral-Directional Characteristics

Figure 7. Concluded.

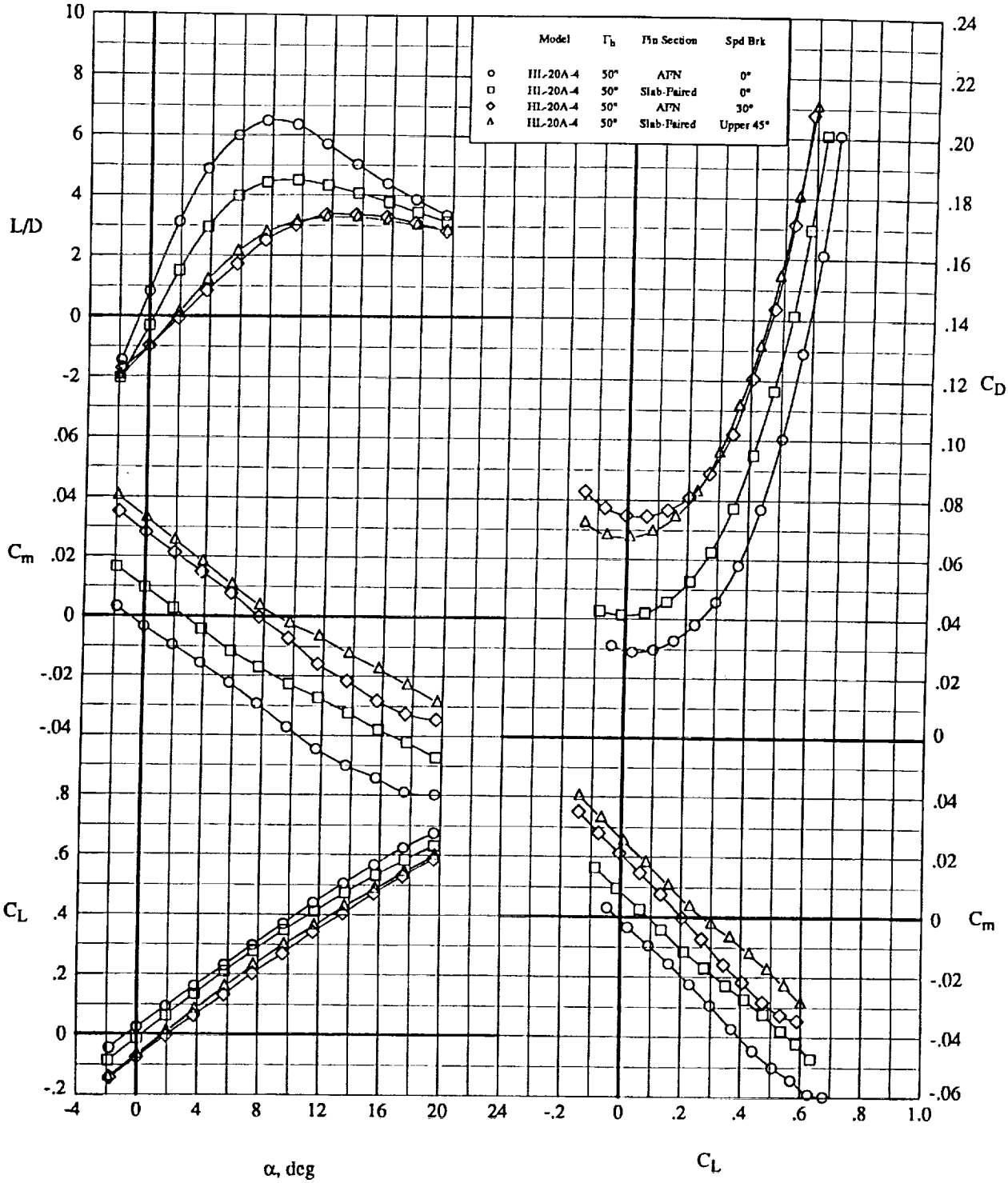

(a) Longitudinal Characteristics

Figure 8. Effect of Speed Brakes on the Aerodynamic Characteristics at $M_\infty = 0.3$ for the HL-20A-4 configuration.

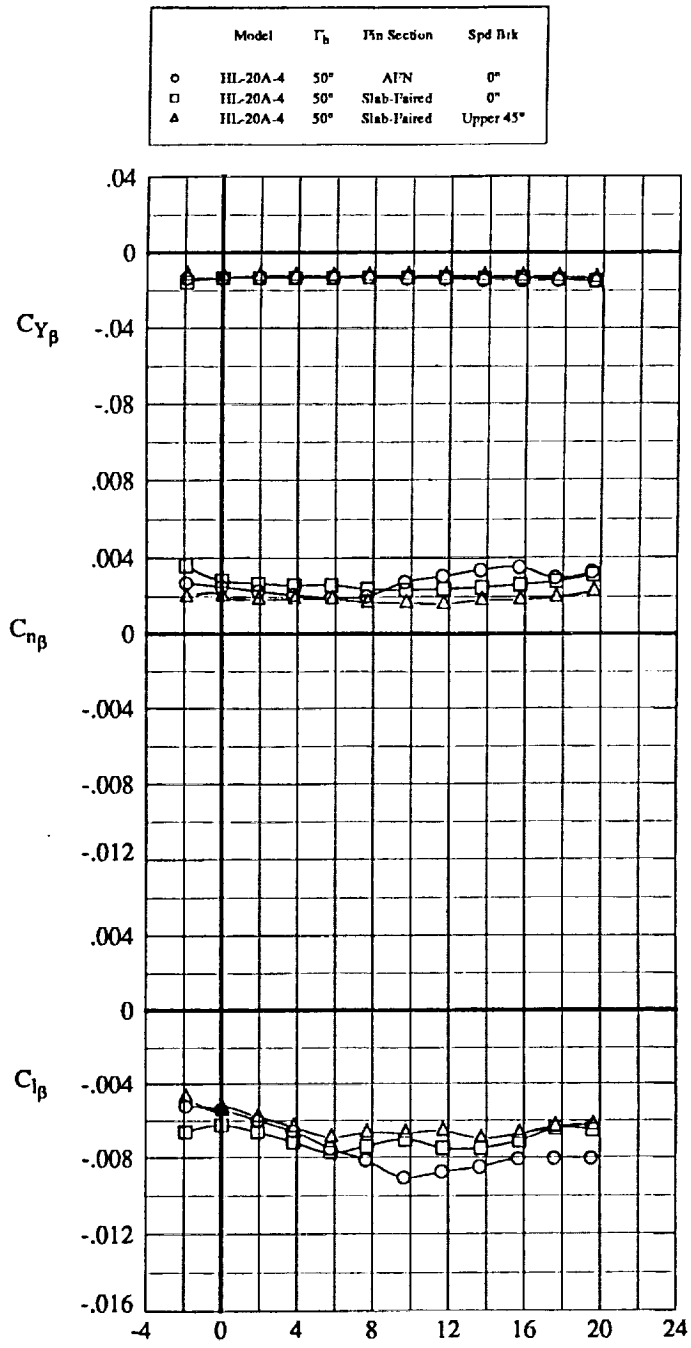

(b) Lateral-Directional Characteristics

Figure 8. Concluded.

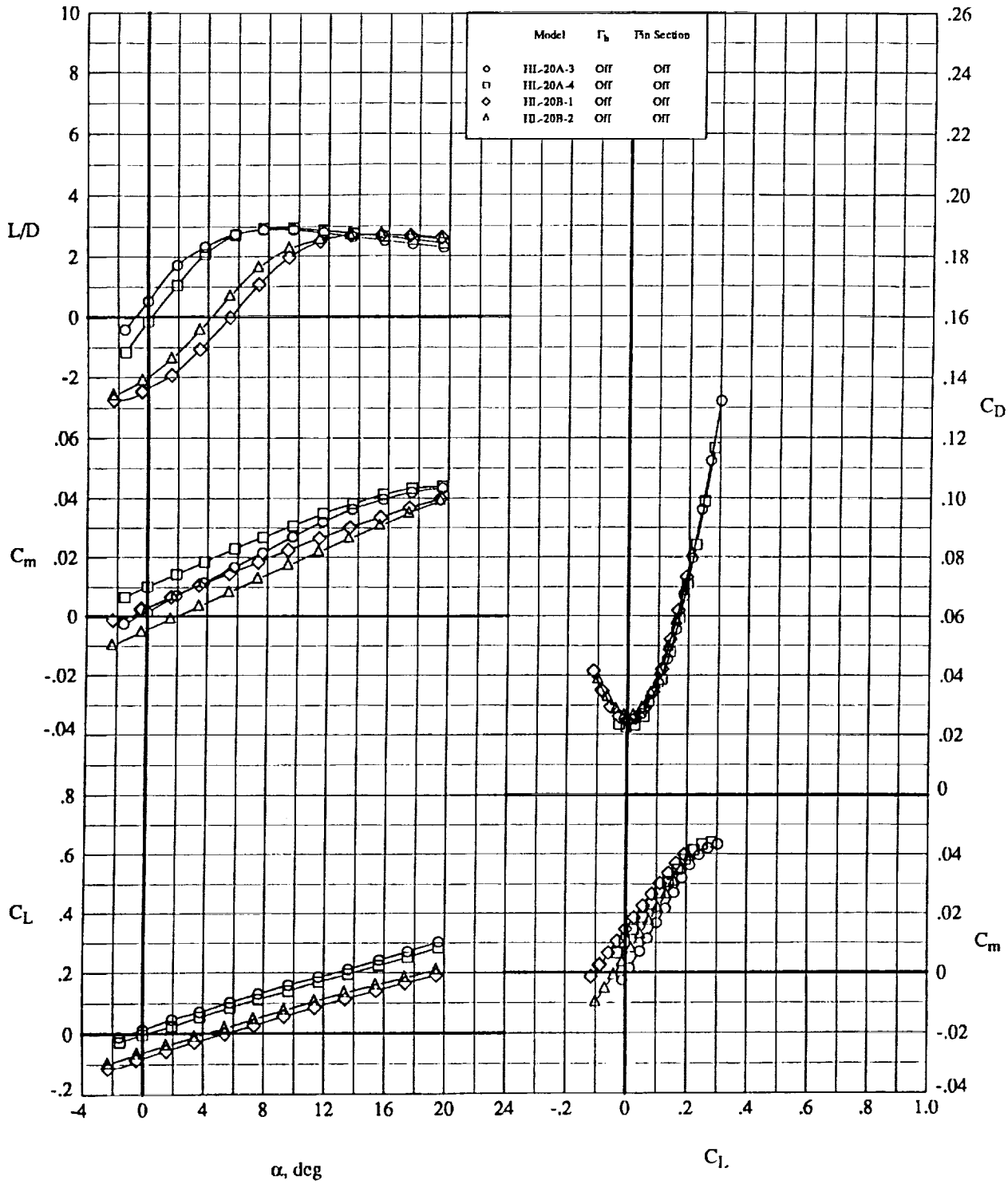

Figure 9. Effect of Removal of Upper Surface Downslope on the Longitudinal Aerodynamic Characteristics at $M_\infty = 0.3$ for configurations with the tip fin off.

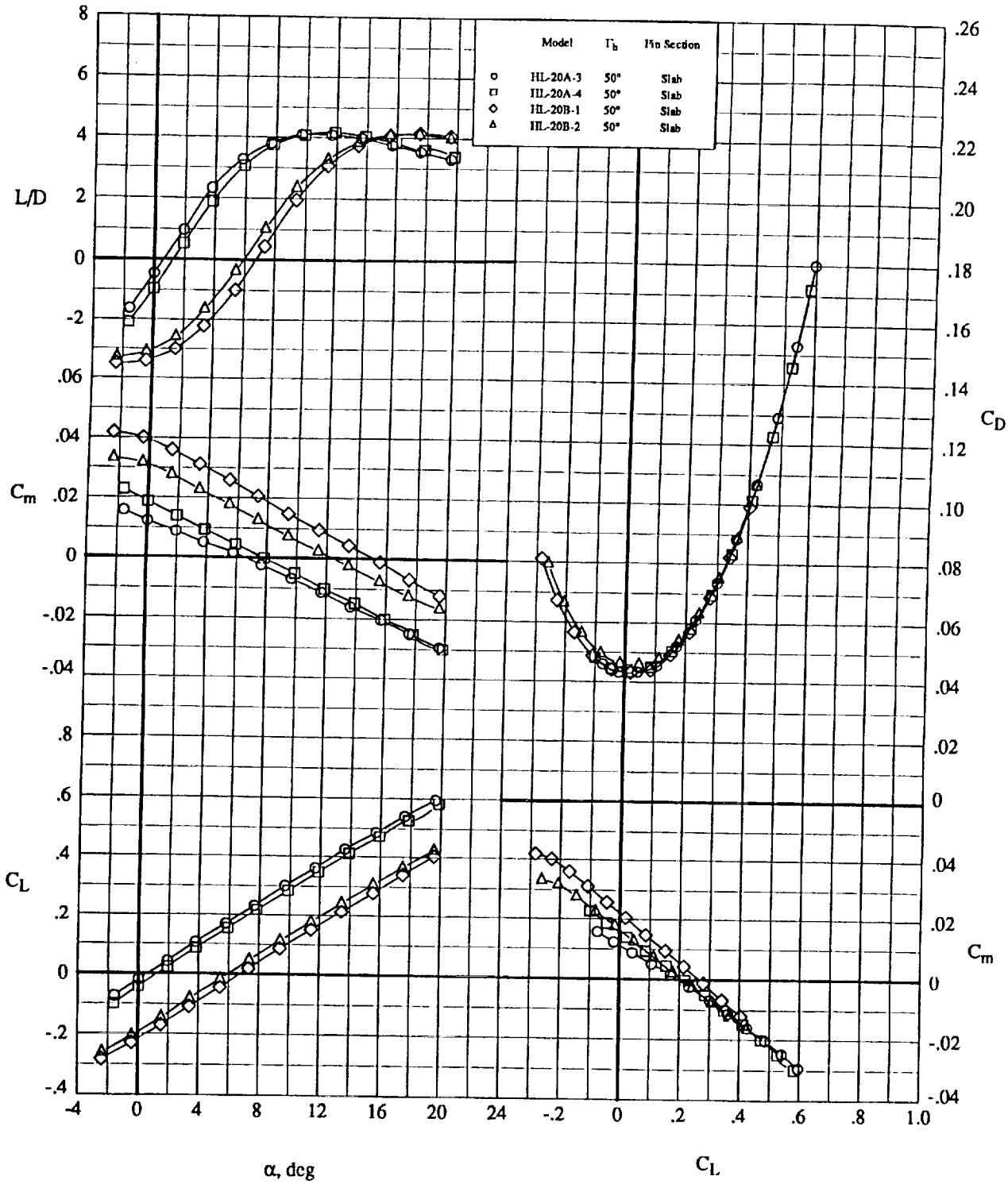

Figure 10. Effect of Removal of Upper Surface Downslope on the Longitudinal Aerodynamic Characteristics at $M_\infty = 0.3$ for configurations with the slab tip fin at $\Gamma_h = 50°$.

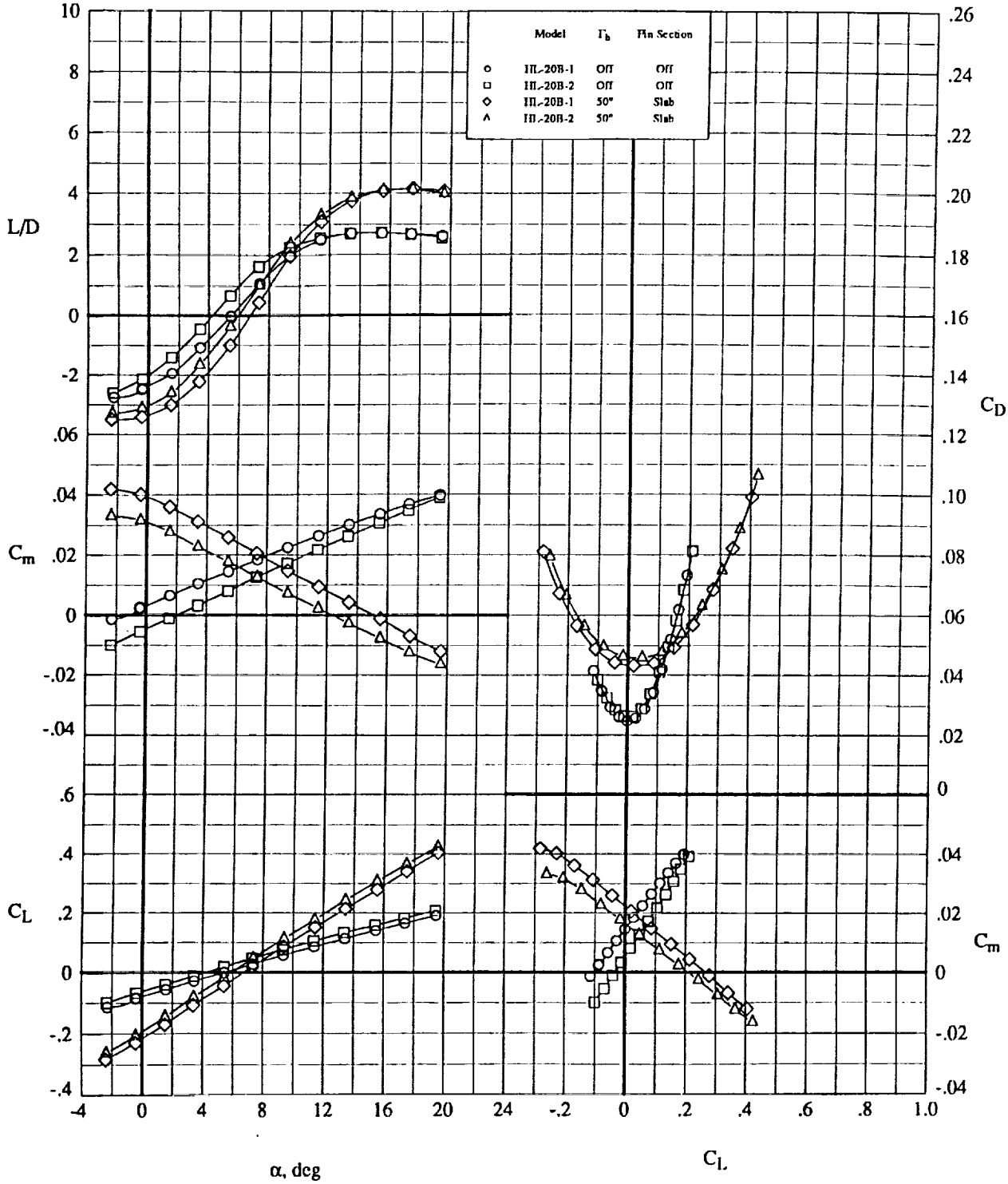

Figure 11. Effect of Body Contouring and Camber on the Longitudinal Aerodynamic Characteristics at $M_\infty = 0.3$ for the HL-20B Series bodies, with and witout $\Gamma_h = 50°$ slab fins.

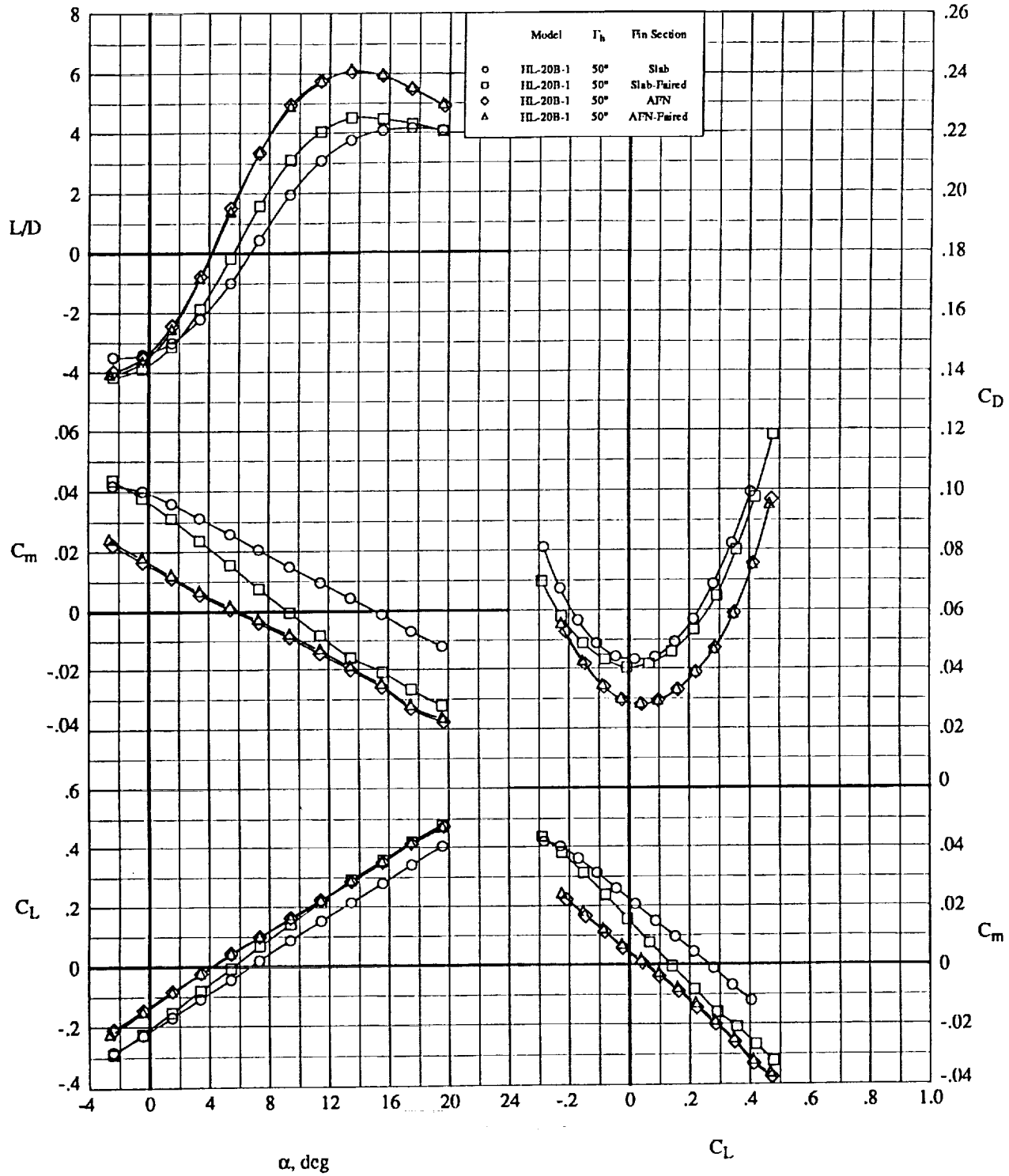

(a) Longitudinal Characteristics

Figure 12. Effect of Fin Section and Fairing on the Aerodynamic Characteristics at $M_\infty = 0.3$ for the HL-20B-1 configuration.

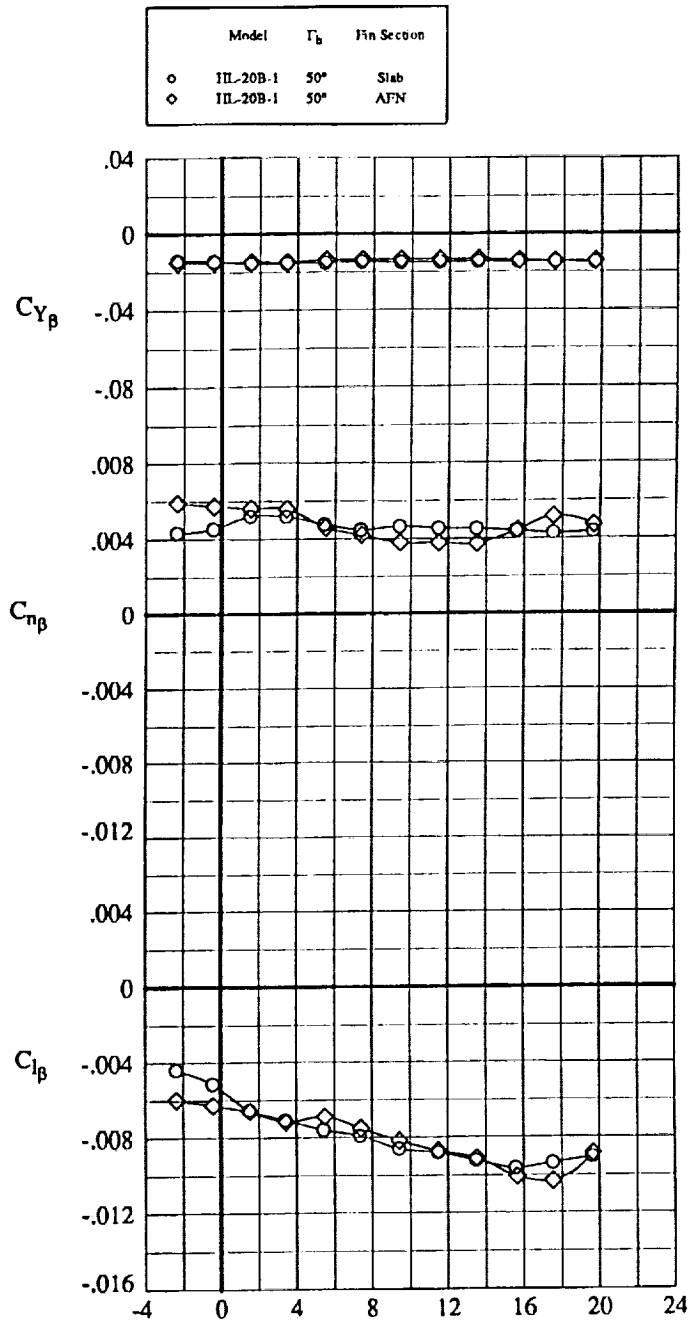

(b) Lateral-Directional Characteristics

Figure 12. Concluded.

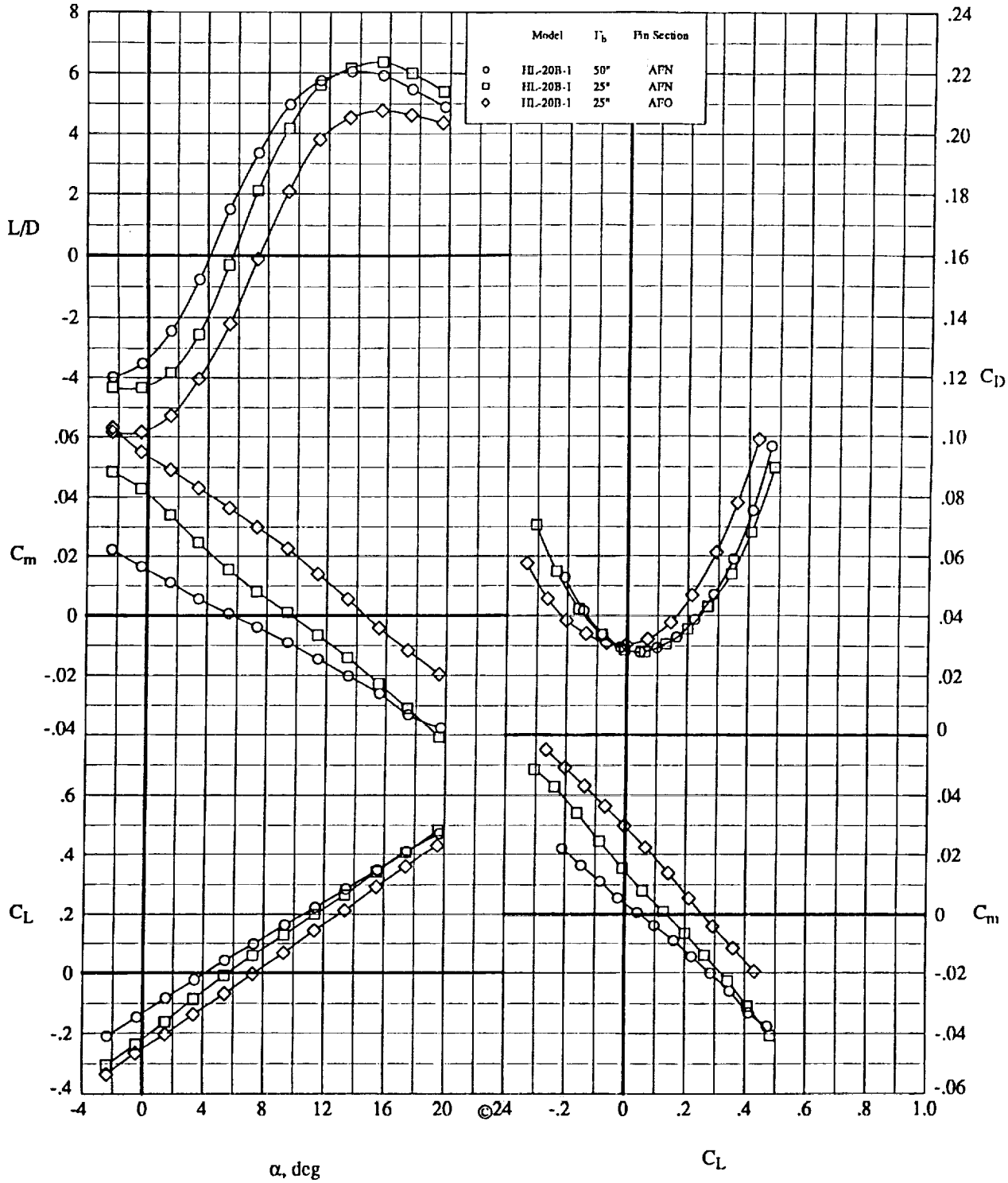

(a) Longitudinal Characteristics

Figure 13. Effect of Fin Dihedral and Airfoil Section on the Aerodynamic Characteristics at $M_\infty = 0.3$ for the HL-20B-1 configuration.

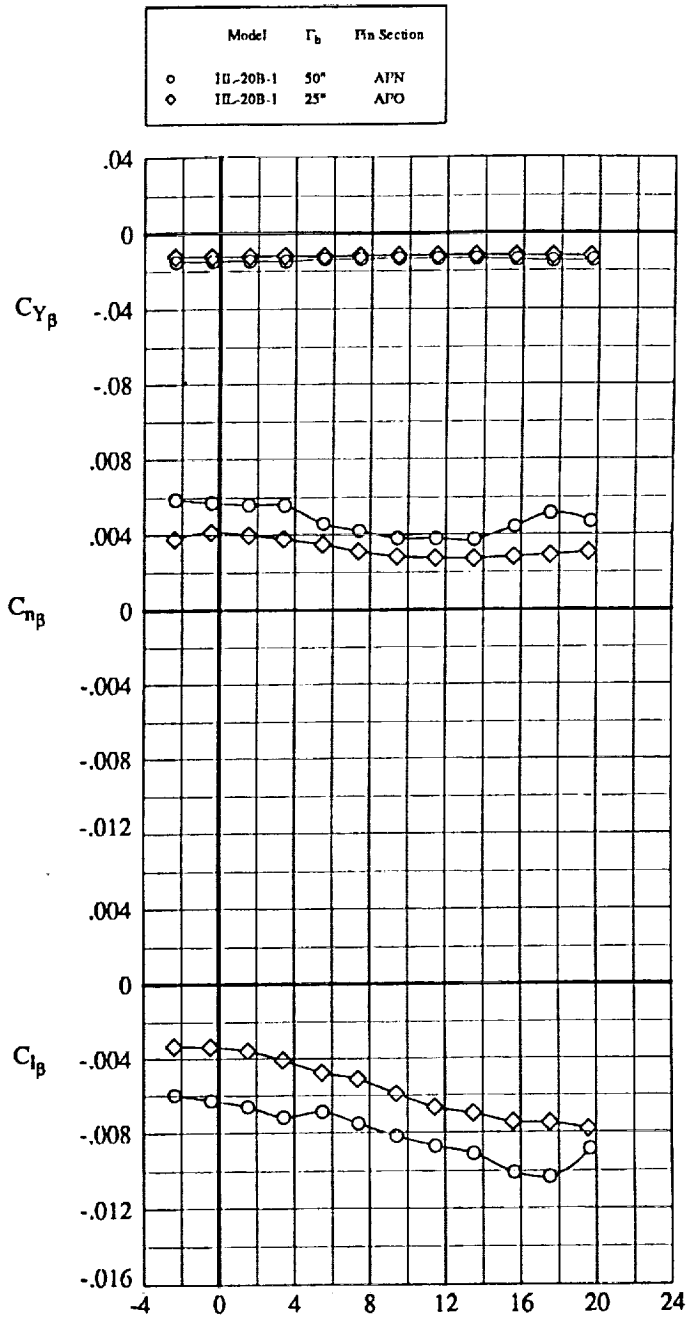

(b) Lateral-Directional Characteristics

Figure 13. Concluded.

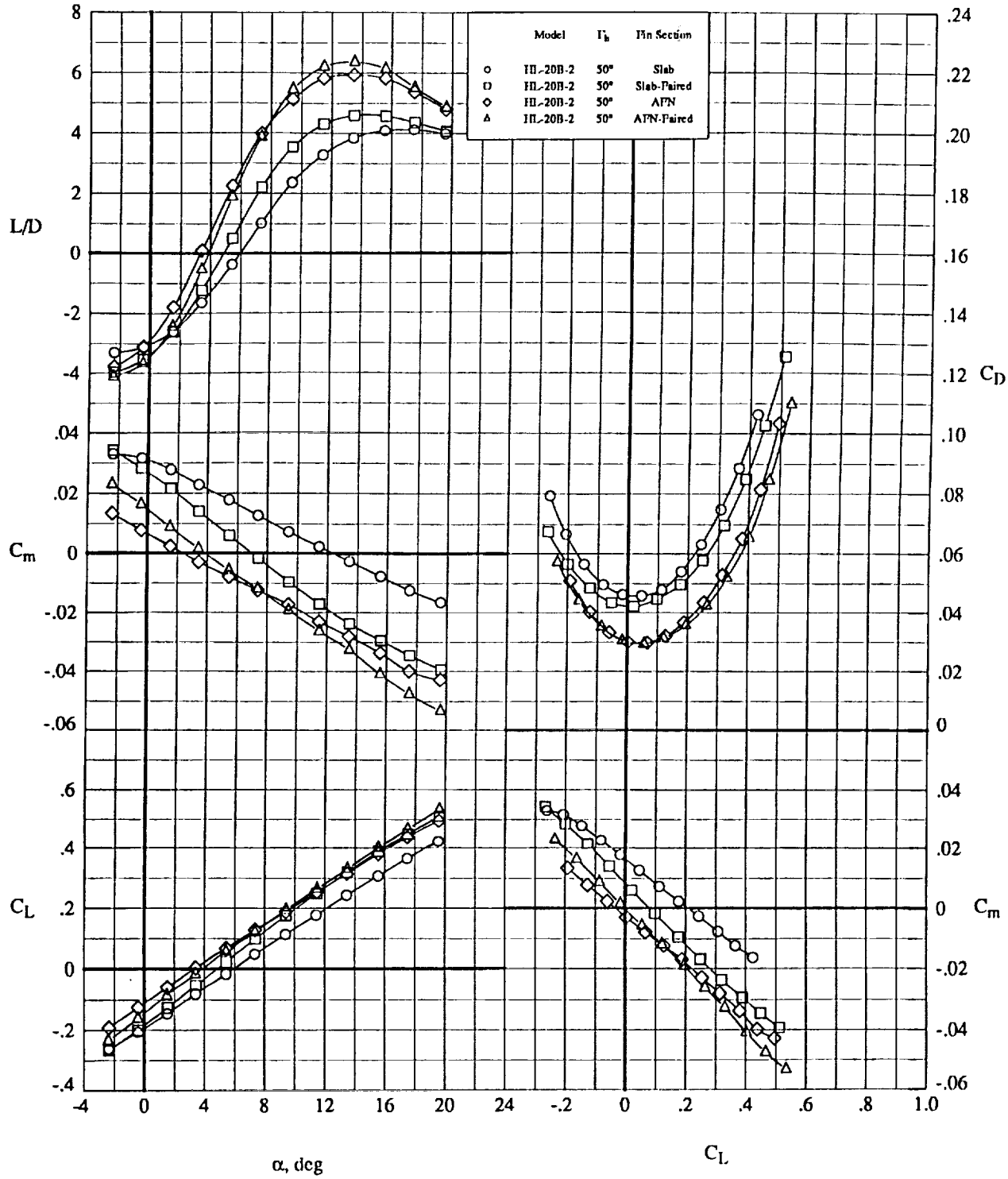

(a) Longitudinal Characteristics

Figure 14. Effect of Fin Section and Fairing on the Aerodynamic Characteristics at $M_\infty = 0.3$ for the HL-20B-2 configuration.

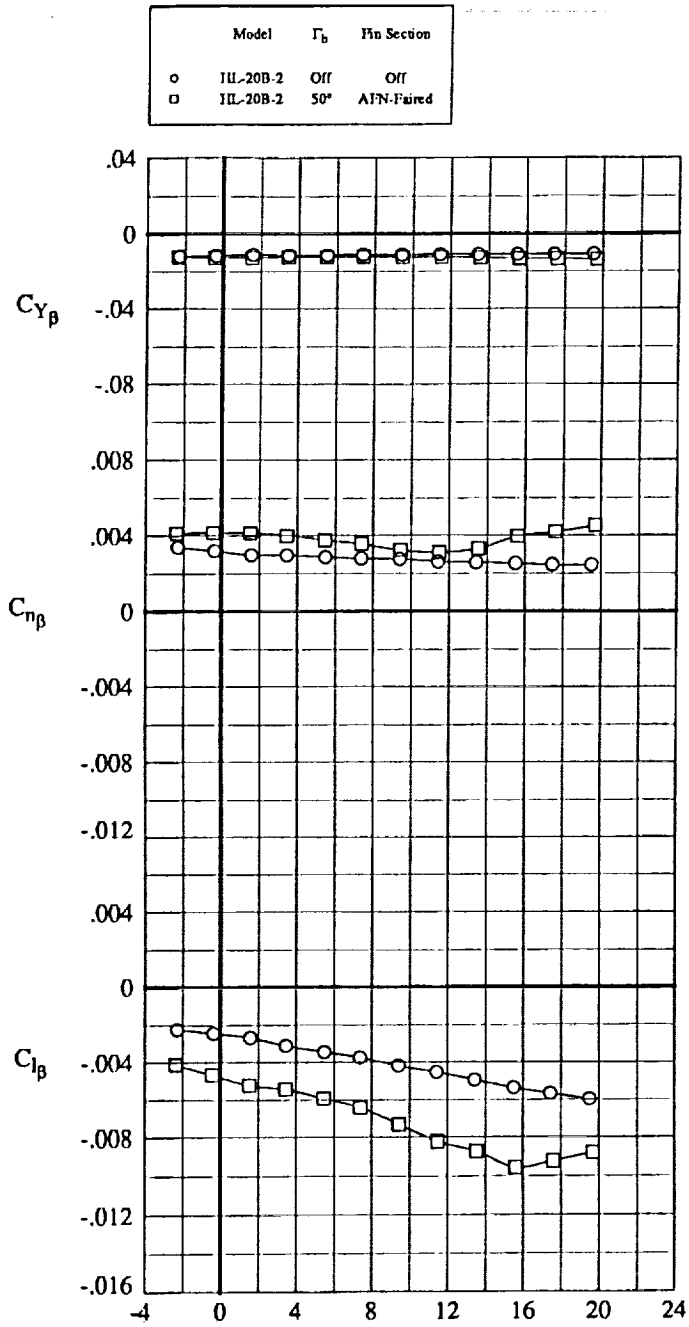

α, deg

(b) Lateral-Directional Characteristics

Figure 14. Concluded.

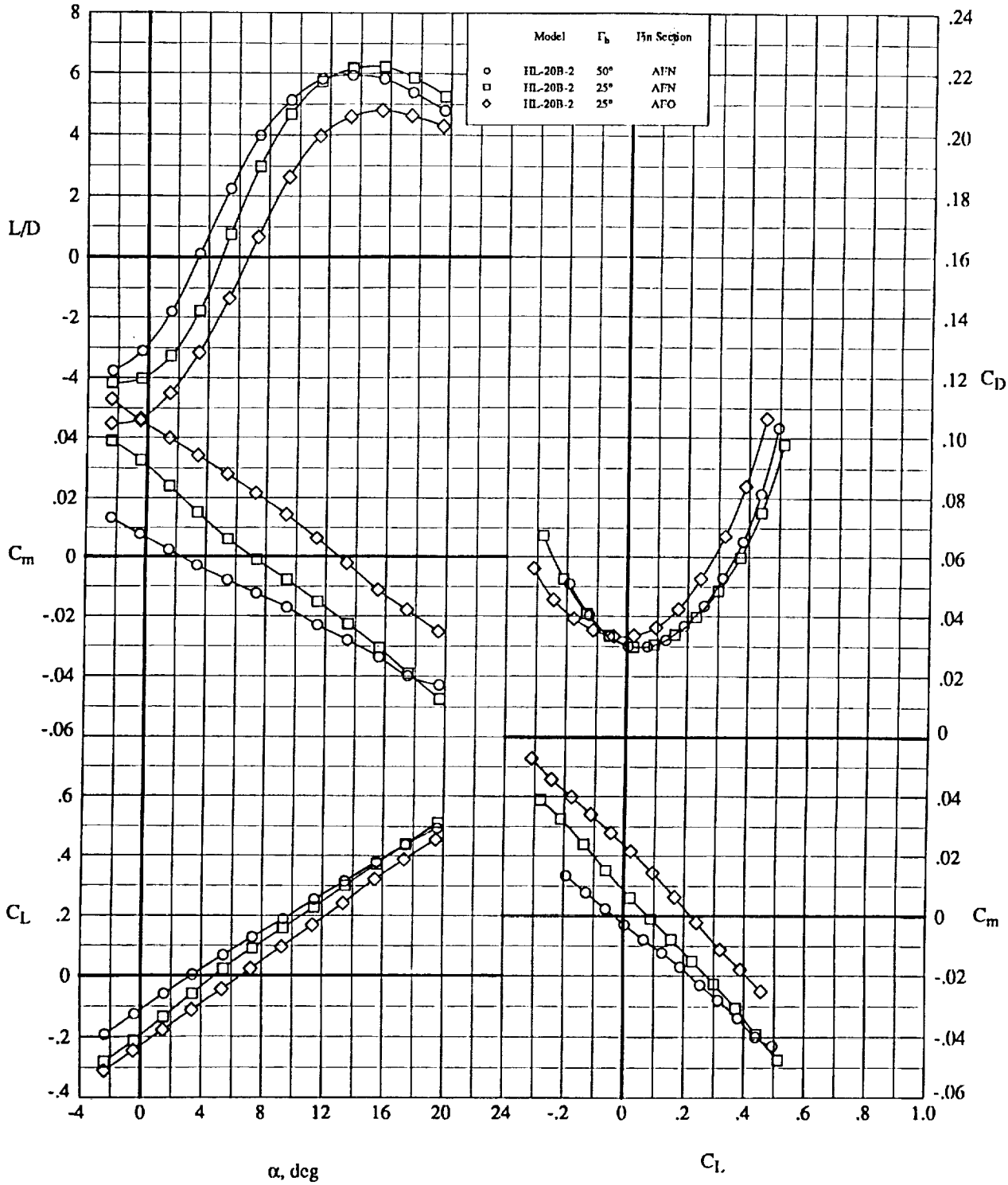

Figure 15. Effect of Fin Dihedral and Airfoil Section on the Aerodynamic Characteristics at $M_\infty = 0.3$ for the HL-20B-2 configuration.

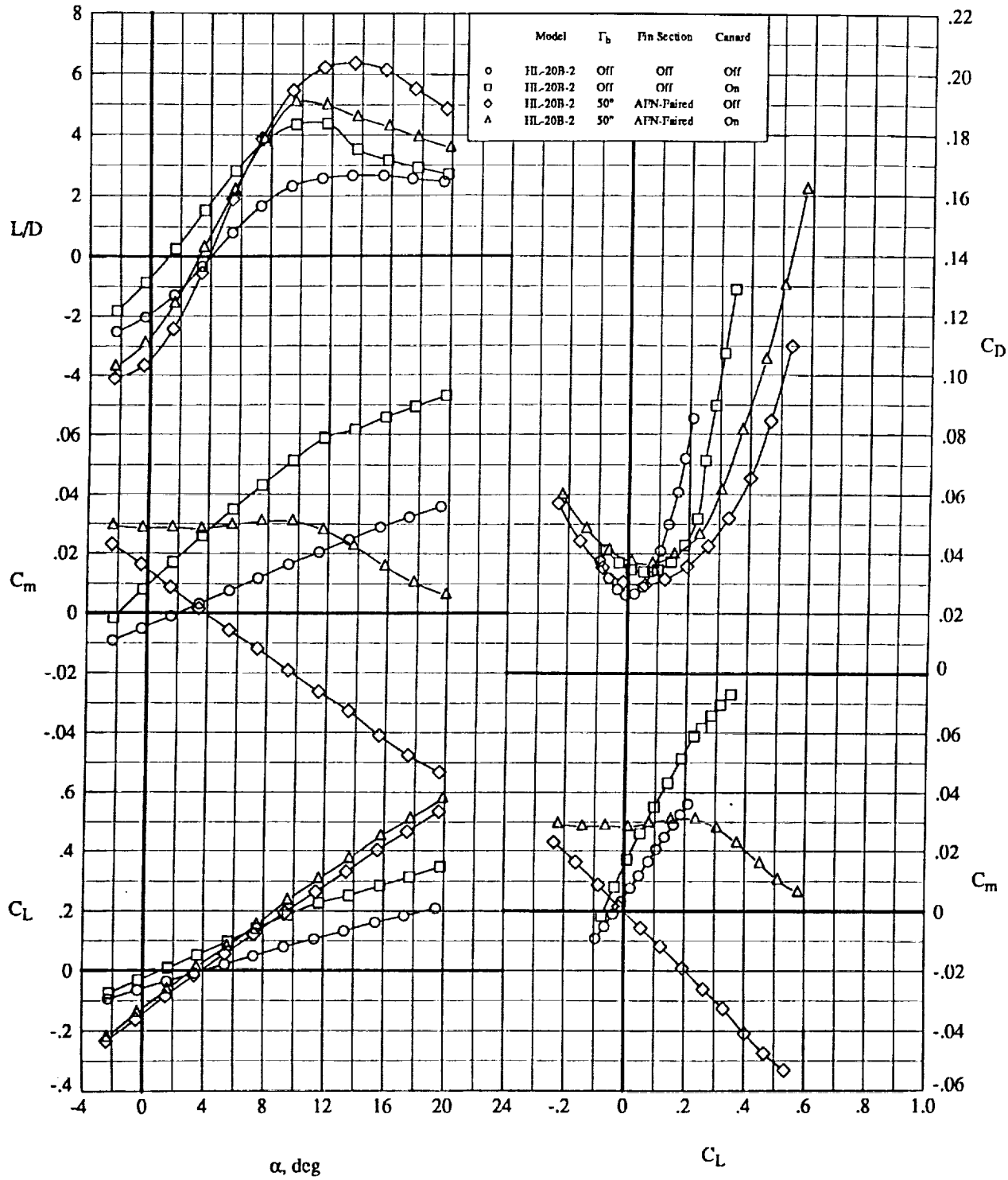

(a) Longitudinal Characteristics

Figure 16. Effect of Addition of Canard on the Aerodynamic Characteristics at $M_\infty = 0.3$ for the HL-20B-2 configuration.

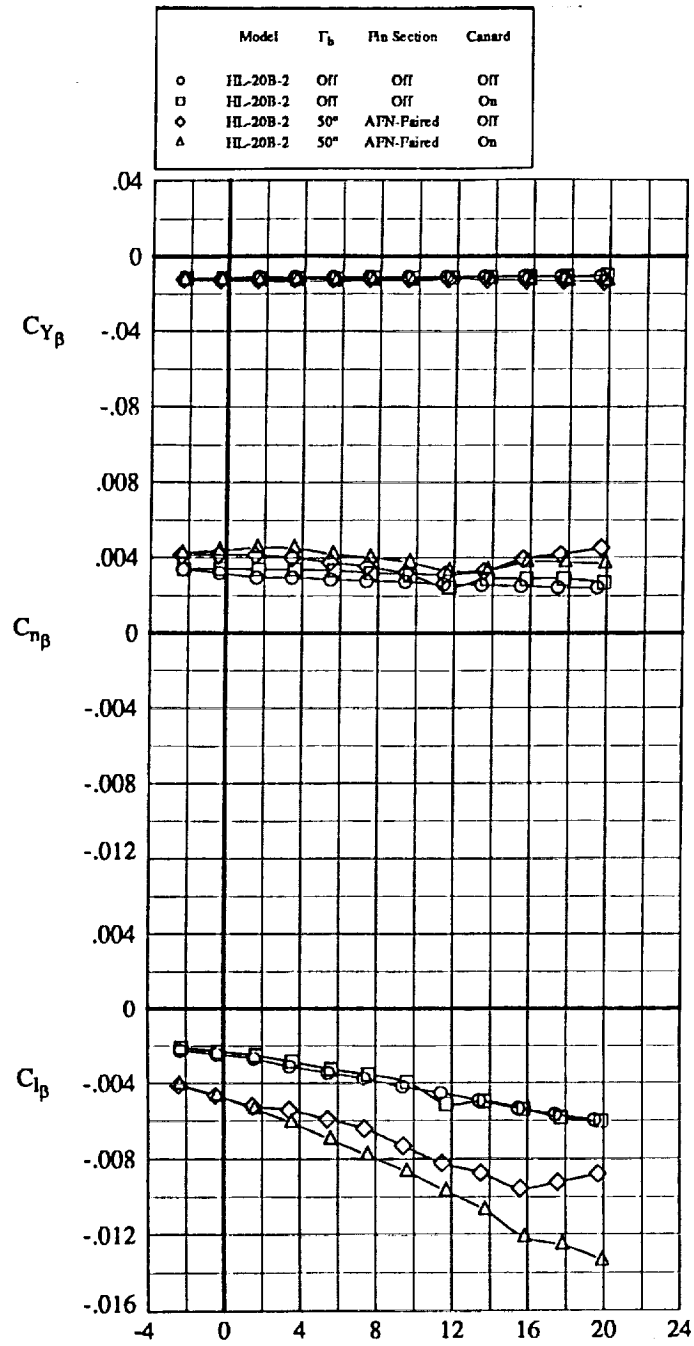

(a) Lateral-Directional Characteristics

Figure 16. Concluded.

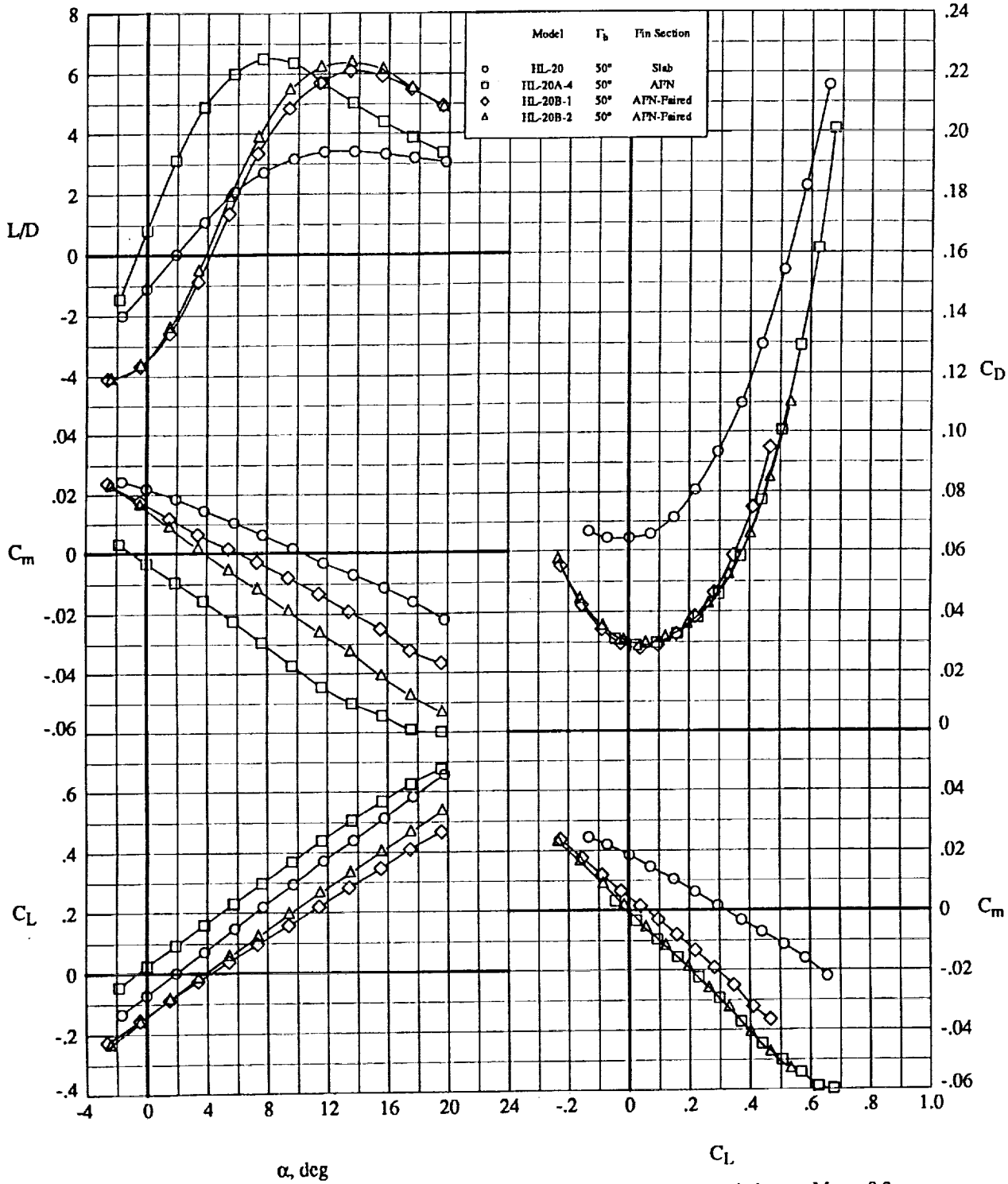

Figure 17. Comparison of the Longitudinal Aerodynamic Characteristics at $M_\infty = 0.3$ for some selected near-optimum performance HL-20A/B configurations and the original HL-20 with $\Gamma_h = 50°$.

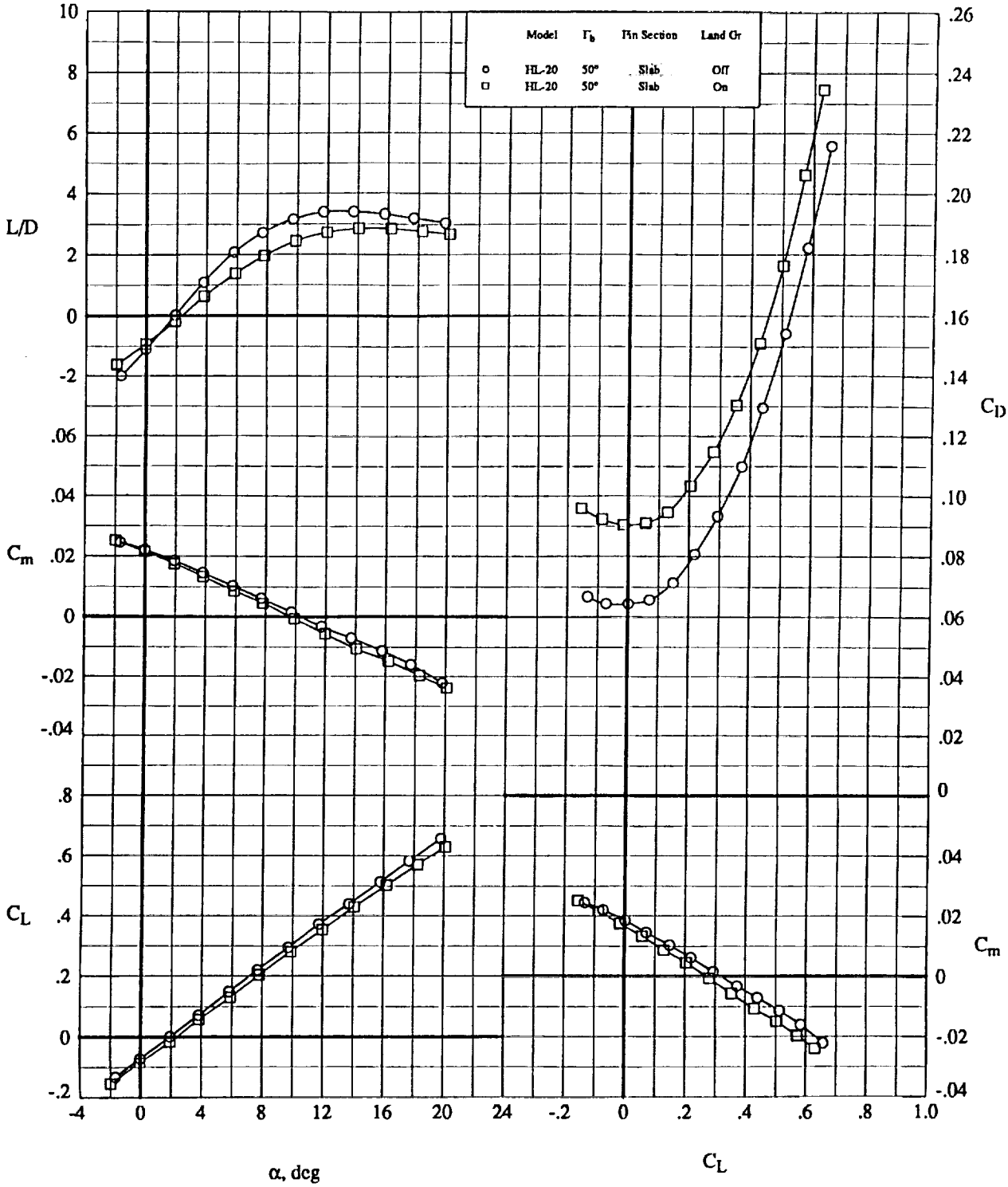

(a) Longitudinal Characteristics

Figure 18. Effect of Landing Gear on the Aerodynamic Characteristics at $M_\infty = 0.3$ for the HL-20 configuration with the slab tip fin at $\Gamma_h = 50°$.

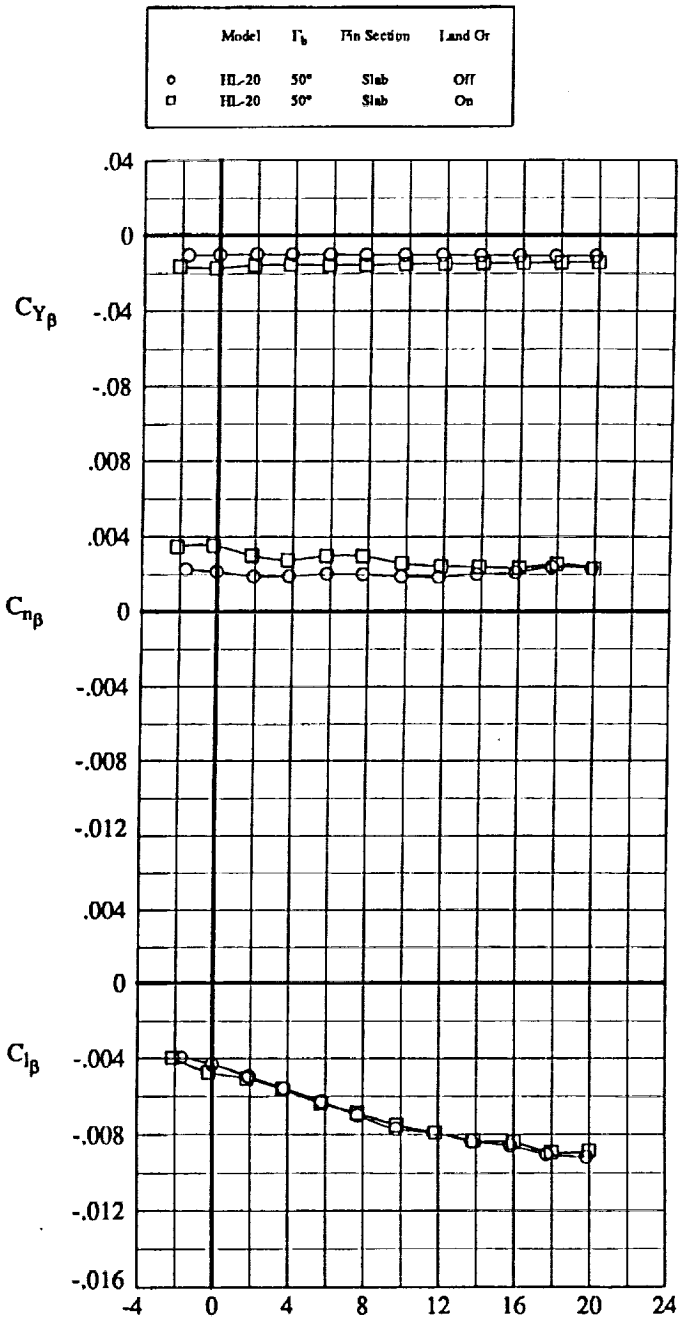

(b) Lateral-Directional Characteristics

Figure 18. Concluded.

REPORT DOCUMENTATION PAGE

Form Approved
OMB No. 0704-0188

1. AGENCY USE ONLY *(Leave blank)*	2. REPORT DATE	3. REPORT TYPE AND DATES COVERED
	December 1995	Technical Memorandum

4. TITLE AND SUBTITLE
A Study to Determine Methods of Improving the Subsonic Performance of A Proposed Personnel Launch System (PLS) Concept

5. FUNDING NUMBERS
242-20-08-02

6. AUTHOR(S)
B. Spencer, Jr., C. H. Fox, Jr., and J. K. Huffman

7. PERFORMING ORGANIZATION NAME(S) AND ADDRESS(ES)
NASA Langley Research Center
Hampton, VA 23681-0001

8. PERFORMING ORGANIZATION REPORT NUMBER

9. SPONSORING / MONITORING AGENCY NAME(S) AND ADDRESS(ES)
National Aeronautics and Space Administration
Washington, DC 20546-0001

10. SPONSORING / MONITORING AGENCY REPORT NUMBER
NASA TM-110201

11. SUPPLEMENTARY NOTES

12a. DISTRIBUTION / AVAILABILITY STATEMENT
Unclassified - Unlimited
Subject Category 02

12b. DISTRIBUTION CODE

13. ABSTRACT *(Maximum 200 words)*

An investigation has been conducted in the Langley 7- by 10-Foot High Speed Wind Tunnel to determine the longitudinal and lateral directional aerodynamic characteristics of a series of personnel launch system concepts. This series of configurations evolved during an effort to improve the subsonic characteristics of a proposed lifting entry vehicle (designated the HL-20). The primary purpose of the overall investigation was to provide a vehicle concept which was inherently stable and trimable from entry to landing while examining methods of improving subsonic aerodynamic performance.

14. SUBJECT TERMS
Subsonic Performance Enhancement

15. NUMBER OF PAGES
81

16. PRICE CODE
A05

17. SECURITY CLASSIFICATION OF REPORT	18. SECURITY CLASSIFICATION OF THIS PAGE	19. SECURITY CLASSIFICATION OF ABSTRACT	20. LIMITATION OF ABSTRACT
Unclassified	Unclassified		

NSN 7540-01-280-5500

Standard Form 298 (Rev. 2-89)
Prescribed by ANSI Std. Z39-18
298-102